



Title	Investigation of Picosecond Optical Phenomena in III-V Quantum Confined Structures
Author(s)	Takeuchi, Atsushi
Citation	大阪大学, 1992, 博士論文
Version Type	VoR
URL	<a href="https://doi.org/10.11501/3063586">https://doi.org/10.11501/3063586</a>
rights	
Note	

*The University of Osaka Institutional Knowledge Archive : OUKA*

<https://ir.library.osaka-u.ac.jp/>

The University of Osaka

**Investigation of Picosecond Optical Phenomena**  
**in**  
**III-V Quantum Confined Structures**

**1992**

**Atsushi Tackeuchi**

**Investigation of Picosecond Optical Phenomena  
in  
III-V Quantum Confined Structures**

**1992**

**ATSUSHI TACKEUCHI**



## **Abstract**

Motivated by the need to understand the ultrafast optical processes related to quantum confinement effects in semiconductor devices, a series of studies have been made about the picosecond nonlinear optical phenomena in excitonic absorption combined with tunneling and diffusion in various quantum wells, wires, and superlattices of III-V compounds. The main intention is to use the fast recovery of the excitonic absorption after its optical bleaching for all-optical device applications.

The present study shows that the recovery time can be reduced to picosecond region, which overcomes the serious difficulty of slow recovery time (on the order of nanoseconds) of excitonic nonlinearity in previous works. This has been achieved by the use of various structures with tunneling or rapid recombination channels as follows:

In tunneling bi-quantum well (TBQ) structure consisting of narrow and wide GaAs quantum wells, photo-excited electrons in the narrow wells escape to the wide wells by non-resonant or resonant tunneling. In non-resonant tunneling, the recovery time is reduced to 1 ps by reducing the AlGaAs barrier thickness to 1.7 nm. This is by three orders of magnitude shorter than that in conventional multiple quantum well (MQW). In resonant TBQ, where photo-excited electrons in the e1-level of narrow wells escape toward the e2-level of wide wells by resonant tunneling, the reduction of absorption recovery time and the increased tail-to-peak ratio in the excitonic absorption change are observed. We also report the fast recovery in the type-II TBQ structure consisting of a series of GaAs

wells, AlGaAs barriers, and AlAs layers. Type-II TBQs have an advantage over type-I TBQs for application because type-II TBQ have no significant optical absorption except in the GaAs wells. For a AlGaAs barrier thickness of 1.1 nm, the recovery time is found to be 8 ps.

Another approach to reduce the recovery time is the use of fast surface recombination on the side-walls of MQW wires. We made MQW wires as small as 130 nm using focused-ion-beam (FIB) lithography and electron cyclotron-resonance (ECR) chlorine-plasma etching. We show that the strong optical nonlinearity of excitons is preserved for 130-nm-wide wires, and that the recovery time is as small as 11 ps.

As an another aspect of rapid decay processes, the first direct observation is reported of spin relaxation in GaAs/AlGaAs MQW using time-resolved polarization absorption measurement. We obtained a fast decay of spin-up carriers and the corresponding fast accumulation of spin-down carriers with the time constant of 32 ps at room temperature. The relaxation processes show clear symmetrical behavior in time dependence, as expected from simple rate equations. Finally, we characterize InGaAs/InAlAs resonant tunneling barrier (RTB) diodes using electro-optic sampling. The switching time from peak to valley is decreased with the reduction of the InAlAs barrier thickness. A new equivalent circuit model of RTB diodes, which includes the quantum mechanical state lifetime phenomenologically, describes the switching behavior fairly well.

## CONTENTS

<b>CHAPTER 1 Introduction</b>	<b>1</b>
 <b>CHAPTER 2 Fast Recovery of Excitonic Absorption Bleaching in Tunneling Bi-Quantum Well Structures</b>	 <b>9</b>
2.1 Introduction	9
2.2 Proposal of Tunneling Bi-Quantum Well structures	9
2.3 Time resolved absorption measurement	11
2.3.1 Sample structures	11
2.3.2 Measurement system	13
2.3.3 Relation between absorption bleaching and carrier density	15
2.3.4 Verification of fast absorption recovery in Tunneling Bi-Quantum well	16
2.4 Discussion	18
2.5 Summary	24
 <b>CHAPTER 3 Time Evolution of Excitonic Absorption Bleaching in Resonant Tunneling Bi-Quantum-well Structures</b>	 <b>28</b>
3.1 Introduction	28
3.2 Experiment and Discussion	29
3.2.1 Sample structures and Absorption spectra	29
3.2.2 Time resolved absorption measurement	30
3.2.3 Comparison with e2-hh2 excitonic absorption change in MQW	34
3.3 Summary	37

<b>CHAPTER 4 Time Resolved Studies of Excitonic Absorption Bleaching in Type-II GaAs/AlGaAs/AlAs Tunneling Bi-Quantum well</b>	<b>39</b>
4.1 Introduction	39
4.2 Experiment	42
4.2.1 Sample structures	42
4.2.2 Time resolved absorption measurement	44
4.3 Discussion	48
4.4 Summary	50
 <b>CHAPTER 5 Picosecond Excitonic Absorption Recovery of 100-nm GaAs/AlGaAs Narrow Multiple-Quantum-Well wires</b>	 <b>54</b>
5.1 Introduction	54
5.2 Experiment	56
5.2.1 Sample structures and Fabrication process	56
5.2.2 Absorption spectra of MQW wires	58
5.2.3 Time resolved absorption measurement	60
5.3 Discussion	63
5.4 Summary	65
 <b>CHAPTER 6 Direct Observation of Picosecond Spin Relaxation of Excitons in GaAs/AlGaAs Quantum Wells using Spin-dependent Optical Nonlinearity</b>	 <b>67</b>
6.1 Introduction	67
6.2 Rate equations of spin relaxation	67
6.3 Experiment	71
6.4 Discussion	76
6.5 Summary	79

<b>CHAPTER 7 Picosecond Characterization of InGaAs/InAlAs Resonant Tunneling Barrier Diode by Electro-Optic Sampling</b>	<b>82</b>
7.1 Introduction	82
7.2 Experiment	83
7.2.1 Sample structures of RTB diodes	83
7.2.2 Electro-optic sampling of RTB diodes	85
7.3 Discussion	88
7.4 Summary	94
 <b>CHAPTER 8 Conclusions</b>	 <b>98</b>
 <b>Acknowledgements</b>	 <b>101</b>
 <b>Publications and Presentations</b>	 <b>102</b>
 <b>Personal History</b>	 <b>106</b>



## CHAPTER 1

### Introduction

Recent progress of semiconductor device is outstanding in two respects: improvements in switching speed and the discovery of new properties. Present devices have switching speeds in excess of 10 ps and new properties such as room temperature excitons in quantum wells and negative differential resistance in tunneling barrier structures. These new properties are related to quantum confinement effects. Previously, the confinement effect was not easily observed in semiconductor structures. However, because of nanostructure fabrication technology, that effect has become easily observable and applicable. Today, an understanding of ultrafast phenomena related to quantum effects governing device operation is very important for further development. In this thesis, we investigate ultrafast phenomena related to quantum wells and superlattices.

Quantum wells and superlattices were introduced in 1970 by Esaki et al.<sup>1)</sup> They showed the possibility that Bloch oscillation would occur in the superlattice under an electric bias. The report stimulated many researcher to study the fine layered structures. In the 1970s, Dingle et al. studied the optical properties of quantum wells and demonstrated that quantum confinements of carriers show new properties.<sup>2)</sup> The development of the epitaxial growth techniques such as molecular beam epitaxy (MBE) and metal-organic chemical vapor deposition (MOCVD) was indispensable to the fabrication of fine layered structures. In the 1980s, these structures appeared in applications such as high electron mobility transistor (HEMT),<sup>3)</sup> resonant hot electron transistor (RHET),<sup>4)</sup> and quantum well lasers.<sup>5,6,7)</sup>

Currently, we are interested in two properties for the application of such structures. One is the enlarged optical nonlinearity at the excitonic absorption peak in quantum wells. The photo-excitation of the excitons in semiconductor such as GaAs causes large absorption bleaching with a time constant shorter than 1 ps<sup>8)</sup> (Fig.1-1). This allows one light to control another light, which means all-optical operation, due to the change in the optical constant of the nonlinear optical material. In 1979, Gibbs et al. showed an all-optical bi-stability using the GaAs etalon at low temperature.<sup>9)</sup> In quantum wells, excitons exist even at room temperature and show a larger excitonic bleaching than semiconductor bulk. The magnitude of the absorption bleaching in GaAs/AlAs quantum wells is three times larger than that of bulk GaAs for the same pumped carrier density.<sup>10)</sup> In 1985, at room temperature, 1-ps all-optical switching was done using the

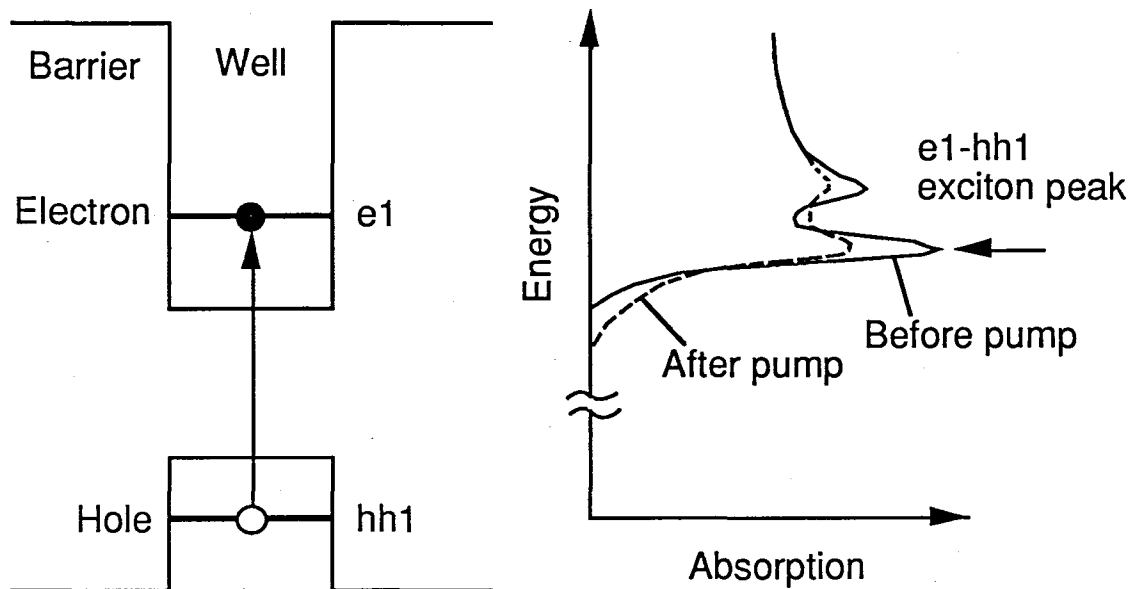


Fig. 1-1. Excitonic absorption bleaching in quantum well.

GaAs/AlGaAs quantum well etalon.<sup>11)</sup> A serious problem of this phenomenon, however, is the slow recovery of optical properties such as absorption. The typical recovery time of excitonic absorption after its bleaching in a GaAs/AlGaAs MQW is 30 ns at 300 K.<sup>12)</sup> This is determined mainly by the radiative recombination of carriers which limits the time response of devices using excitonic optical nonlinearity. The recovery time can be reduced by surface recombination,<sup>13,14)</sup> proton-bombardment,<sup>15)</sup> or ac Stark effect.<sup>16)</sup> The ac Stark effect is fast but is known to be inefficient in changing optical properties. The other methods have shown no ultrafast recovery on the order of a picosecond.

The other interesting property is a tunneling effect in superlattices such as resonant tunneling barrier (RTB) diodes.<sup>17)</sup> The RTB consists of a quantum well surrounded by two barriers as shown in Fig. 1-2. In this structure, a negative differential resistance (NDR) occurs under an electric bias. The applications of resonant tunneling use the switching over its NDR region to do a new logic operation. There is a new aspect about the switching process, since it is not governed by electric factors such as RC time constant alone. The new factor is a quantum-mechanical state-lifetime,<sup>4-6)</sup>  $\tau_s$  ( $= \hbar / \Delta E_{FWHM}$ , where  $\Delta E_{FWHM}$  is the full energy width at half maximum of tunneling probability), of carriers in the RTB diode's quantum well. The carriers confined in the well need a finite time for escape using tunneling. Usually the statelifetime is equal or faster than picoseconds. This made the analysis of the tunneling phenomena difficult.

To study these ultrafast phenomena, we used pump-probe measurement (Fig.1-3). In this procedure, after the pump pulses excite

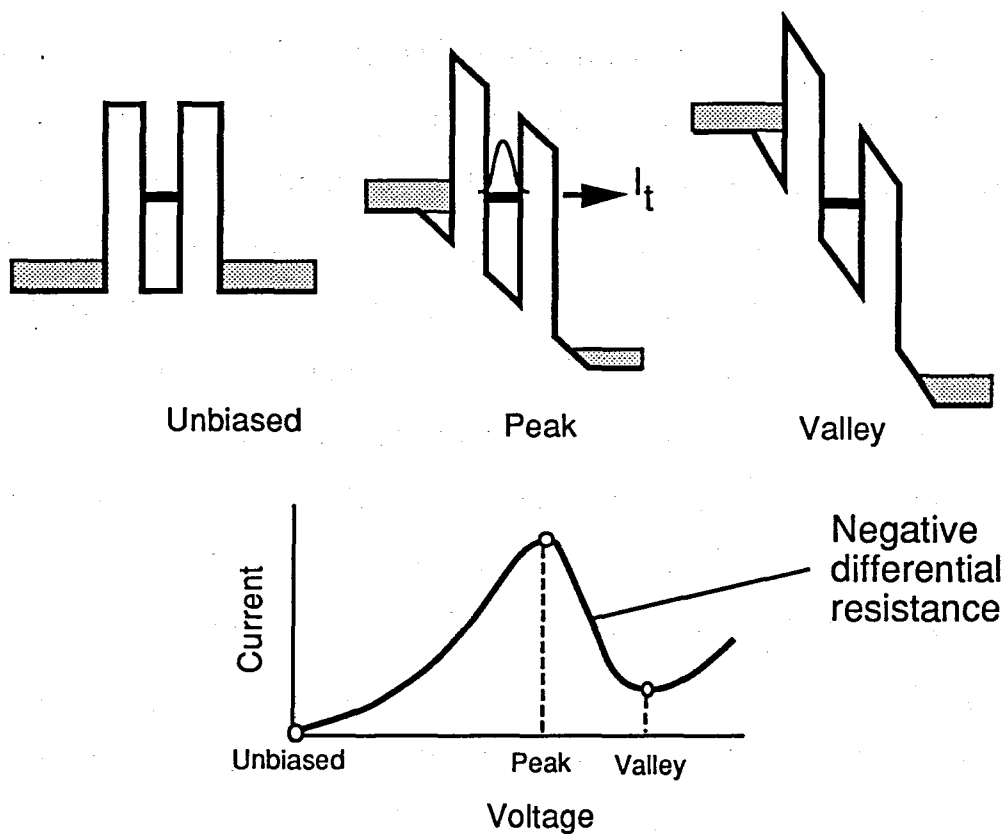


Fig. 1-2. Resonant tunneling barrier structure.

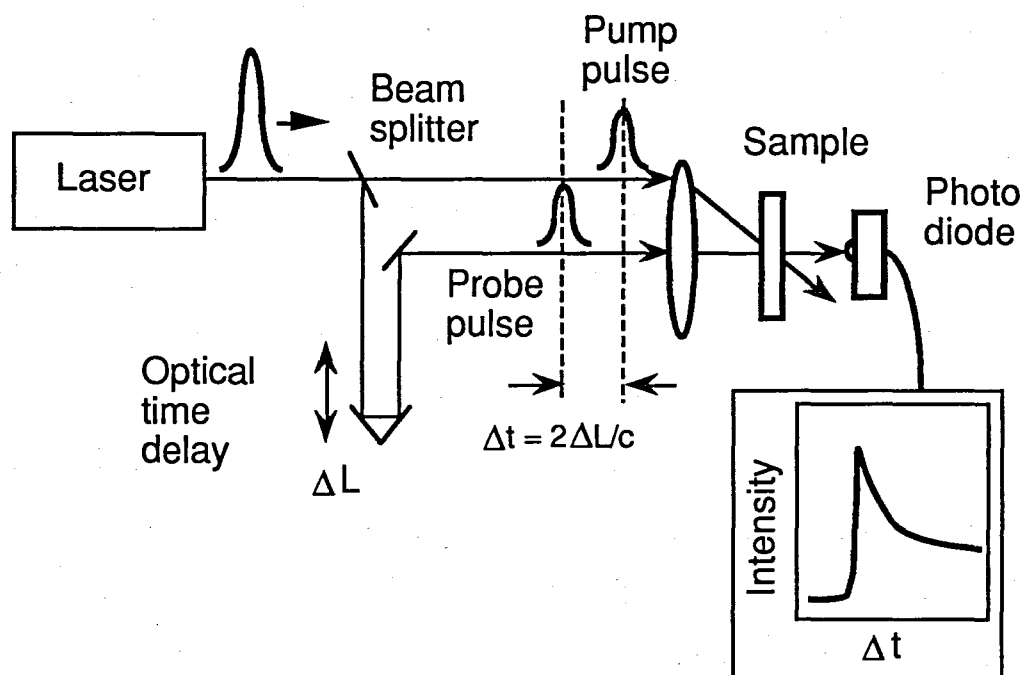


Fig. 1-3. Pump-probe time resolved measurement system.

the samples, the other pulses probe the changes in sample properties. Since the time delay between the pump and probe pulses is caused by changing optical path length, the measurement's time-resolution is mainly determined by optical pulse width independent of laser pulse jitter. The typical time resolution of our measurement system is 1-2 ps, which is equal to the optical pulse width.

The thesis focuses on picosecond phenomena related to the excitonic absorption bleaching in quantum wells and the tunneling phenomena in superlattices. In particular, fast recovery of excitonic absorption after its bleaching in quantum wells is our main concern for the all-optical device application. This study shows that the recovery time can be reduced to the picosecond region, by using various structures with tunneling or rapid combination channels.

In chapter 2, we describe the proposal of the tunneling bi-quantum well (TBQ) structure and the verification of the fast recovery of excitonic absorption after its bleaching in TBQs. The TBQ consists of narrow and wide wells, where the tunneling effect is used to realize fast absorption recovery. Chapter 3 concerns the absorption recovery of the resonant TBQs and Chapter 4 examines type-II TBQs. Carriers are transported in the resonant TBQ by resonant tunneling faster than by non-resonant process. The type-II TBQ consists of GaAs wells, AlGaAs barriers, and AlAs layers, which show no significant optical absorption below the energy gap of the GaAs wells. Chapter 5 describes picosecond absorption recovery of the multiple quantum well wires fabricated using FIB lithography. Photo-excited carriers in MQW wires diffuse toward side walls and recombine on the side wall surfaces with picoseconds lifetimes. Chapter 6 shows direct

observation of spin relaxation in MQW. Spin relaxation process at room temperature was observed using spin-dependent optical nonlinearity. Chapter 7 uses electro-optic sampling to characterize the resonant tunneling barrier diode. A new equivalent circuit model including quantum effect is proposed. Finally Chapter 8 concludes the thesis.



## REFERENCES

- 1) L. Esaki and R. Tsu: IBM J. Res. Dev., 14 (1970) 61.
- 2) R. Dingle, Festkörperprobleme, ed. H. J. Queisser vol. XV, p. 21, (Pergamon, 1975).
- 3) T. Mimura, S. Hiyamizu, T. Fujii, and K. Nanbu: Jpn. J. Appl. Phys., 19 (1980) L225.
- 4) N. Yokoyama, K. Imamura, S. Muto, S. Hiyamizu and H. Nishi: Jpn. J. Appl. Phys., 24, L853 (1985).
- 5) J. P. van der Ziel, R. Dingle, R. C. Miller, W. Wiegmann, and W. A. Nordland Jr.: Appl. Phys. Lett., 26 (1975) 463.
- 6) N. Holonyak, Jr., R. M. Kolbas, R. D. Dupuis, and P. D. Dapkus: IEEE J. QE. (1980) 170.
- 7) W. T. Tsang: Appl. Phys. Lett., 39 (1981) 786.
- 8) W. H. Knox, R. L. Fork, M. C. Downer, D. A. B. Miller, D. S. Chemla, C. V. Shank, A. C. Gossard, and W. Wiegmann: Phys. Rev. Lett. 54, 1306 (1985).
- 9) H. M. Gibbs, S. L. McCall, T. N. C. Venkatesan, A. C. Gossard, A. Passner and W. Wiegmann: Appl. Phys. Lett. 35 (1979) 451.
- 10) S. H. Park, J. F. Morhange, A. D. Jeffery, R. A. Morgan, A. Chavez-Pirson, H. M. Gibbs, S. W. Koch, N. Peyghambarian, M. Derstine, A. C. Gossard, J. H. English, and W. Weigmann: Appl. Phys. Lett. 52, 1201 (1988).
- 11) A. Migus, A. Antonetti, D. Hulin, A. Mysyrowicz, H. M. Gibbs, N. Peyghambarian and J. L. Jewell: Appl. Phys. Lett. 46 (1985) 70.
- 12) D. S. Chemla, D. A. B. Miller, P. W. Smith, A. C. Gossard, and W. Wiegmann: IEEE J. Quantum Electron. QE-20, 265 (1984).
- 13) Y. H. Lee, H. M. Gibbs, J. L. Jewell, J. F. Duffy, T. Venkatesan, A. C. Gossard, W. Wiegmann, and J. H. English: Appl. Phys. Lett. 49, 486 (1986).

- 14) J. L. Jewell, A. Scherer, S. L. McCall, A. C. Gossard, and J. H. English: Appl. Phys. Lett. 51, 94 (1987).
- 15) Y. Silberberg, P. W. Smith, D. A. B. Miller, B. Tell, A. C. Gossard, and W. Wiegmann: Appl. Phys. Lett. 46, 701 (1985).
- 16) A. Von Lehmen, D. S. Chemla, J. E. Zucker and J. P. Heritage: Opt. Lett. 11, 609 (1986).
- 17) R. Tsu, and L. Esaki: Appl. Phys. Lett. , 22 (1973) 562.
- 18) B. Ricco and M. Ya. Azbel: Phys. Rev. B29, 1970 (1984).
- 19) H. C. Liu and D. D. Coon: Appl. Phys. Lett. 50, 1246 (1987).
- 20) T. C. L. G. Sollner, E. R. Brown, W. D. Goodhue and H. Q. Le: Appl. Phys. Lett. 50 (1987) 332.

## CHAPTER 2

# Fast Recovery of Excitonic Absorption Bleaching in Tunneling Bi-Quantum-Well Structures

## 2.1 Introduction

The optical nonlinearity of excitons in multiple quantum wells (MQWs) is currently attracting wide interest with regard to possible applications in optical switching and computing.<sup>1,2)</sup> Nonlinear absorption and refraction changes occur in these structures with a time constant shorter than 1 ps due to the photoexcitation of exciton peak.<sup>3)</sup> However, the slow recovery of optical properties such as absorption is a serious problem (Fig. 2-1). The typical recovery time of excitonic absorption after its bleaching in a GaAs/AlGaAs MQW is 30 ns at 300 K.<sup>4)</sup> This is determined mainly by the radiative recombination of carriers which limits the time response of devices using excitonic optical nonlinearity. The recovery time can be reduced by surface recombination,<sup>5,6)</sup> proton-bombardment,<sup>7)</sup> or ac Stark effect.<sup>8)</sup> The ac Stark effect is fast but is known to be inefficient in changing optical properties. The other methods have shown no ultrafast recovery on the order of a picosecond.

## 2.2 Proposal of Tunneling Bi-quantum Well structures

To reduce recovery time without sacrificing efficiency, we proposed a superlattice structure using carrier tunneling, which we call a tunneling bi-quantum-well (TBQ).<sup>9)</sup> The TBQ consists of a series of narrow and wide wells as shown in Fig. 2-2. In this structure, we make use of the optical nonlinearity at the exciton level in the narrow well.

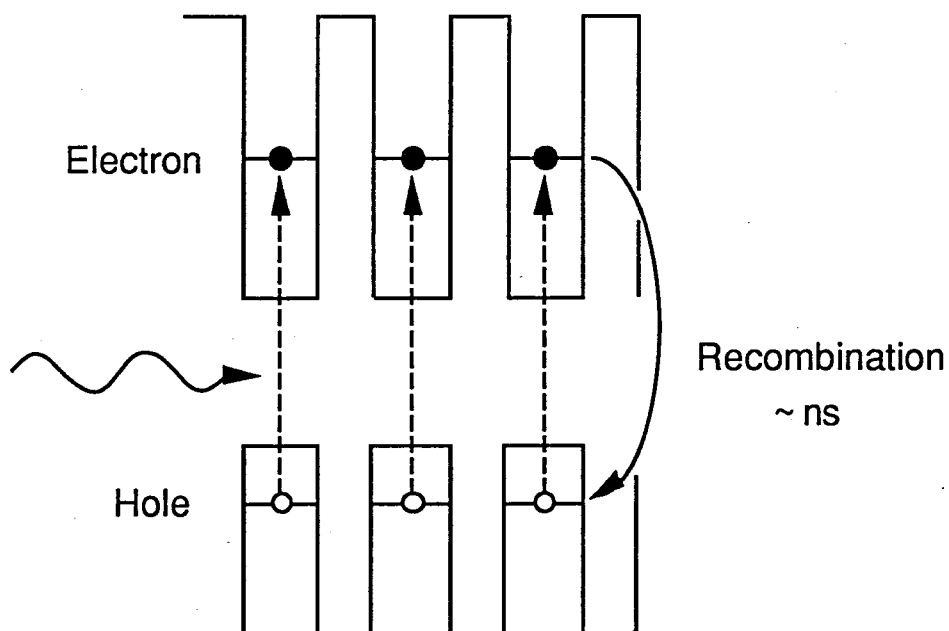


Fig. 2-1. Slow carrier recombination in MQW. The typical recovery time from excitonic absorption bleaching in a GaAs/AlGaAs MQW is on the order of nanoseconds.

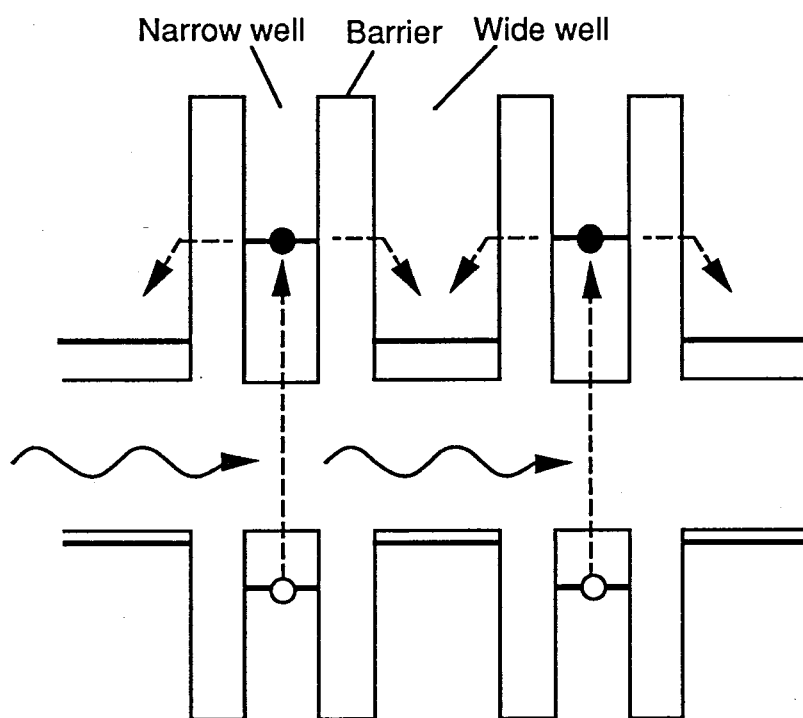


Fig. 2-2. Energy band diagram of TBQ structures. Photoexcited carriers in narrow wells escape toward wide wells by tunneling.

Since the energy level structure in the narrow and wide wells differ, photoexcited carriers in the narrow wells can escape toward the wide wells by tunneling and relax into their lowest energy level. This process recovers the optical constants of the excited narrow well much faster than radiative recombination. It is possible to control the recovery time by changing tunneling time.

## **2.3 Time resolved absorption measurement**

### **2.3.1 Sample structures**

The TBQ structures we studied consist of 50 periods of narrow GaAs quantum wells 4.5 nm thick and wide quantum wells 9.0 nm thick. We varied the thickness of  $\text{Al}_{0.51}\text{Ga}_{0.49}\text{As}$  barriers,  $L_B$ , from 5.1 nm (18 MLs) to 1.7 nm (6 MLs) to study the dependence of recovery time on barrier thickness. All structures were grown on a semi-insulating (100) GaAs substrate by molecular beam epitaxy. After the growth, the substrate was removed by selective etching over a part of the sample.

Figure 2-3 shows the absorption spectra of TBQ structures at room temperature. Absorption peaks near 840 nm show the lowest electron-heavy-hole and electron-light-hole excitons in the wide wells. Absorption peaks near 790 nm show the lowest electron-heavy-hole excitons in the narrow wells. Note the reduction of the oscillator strength of excitons compared with that of the continuum as the barriers become thinner. The reduced excitonic oscillator strength is attributed to the reduced confinement of excitons in the wells. Another notable feature is the energy shift of the excitonic absorption peak in

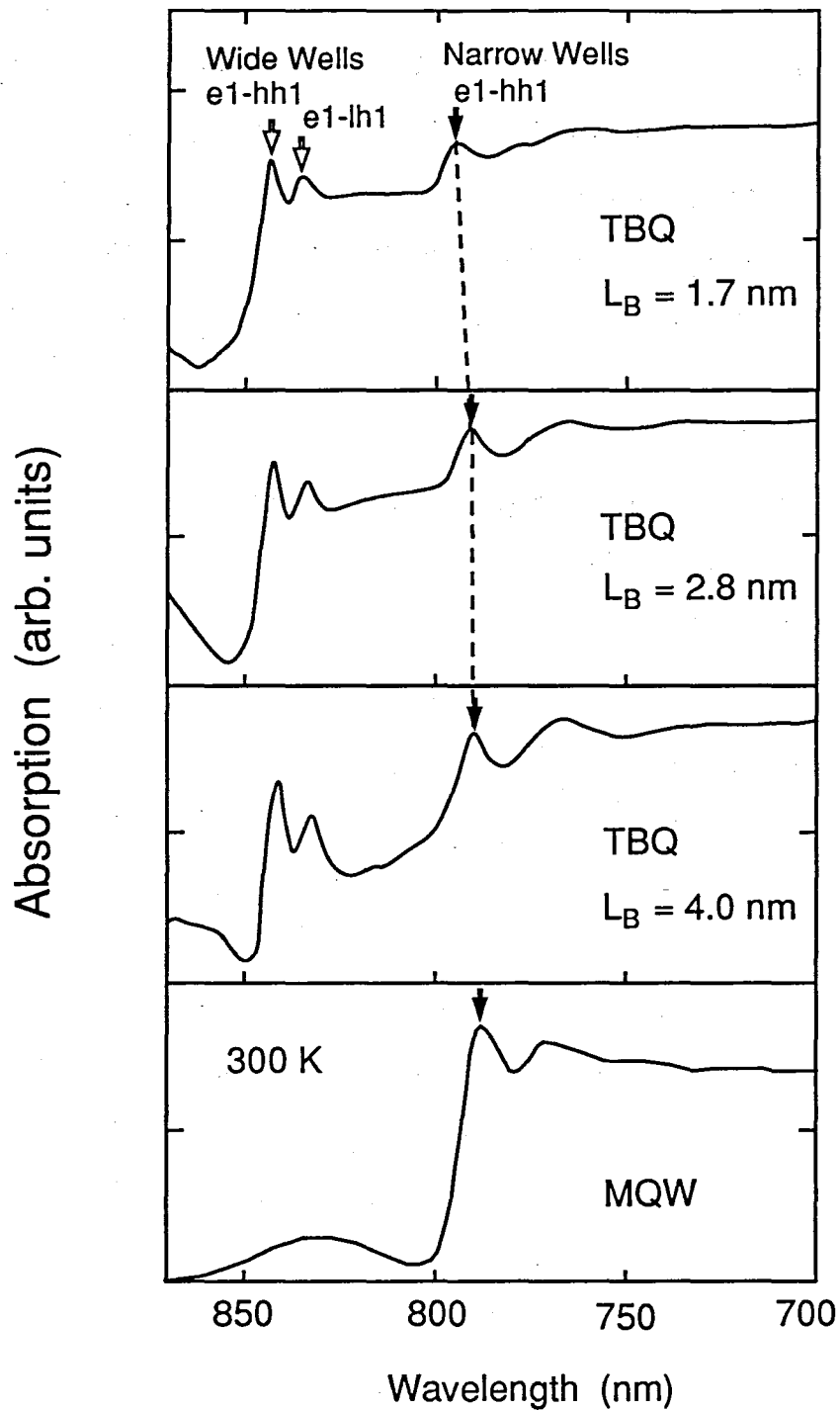


Fig. 2-3. Absorption spectra of TBQs and MQW. Absorption peaks near 840 nm show the lowest electron-heavy-hole and electron-light-hole excitons in the wide wells. Absorption peaks near 790 nm show the lowest electron-heavy-hole excitons in the narrow wells.



the narrow wells. The electron-heavy-hole exciton peaks shift from 789 nm to 794 nm as the barrier thickness decreases from 5.1 nm to 1.7 nm. This energy shift also comes from the reduced confinement of excitons. Masselink et al. observed a similar reduction of exciton oscillator strengths and the similar red shift of the excitonic absorption peaks with the reduced barrier thickness in conventional MQWs.<sup>10)</sup>

### 2.3.2 Measurement system

We made time-resolved pump-probe absorption measurements (Fig.2-4), which is a kind of sampling measurements. In the pump probe absorption measurement, we use a beamsplitter to divide optical pulses to the pump and probe pulses. If the optical path length of the pump beam and that of the probe beam are equal, the both pulses arrive at the sample just on the same time. By changing the optical path length, we generate the time difference between the pump and the probe pulses. Since this measurement is not affected by the optical pulse's jitter, the time resolution of the measurements system is determined mainly by the width of the optical pulses. As for the optical pulse source, we used a tunable mode-locked styryl dye laser synchronously pumped by compressed YAG (yttrium aluminum garnet) laser pulses. The optical tunability of the laser is important for the accurate excitation of the excitonic absorption peaks. The dye laser generates optical pulses of 1 ps duration at 12 ns intervals between 780 nm and 830 nm. In these experiments, we used the lock-in amplification with an electro-optic modulator of 6 MHz chopping. Dye lasers make a larger noise in kHz than in MHz region. The optical

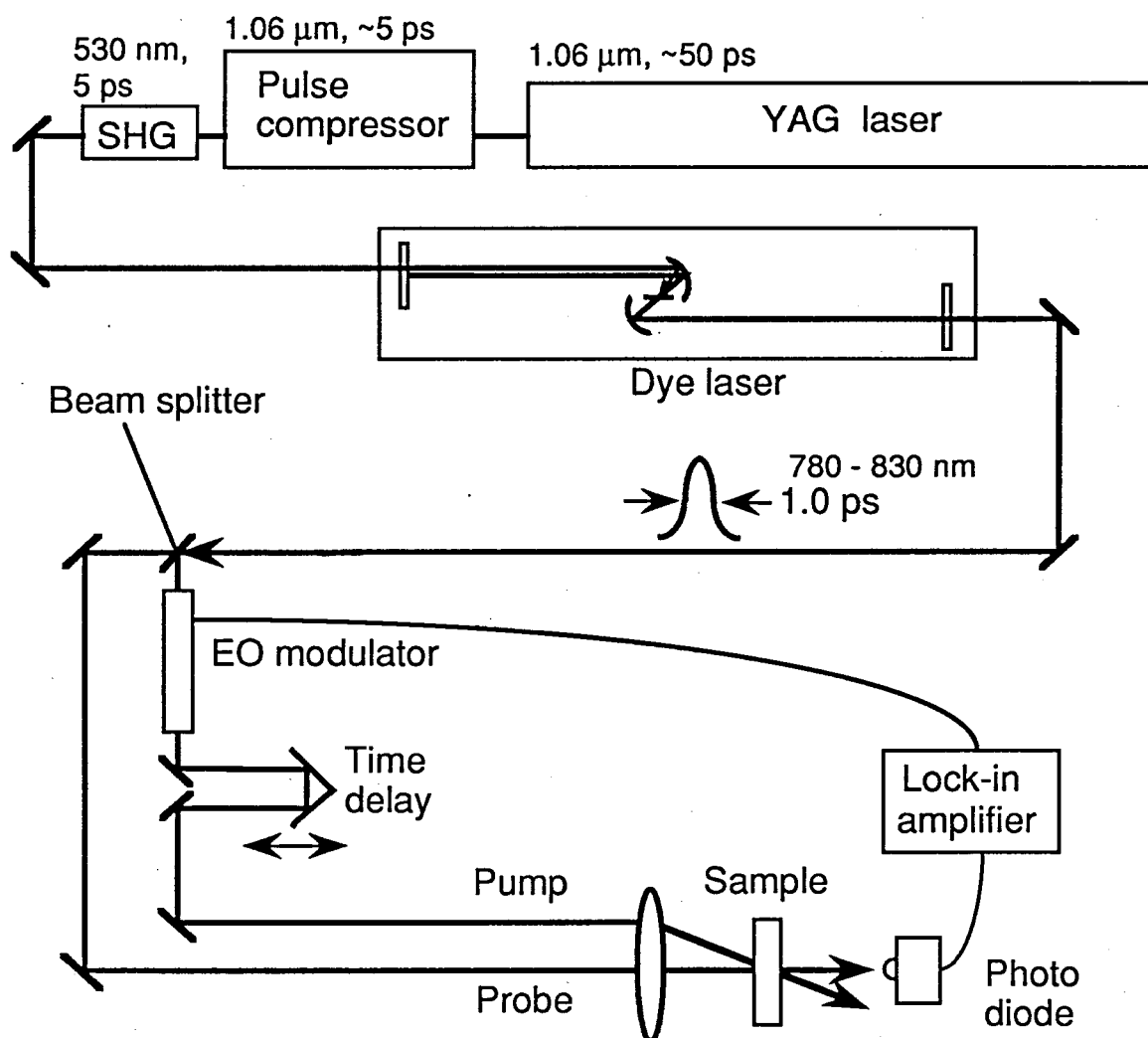


Fig. 2-4. Time resolved absorption measurement system. The tunable mode-locked styryl dye laser was synchronously pumped by compressed YAG laser pulses. The dye laser generates optical pulses of 1 ps duration at 12 ns intervals between 780 nm and 830 nm. We used the lock-in amplification with an electro-optic modulator of 6 MHz chopping. The optical delay of 660 ps stroke is moved by a stepping motor.

delay of 660 ps stroke was moved by a stepping motor. The pump beam was focused on a 15- $\mu\text{m}$ -diameter spot and its intensity was 0.5 mW in front of the sample. The density of photoexcited electrons per well is calculated to be low ( $\sim 2 \times 10^{10} \text{ cm}^{-2}$ ). To see the time dependence of the optical response of the system, we measured optical absorption.

### 2.3.3 Relation between absorption bleaching and carrier density

Absorption bleaching in quantum wells comes from phase-space filling and exchange effect.<sup>12,13)</sup> Both effects are the consequences of the Pauli exclusion principle. In the small signal regime,<sup>4)</sup> the relation between the carrier density,  $N$ , and the absorption coefficient,  $\alpha(N)$ , is written as

$$\alpha(N) = \frac{\alpha_0}{1 + \frac{N}{N_s}}, \quad (2-1)$$

where  $\alpha_0$  is the initial absorption coefficient. The saturation intensity,  $N_s$ , is about  $1 \times 10^{12} \text{ cm}^{-2}$  in the 100-Å-thick GaAs quantum wells.<sup>4,14)</sup> Since the carrier density in our experiment is sufficiently low ( $\sim 2 \times 10^{10} \text{ cm}^{-2}$ ), the relation becomes

$$\alpha(N) = \alpha_0 \left( 1 - \frac{N}{N_s} \right). \quad (2-2)$$

The absorption change,  $\Delta\alpha = \alpha(N) - \alpha_0$ , is proportional to the carrier

density,  $N$ , in the region of small  $N$ .

#### **2.3.4 Verification of fast absorption recovery in Tunneling Bi-Quantum well<sup>11)</sup>**

Figure 2-5 shows the observed time dependence of transmission at the lowest heavy-hole exciton peak in the narrow wells. After photoexcitation, the conventional MQW with 50 periods of 4.5-nm-thick GaAs wells and 4.0-nm-thick  $\text{Al}_{0.51}\text{Ga}_{0.49}\text{As}$  barriers does not show a clear absorption recovery in this time region. In contrast, TBQs show much faster recovery times of 16 ps for 4.0-nm-thick barriers and 6 ps for 2.8-nm-thick barriers. Note that the recovery time of the TBQ is remarkably reduced as barriers become thin.

The absorption change of TBQ with 4.0-nm barriers was about 50% that of conventional MQW for the same pumping power,<sup>9)</sup> indicating that the efficiency of TBQ is comparable to that of MQW under the resonant excitation. This is contrasted with the very low efficiency of ac Stark effect. The transmission change of ac Stark effect is more than one order of magnitude smaller than that of the resonant excitation if we detune more than 36 meV to avoid real excitation by longitudinal optical (LO) phonon absorption.<sup>8)</sup> In Fig. 2-5, we also notice the slow recovery tail after the fast relaxation. These tails have a time constant slower than 1 ns and have a magnitude of 40 to 50% of the initial absorption change. Since calculated tunneling times for holes are about three to six orders of magnitude slower than that of electrons, the slow recovery tail can be attributed to the free holes remaining in the narrow wells.

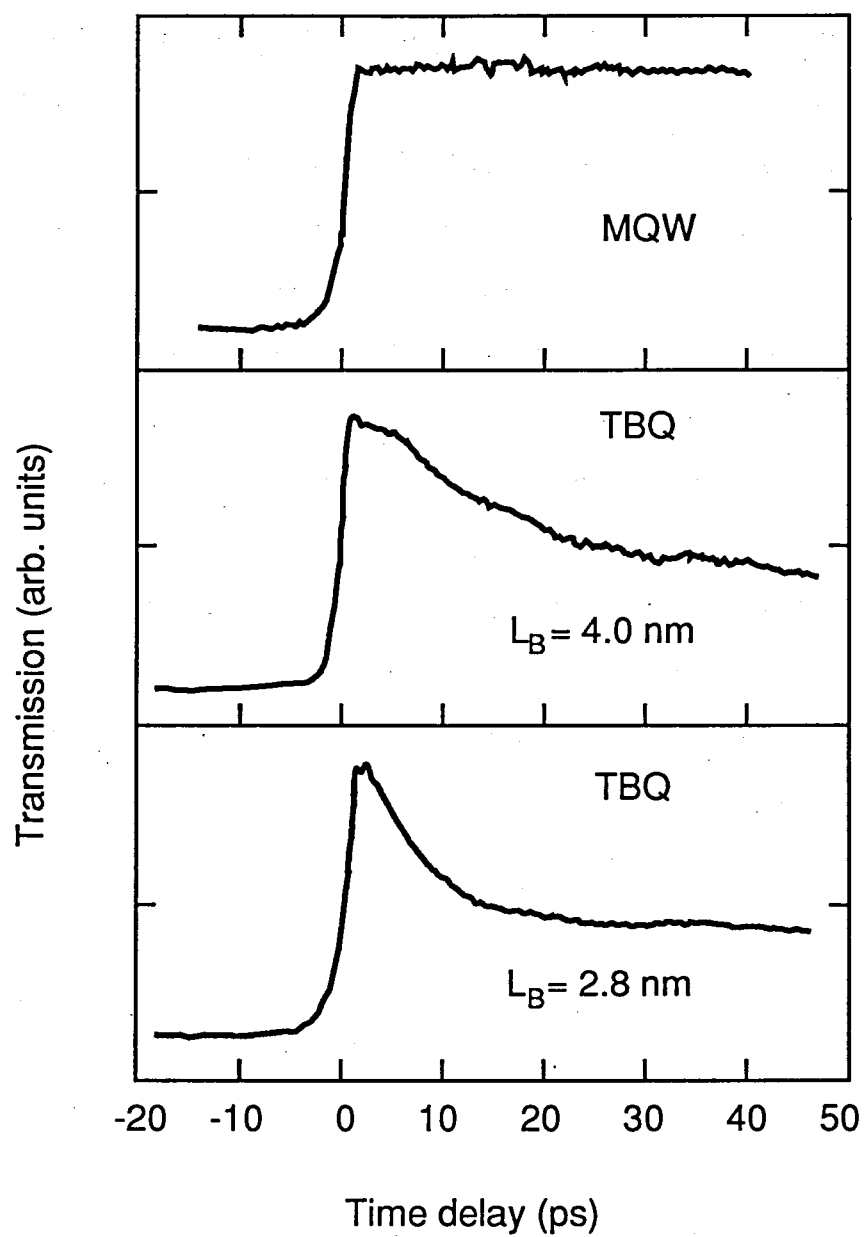


Fig. 2-5. Time resolved absorption change in MQW and TBQs.

For 1.7-nm-thick barriers, we observed a much faster relaxation, 1 ps, as shown in Fig. 2-6. The relative magnitude of the initial absorption change compared with the slow recovery tail is smaller than that of TBQs with larger barrier thicknesses. This reduced peak transmission change occurs because the relaxation time becomes comparable to the optical pulse duration of 1 ps. It was confirmed by taking a numerical convolution of a decay curve and the optical pulse actually measured by an auto-correlator. For the decay curve, we assumed 1-ps exponential recovery with 60% magnitude (due to electrons) and much slower exponential recovery ( $> 1$  ns) with 40% magnitude (due to holes). The simulated curve (dashed curve in Fig. 2-6) agrees well with the experimental result (solid line in Fig. 2-6). To observe the initial absorption relaxation of 1 ps without simulation, much shorter optical pulses (about 0.1 ps) are needed. Note that the 1-ps recovery time is three orders of magnitude faster than the few nanoseconds recovery of the conventional MQW. This is also the fastest tunneling processes ever observed, to our knowledge.

## 2.4 Discussion

The semilogarithmic plot of the experimental recovery time as a function of barrier thickness is shown by solid circles in Fig. 2-7. The dashed line indicates the calculated lifetime of electrons at the lowest quantum level of the narrow well, given that the wide well is infinitely wide.<sup>9,15)</sup> This is, in other words, the state-lifetime of the virtual state of resonant tunneling barrier structures. The rough proportionality between the observed recovery time and calculated lifetime shows that



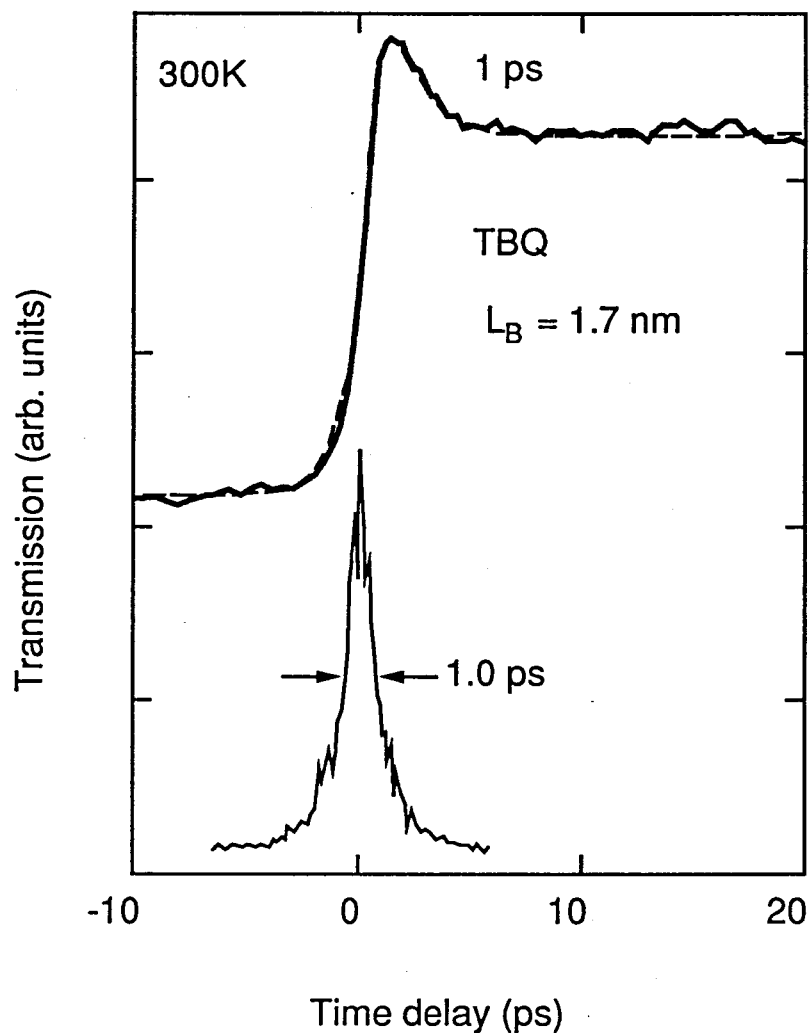


Fig. 2-6. Time-resolved absorption change of the excitonic absorption peak for TBQ with 1.7-nm-thick barriers and auto-correlation of optical pulses of 1 ps (assumed  $\text{sech}^2(1.76 t/\Delta t)$  pulse shape;  $\Delta t$ , pulse width) duration. The dashed line shows the result of convolution (see text).

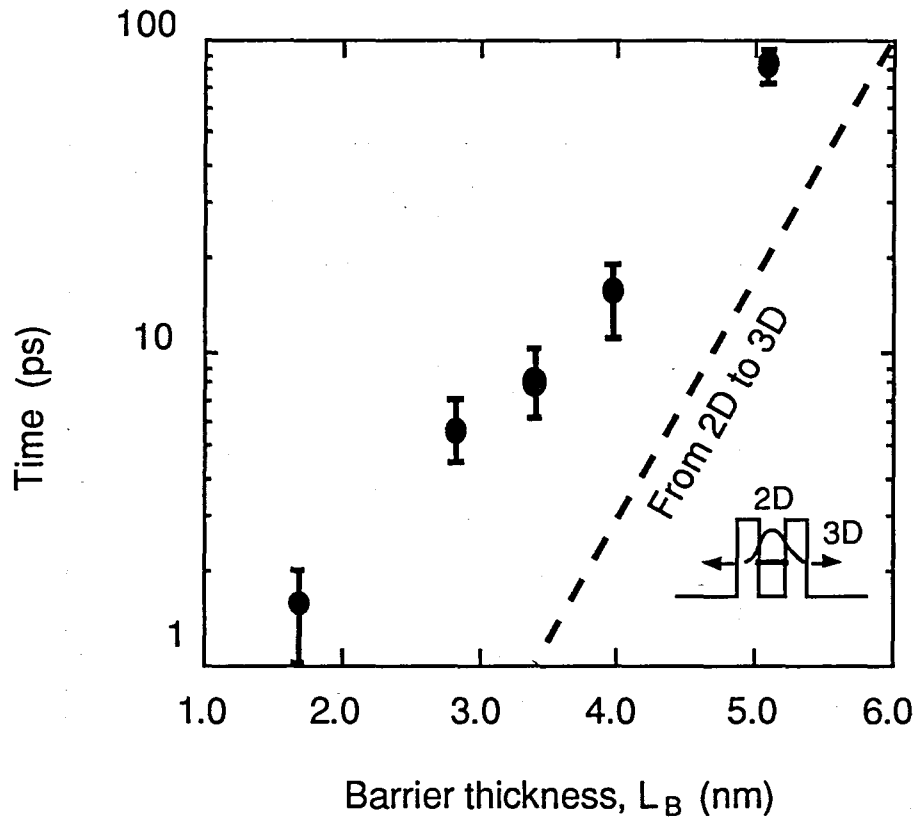


Fig. 2-7. The dependence of recovery time on barrier thickness. The dashed line indicates the calculated lifetime of electrons at the lowest quantum level of the narrow well, given that the wide well is infinitely wide. This is, in other words, the state-lifetime of the virtual state of resonant tunneling barrier structures.

absorption recovery is governed mainly by tunneling. This result also indicates the high controllability of the relaxation time using tunneling. We expect that the TBQ with barriers less than 1.7 nm thick will have a subpicosecond recovery time.

In the TBQ, the relaxation of electrons from the lowest energy level in the narrow well to that of the wide well is a kind of inter-subband relaxation,<sup>16)</sup> because these levels, if they are arranged in a

periodic sequence, form superlattice minibands extending over narrow and wide wells. Also, because the energy difference between the lowest energy levels in the narrow wells and that in the wide wells is greater than 36 meV, relaxation with LO-phonon emission is regarded to be the main relaxation process.<sup>16,17)</sup> To confirm the dominant scattering mechanism, we calculated the tunneling time including LO phonon emission. We used the formalism given by Price<sup>18)</sup> to calculate the scattering rate of two-dimensional (2D) electron gas by generalizing it to treat a superlattice.

In the calculation,<sup>19)</sup> we used some simple assumptions: For electrons, we used the effective mass of  $m^*(x) = (0.067 + 0.083x) \cdot m_0$  for both  $x = 0$  and  $x = 0.51$ . The nonparabolic correction was treated by  $k \cdot p$  perturbation to express the mass reduction of tunneling electrons. For LO phonons, we assumed bulk GaAs phonon modes and neglected complexities coming from the superlattice. We also assumed the Frölich interaction between an electron and a LO phonon. The tunneling time by the LO phonon emission (LOE) or absorption (LOA) is expressed as

$$\frac{1}{\tau_{\text{LOE}}} = \frac{m^* e^2 \hbar \omega_{\text{LO}}}{8\pi^2 \hbar^3 \epsilon_0} \left( \frac{1}{\kappa_\infty} - \frac{1}{\kappa_0} \right) (N_q + 1) \times \int_0^{2\pi} d\theta \int_{-\infty}^{+\infty} \frac{|I(q_z, k_z)|^2}{q_-^2 + q_z^2} dq_z, \quad (2-3)$$

$$\frac{1}{\tau_{LOA}} = \frac{m^* e^2 \hbar \omega_{LO}}{8\pi^2 \hbar^3 \epsilon_0} \left( \frac{1}{\kappa_\infty} - \frac{1}{\kappa_0} \right) N_q$$

$$\times \int_0^{2\pi} d\theta \int_{-\infty}^{+\infty} \frac{|I(q_z, k_z)|^2}{q_+^2 + q_z^2} dq_z, \quad (2-4)$$

$$I(q_z, k_z) \equiv \int_0^{L_z} \psi_{0, k_z - q_z}^*(z) \exp(ik_z z) \psi_{1, k_z}(z) dz, \quad (2-5)$$

$$q_\pm^2 \equiv k_\pm^2 + k^2 - 2 k_\pm k \cos\theta, \quad (2-6)$$

$$\frac{\hbar^2 k_\pm^2}{2m^*} \pm \hbar \omega_{LO} + E_0 = \frac{\hbar^2 k^2}{2m^*} + E_1 \quad (2-7)$$

Here,  $E_1$  ( $E_0$ ) is the energy minimum of superlattice miniband M1 (M0) whose electron envelope function is localized in the narrow (wide) well;  $k_z$  and  $k$  are perpendicular and parallel (to the interface) wave vectors of an electron in the miniband, M1; and  $\psi_{1, k_z}(z)$  [ $\psi_{0, k_z - q_z}(z)$ ] is the corresponding envelope function, normalized in superlattice period,  $L_s$ .  $N_q = 1 / [\exp(\hbar \omega_{LO} / k_B T) - 1]$  is the occupation number of LO phonons at temperature  $T$  ( $= 300K$ ). The net tunneling rate is given by averaging Eq.(2-3) or (2-4) over a Fermi-Dirac distribution of electrons at 300 K.

Similarly we calculated the tunneling times for deformation potential (DP),

$$\frac{1}{\tau_{DP}} = \frac{\epsilon_1^2 k_B T m^*}{2\pi \hbar^3 \rho c_s^2} \int_{-\infty}^{\infty} |I(q_z, k_z)|^2 dq_z, \quad (2-8)$$

and the tunneling times for alloy scattering (AL),

$$\frac{1}{\tau_{AL}} = \frac{0.25 U_0^2 \Omega m^*}{2\pi \hbar^3} \int_{-\infty}^{\infty} |I(q_z, k_z)|^2 dq_z. \quad (2-9)$$

Here,  $\epsilon_1$ ,  $\rho$  and  $c_s$  are the deformation potential, the density and the velocity of sound, respectively.  $U_0$  is the Nordheim-Brooks' alloy potential<sup>20)</sup> and  $\Omega$  the volume of unit cell.

The calculated tunneling time is summarized in Fig. 2-8 as a function of barrier thickness,  $L_B$ . All the tunneling times vary exponentially with  $L_B$  and the line slopes don't depend on the scattering mechanisms. The dependence of the tunneling time on the barrier thickness comes from the overlap integral of the wavefunctions of the electron states for the narrow and wide wells. The difference of the scattering mechanism affects only the magnitude of the tunneling time, which results in a parallel shift in the semilogarithmic plot. Note that the LO phonon emission is by far the fastest process and shows a relatively good agreements with the experiment. We can almost neglect other scattering mechanisms. The tunneling of the present TBQ is mainly governed by the LO-phonon emission.

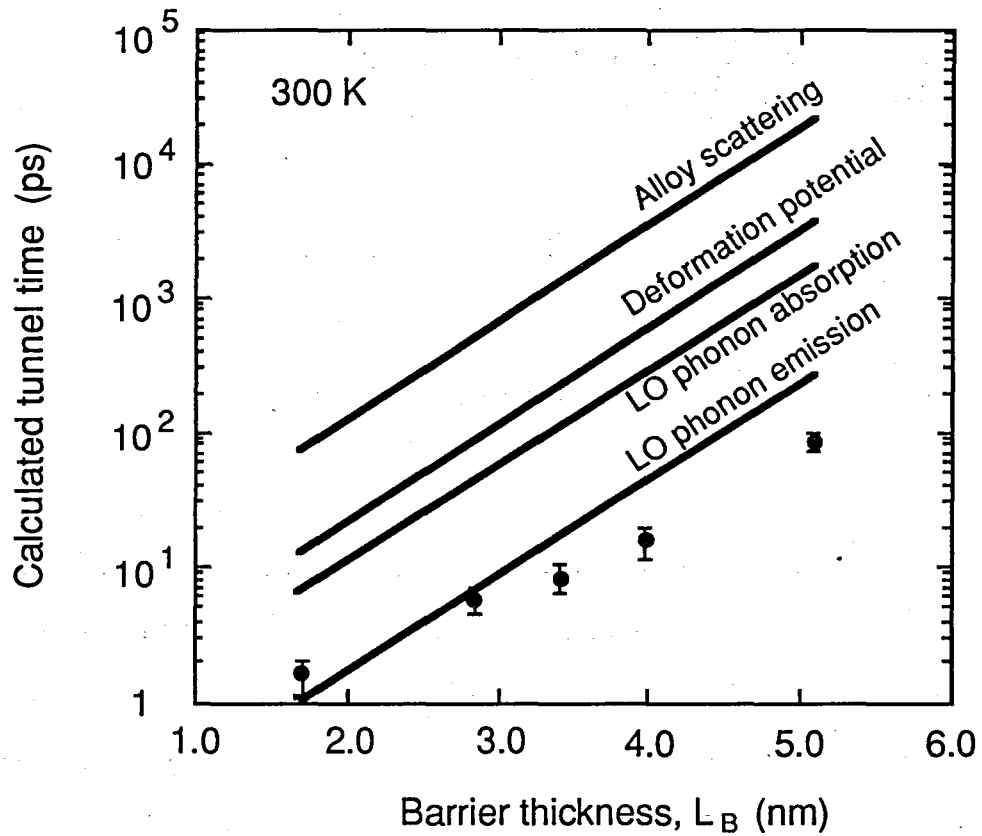


Fig. 2-8. Calculated tunneling times for various scattering mechanisms. All tunneling times vary exponentially with  $L_B$ . Experimental recovery times are also shown.

## 2.5 Summary

In conclusion, fast recovery from the excitonic absorption bleaching in TBQ structures was proposed and demonstrated. The TBQ has a new feature that conventional superlattices will never have, that is, the control of relaxation time using tunneling. With the reduction of tunneling barrier thickness down to 1.7 nm, the recovery time is reduced to as short as 1 ps. This is by three orders of magnitude shorter than the recovery time (a few nanoseconds) of conventional



MQWs. We calculated the tunneling times for various scattering mechanisms and showed that the LO phonon emission process is the fastest one. The calculated tunneling time with LO phonon emission shows a semi-quantitative agreement with experiment. The 1-ps recovery is the fastest tunneling process ever observed, to our knowledge. We believe that this result indicates the high potential of the TBQ as a breakthrough in the problem of the slow-carrier recombination in semiconductors.

## REFERENCES

- 1) H. M. Gibbs, S. S. Tarng, J. L. Jewell, D. A. Weinberger, K. Tai, A. C. Gossard, S. L. McCall, A. Passner, and W. Wiegmann: Appl. Phys. Lett. 41 (1982) 221.
- 2) A. Migus, A. Antonetti, D. Hulin, A. Mysyrowicz, H. M. Gibbs, N. Peyghambarian, and J. L. Jewell: Appl. Phys. Lett. 46 (1985) 70.
- 3) W. H. Knox, R. L. Fork, M. C. Downer, D. A. B. Miller, D. S. Chemla, C. V. Shank, A. C. Gossard, and W. Wiegmann: Phys. Rev. Lett. 54 (1985) 1306.
- 4) D. S. Chemla, D. A. B. Miller, P. W. Smith, A. C. Gossard, and W. Wiegmann: IEEE J. Quantum Electron. QE-20 (1984) 265.
- 5) Y. H. Lee, H. M. Gibbs, J. L. Jewell, J. F. Duffy, T. Venkatesan, A. C. Gossard, W. Wiegmann, and J. H. English: Appl. Phys. Lett. 49 (1986) 486.
- 6) J. L. Jewell, A. Scherer, S. L. McCall, A. C. Gossard, and J. H. English: Appl. Phys. Lett. 51 (1987) 94.
- 7) Y. Silberberg, P. W. Smith, D. A. B. Miller, B. Tell, A. C. Gossard, and W. Wiegmann: Appl. Phys. Lett. 46 (1985) 701.
- 8) A. Von Lehmen, D. S. Chemla, J. E. Zucker and J. P. Heritage: Opt. Lett. 11 (1986) 609.
- 9) A. Tackeuchi, S. Muto, T. Inata, and T. Fujii: Jpn. J. Appl. Phys. 28 (1989) L1098.
- 10) W. T. Masselink, P. J. Pearah, J. Klem, C. K. Peng, and H. Morkoç: Phys. Rev. B32 (1985) 8027.
- 11) A. Tackeuchi, S. Muto, T. Inata, and T. Fujii: Appl. Phys. Lett. 58 (1991) 1670.
- 12) S. Schmitt-Rink, D. S. Chemla, and D. A. B. Miller: Phys. Rev. B32 (1985) 6601.
- 13) W. H. Knox, C. Hirlimann, D. A. B. Miller, J. Shah, D. S. Chemla, and C. V. Shank: Phys. Rev. Lett. 56 (1986) 1191.

- 14) S. H. Park, J. F. Morhange, A. D. Jeffery, R. A. Morgan, A. Chavez-Pirson, H. M. Gibbs, S. W. Koch, N. Peyghambarian, M. Derstine, A. C. Gossard, J. H. English, and W. Weigmann: Appl. Phys. Lett. 52 (1988) 1201.
- 15) M. Tsuchiya, T. Matsusue, and H. Sakaki: Phys. Rev. Lett. 59 (1987) 2356.
- 16) N. Sawaki, R. A. Höpfel, E. Gornik, and H. Kano: Appl. Phys. Lett. 55 (1989) 1996.
- 17) A. Seilmeier, M. Worner, G. Abstreiter, G. Weimann, and W. Schlapp: Superlattices and Microstructures 5 (1989) 569.
- 18) P. J. Price: Annal. Phys. 133 (1981) 217; see also K. Hirakawa and H. Sakaki: Phys. Rev. B 12 (1986) 8291.
- 19) S. Muto, T. Inata, A. Tackeuchi, Y. Sugiyama, and T. Fujii: Appl. Phys. Lett. 58 (1991) 2393.
- 20) L. Nordheim: Ann. Phys. 9 (1931) 607.

## CHAPTER 3

# Time Evolution of Excitonic Absorption Bleaching in Resonant Tunneling Bi-Quantum-Well Structures

### 3.1 Introduction

In chapter 2, we reported a 1-ps absorption recovery in GaAs/AlGaAs TBQ structures by reducing the barrier thickness to 1.7 nm.<sup>1-3)</sup> This showed that electrons can escape from the narrow wells in the picosecond region even in nonresonant tunneling. In resonant TBQ structures, in which the ground electron level in the narrow well has the same energy as the second level in the wide well as shown in Fig. 3-1, faster absorption recovery is expected. Resonant tunneling of electrons was studied using photoluminescence measurements at low temperature,<sup>4-8)</sup> and the reduction of the tunneling time at resonance was reported. In the application of the TBQ to optical devices, information regarding optical nonlinearities such as excitonic absorption bleaching at room temperature is important. In this chapter, we describe the study about the time evolution of excitonic absorption bleaching in resonant TBQ structure at room temperature.<sup>9)</sup> In resonant TBQ structure, we have observed the reduction of the absorption recovery time and the increase of the tail-to-peak ratio of the absorption change. To clarify the origin of the enhanced tail-to-peak ratio, we have also studied the change in the e2-hh2 excitonic absorption of conventional MQW.

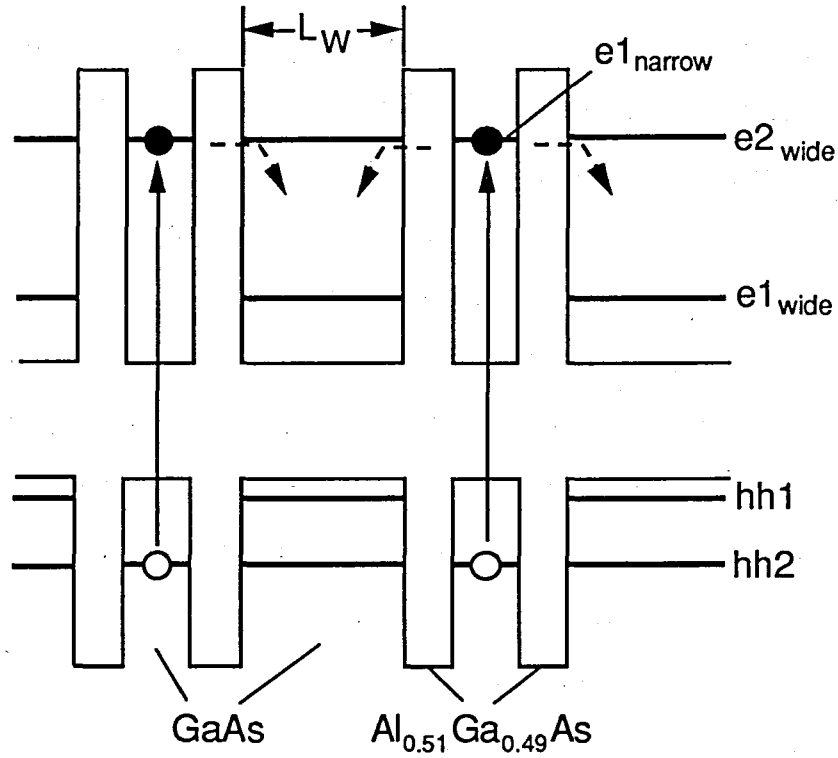


Fig. 3-1. Schematic energy level diagram of resonant TBQ structures. The ground electron level in the narrow well,  $e1_{\text{narrow}}$ , has the same energy as the second level in the wide well,  $e2_{\text{wide}}$ .

### 3.2 Experiment and Discussion

#### 3.2.1 Sample structures and Absorption spectra

The TBQ structures we studied consist of 50 periods of narrow GaAs quantum wells, each 4.5 nm thick, and  $\text{Al}_{0.51}\text{Ga}_{0.49}\text{As}$  barriers, each 4.0 nm thick. We varied the thickness,  $L_W$ , of wide quantum wells from 9.0 nm (32 MLs) to 13.0 nm (46 MLs) to realize the resonant tunneling condition (Fig. 3-1). All structures were grown on a semi-insulating (100) GaAs substrate by molecular beam epitaxy. After the growth, the substrate was removed by selective etching over a

part of the sample.

Figure 3-2 shows the absorption spectra of TBQ structures at room temperature. Absorption peaks around 850 nm show the lowest electron-heavy-hole excitons in the wide wells. Absorption peaks near 790 nm show the lowest electron-heavy-hole excitons,  $e1\text{-hh}1$ , in the narrow wells. The second electron-heavy-hole exciton peak,  $e2\text{-hh}2$ , in the wide wells shifts from 806 nm to 767 nm with the reduction in the wide well thickness from 13.0 to 9.0 nm. For 10.7-nm-thick wide wells, these two exciton peaks coincide. Considering the energy broadening of the electron levels due to the well-thickness fluctuation of 1 monolayer, the coincidence of these exciton peaks means that the ground electron level in the narrow well,  $e1_{\text{narrow}}$ , and the second electron level in the wide wells,  $e2_{\text{wide}}$ , are almost resonant.

### 3.2.2 Time resolved Absorption measurement

We used a conventional time-resolved pump-probe absorption method, which uses lock-in amplification. Optical pump and probe pulses of 1-ps duration were produced at 12 ns intervals using a tunable mode-locked styryl-dye laser synchronously pumped by compressed YAG laser pulses. The optical delay of 660 ps stroke was moved by a stepping motor. The pump beam intensity was 0.2 to 0.5 mW at the sample surface and focused on a 15- $\mu\text{m}$ -diameter spot. The density of photoexcited electrons per well was calculated to be low (about  $1$  to  $2 \times 10^{10} \text{ cm}^{-2}$ ).

Figure 3-3 shows the observed time dependence of transmission at the lowest heavy-hole exciton peak,  $e1\text{-hh}1$ , in the narrow wells. The

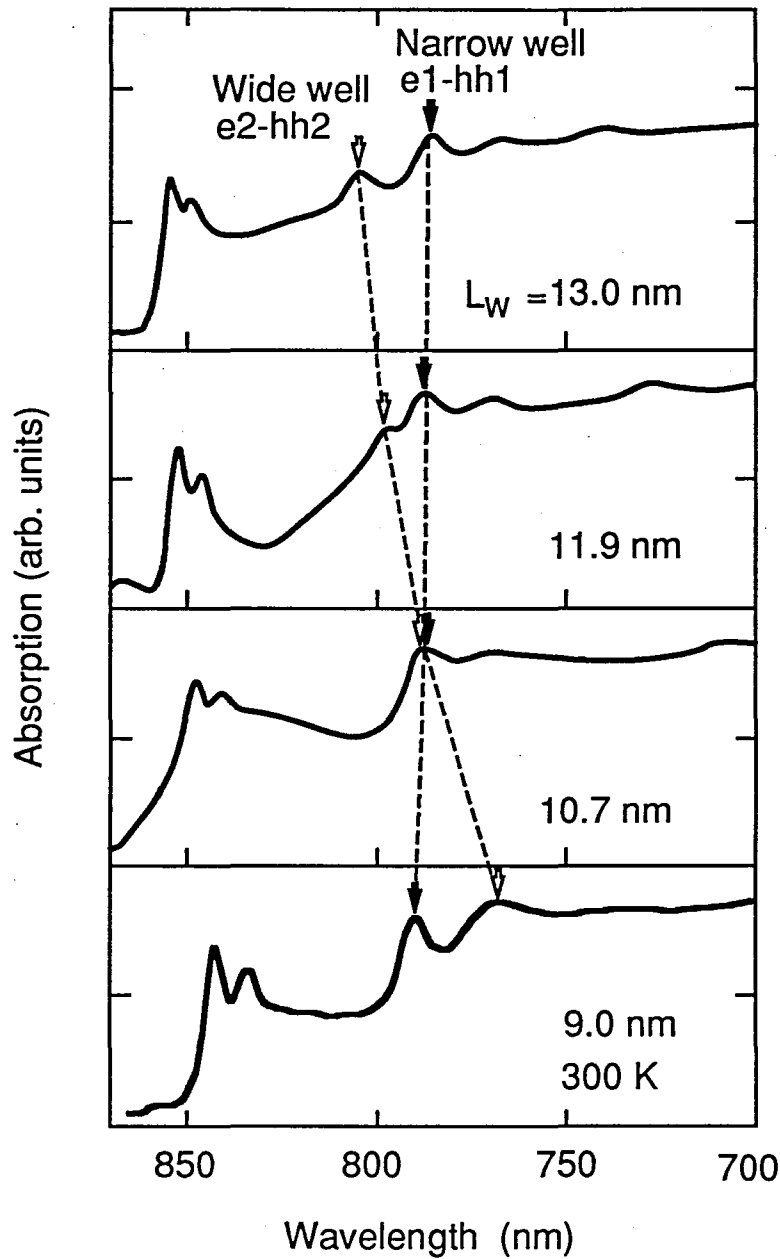


Fig. 3-2. Absorption spectra for TBQ structures at room temperature. Absorption peaks near 790 nm (shown by arrows) show the lowest electron-heavy-hole excitons, e1-hh1, in the narrow wells. The second electron-heavy-hole exciton peak, e2-hh2, in the wide wells (shown by open arrows) shifts from 806 nm to 767 nm with the reduction in the wide well thickness from 13.0 to 9.0 nm. For 10.7-nm-thick wide wells, these two exciton peaks coincide.

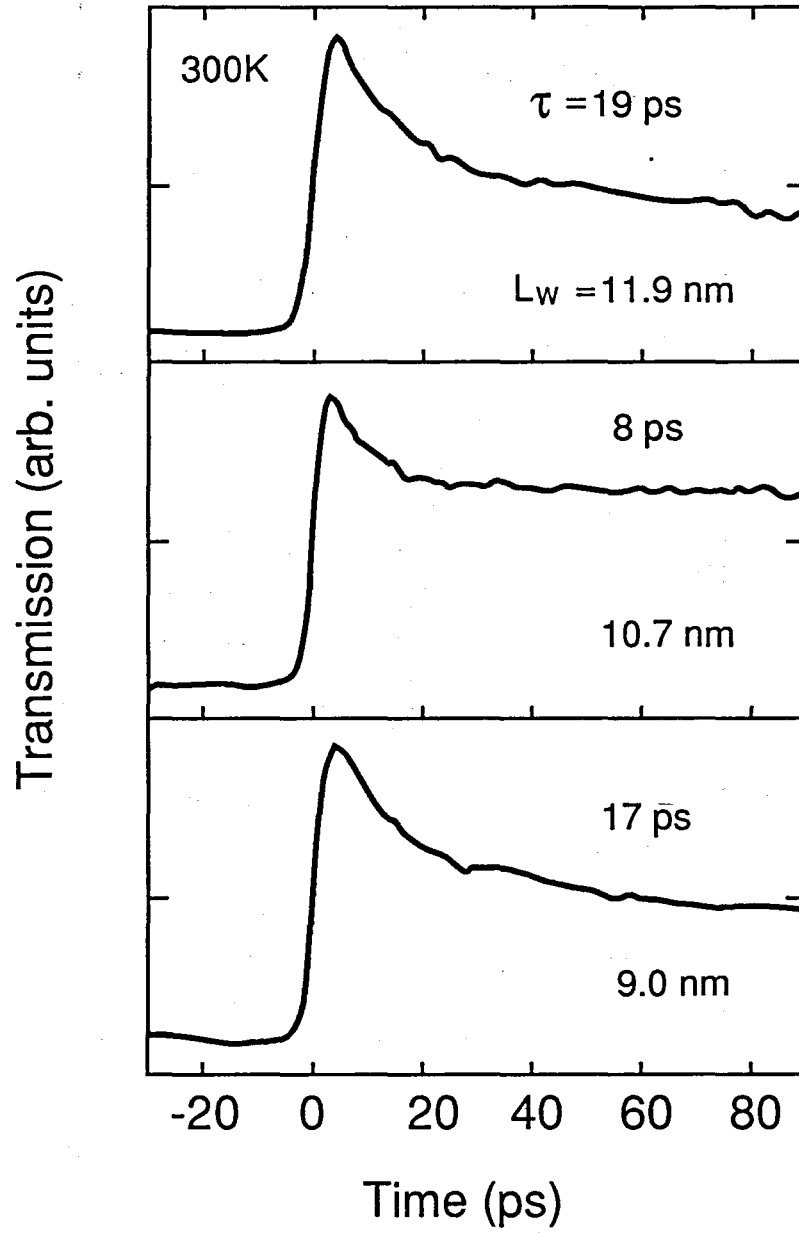


Fig. 3-3. Time resolved transmission change of the lowest heavy-hole exciton peak, e1-hh1, in narrow wells. The time evolution of resonant TBQ structures consist of a fast recovery in the picosecond region due to electron tunneling and a long recovery tail having a time constant longer than one nanosecond.



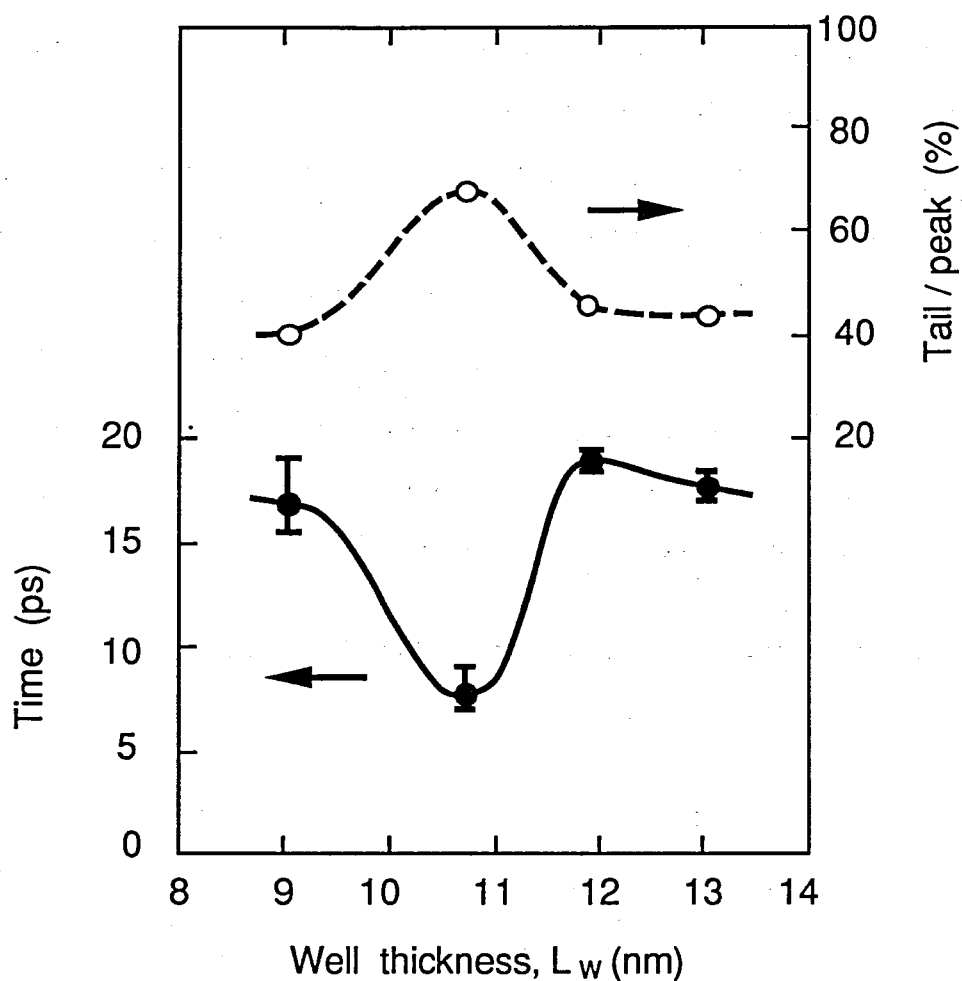


Fig. 3-4. Recovery time and tail-to-peak ratio of TBQ structures. Resonant TBQ structures with 10.7-nm-wide wells showed a faster recovery of 8 ps and a significant enhancement of the tail-to-peak ratio.

time evolution of TBQ structures consists of a fast recovery in the picosecond region due to electron tunneling and a long recovery tail having a time constant longer than one nanosecond. The fast recovery component of the nonresonant TBQ structure is 17 ps for the 9.0-nm-thick wide wells and 19 ps for the 11.9-nm-thick barriers. However, the resonant TBQ structures with 10.7-nm-wide wells show a faster recovery of 8 ps. The observed reduction of the recovery time for

resonant condition is consistent with photoluminescence studies<sup>5-8</sup>) on the resonant tunneling of electrons.

As for the long recovery tail, we observe a significant enhancement of the tail-to-peak ratio in the resonant condition, as shown in Fig. 3-4. The long recovery tail of nonresonant TBQ structures is attributed to the holes left in the narrow wells. The resonant TBQ structure has a tail-to-peak ratio of 67%. This contrasts with the result of nonresonant TBQ structures, in which the tails have ratios of 39 to 46% of the initial absorption change.

### **3.2.3 Comparison with e2-hh2 excitonic absorption change in MQW**

For resonant TBQ structures, note that we measure, not only the e1-hh1 excitonic absorption bleaching of the narrow wells, but also that of the e2-hh2 exciton peaks of the wide wells. To isolate the contribution of the e2-hh2 exciton absorption of wide wells, we also measured the time-resolved absorption change of e2-hh2 excitons of MQW having the same well thickness as the resonant wide wells. The MQW have 55 periods of alternating 4.0-nm-thick  $\text{Al}_{0.51}\text{Ga}_{0.49}\text{As}$  barriers and 10.7-nm-thick GaAs wells (Fig.3-5). The e1-hh1 excitonic absorption of the MQW has a peak at the 851-nm wavelength, and the peak of the e2-hh2 excitonic absorption is at 795-nm. Figure 3-6 shows the time evolution of e2-hh2 excitonic absorption bleaching of the MQW. This figure shows a steplike response without any obvious peak. In this MQW, since the energy difference between the e1 and the e2 levels is greater than the longitudinal optical (LO) phonon energy of 36 meV, an ultrafast intersubband relaxation from

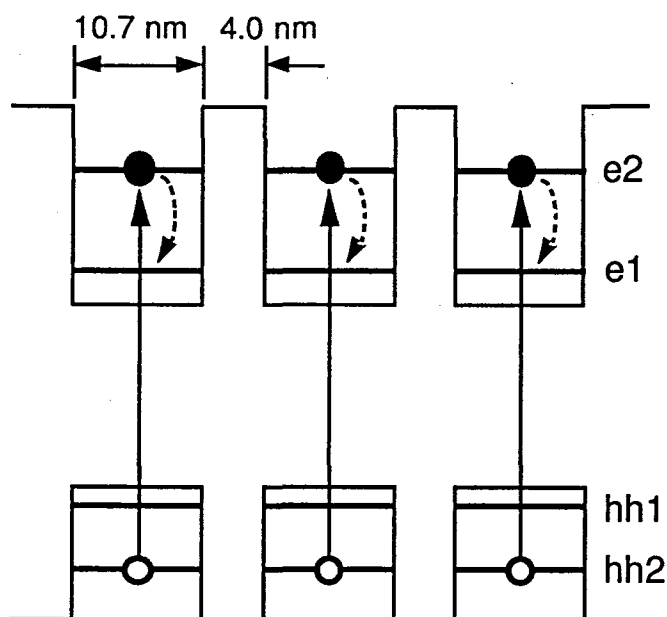


Fig. 3-5. Schematic band diagram of MQW which have 55 periods of alternating 4.0-nm-thick Al<sub>0.51</sub>Ga<sub>0.49</sub>As barriers and 10.7-nm-thick GaAs wells. Arrows show e2-hh2 transitions of the MQW. The dotted arrows show the intersubband relaxation from e2 to e1 level.

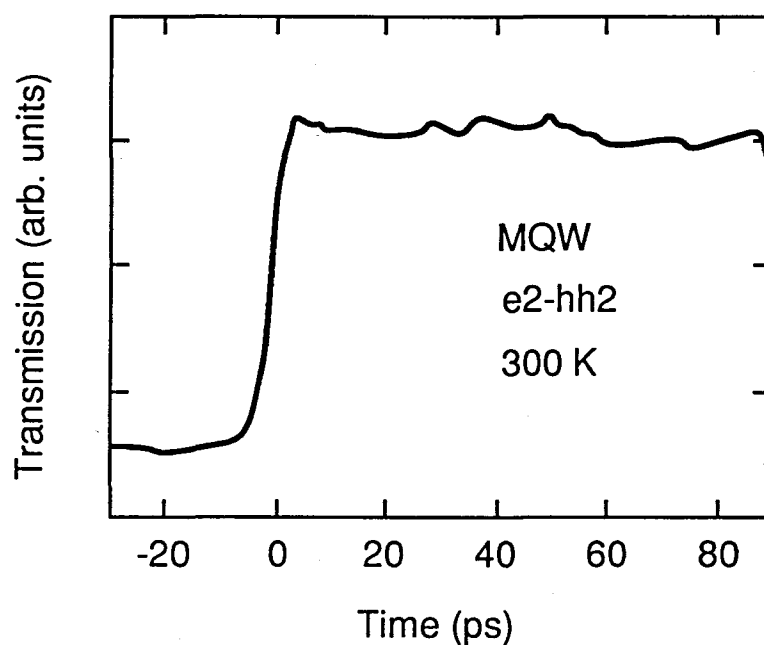


Fig. 3-6. Time resolved transmission of e2-hh2 transition change of MQW.

the e2 to the e1 level is possible through LO-phonon emission. The fact that no peak is observed during our experiments means that the intersubband relaxation time with LO-phonon emission is faster than our time resolution of 1 ps. Tatham et al.<sup>10)</sup> reported that the intersubband relaxation time of electrons with LO-phonon emission is consistently faster than 1 ps. As for the holes, since the energy difference between the h1 and h2 levels is smaller than  $kT$  of 26 meV, a certain number of photo-excited holes are thermally remaining in the hh2 levels. The steplike response is regarded to be due to these holes.

The increase of the tail-to-peak ratio in resonant TBQ structures can be understood likewise as the superimposed contributions of the e1-hh1 excitonic absorption bleaching in the narrow wells and the e2-hh2 excitonic absorption bleaching in the wide wells. It is known that the absorption bleaching in the continuum levels is small.<sup>11)</sup> In nonresonant TBQ structures, only the e1-hh1 excitonic absorption bleaching of the narrow wells can contribute to the observed absorption change. In resonant TBQ structures, the 33% decay in magnitude of the peak is due to the tunneling of electrons from the narrow wells to the wide wells. Also the 67% tail is regarded as the thermally remaining holes in the first excited state of the heavy holes. In the application of resonant TBQ structures at room temperature, the result showed that the energy difference between the hh1 and hh2 levels in wide wells must be larger than  $kT$ , and should preferably be larger than the LO phonon energy of 36 meV to avoid increasing the tail-to-peak ratio.

### 3.3 Summary

In conclusion, we reported the time evolution of the excitonic absorption peak in resonant tunneling bi-quantum-well structures. we studied 4 samples with narrow GaAs quantum wells, each 4.5 nm thick, and  $\text{Al}_{0.51}\text{Ga}_{0.49}\text{As}$  barriers, each 4.0 nm thick. The thickness of wide quantum wells was varied from 9.0 nm (32 MLs) to 13.0 nm (46 MLs) to realize the resonant tunneling condition. We observed the reduction of the absorption recovery time and the increased tail-to-peak ratio in resonant TBQ structures with 10.7 nm barriers. Also, by measuring the e2-hh2 absorption change in MQW, we concluded that the intersubband relaxation time from the e2 level to the e1 level in quantum wells is below our time resolution of 1 ps and that the increased tail-to-peak ratio in resonant TBQ can be attributed to the thermally remaining holes in the first excited subband of heavy holes. For the application of resonant TBQ structures at room temperature, the present result suggests that the energy difference between the hh1 and hh2 levels in wide wells must be larger than  $kT$ , and should preferably be larger than the LO phonon energy of 36 meV to avoid increasing the tail-to-peak ratio.

## REFERENCES

- 1) A. Tackeuchi, S. Muto, T. Inata, and T. Fujii: Jpn. J. Appl. Phys. 28, L1098 (1989).
- 2) A. Tackeuchi, S. Muto, T. Inata and T. Fujii: Appl. Phys. Lett. 58 (1991) 1670.
- 3) S. Muto, T. Inata, A. Tackeuchi, Y. Sugiyama and T. Fujii: Appl. Phys. Lett. 58 (1991) 2393.
- 4) N. Sawaki, R. A. Hopfel, E. Gornik and H. Kano: Appl. Phys. Lett. 55 (1989) 1996.
- 5) M. Tsuchiya, T. Matsusue and H. Sakaki: Proc. 6th Int. Conf. Ultrafast Phenomena, Kyoto, 1988 (Springer-Verlag, Berlin, 1988) p.304.
- 6) D. Y. Oberli, J. Shah, T. C. Damen, C. W. Tu, T. Y. Chang, D. A. B. Miller, J. E. Henry, R. F. Kopf, N. Sauer and A. E. DiGiovanni: Phys. Rev. B 40 (1989) 3028.
- 7) M. G. W. Alexander, M. Nido, W. W. Rühle and K. Köhler: Phys. Rev. B 41 (1990) 12295.
- 8) B. Deveaud, F. Clerot, A. Chomette, A. Regreny, R. Ferreira and G. Bastard: Europhys. Lett. 11 (1990) 367.
- 9) A. Tackeuchi, T. Inata, S. Muto, and T. Fujii: Jpn. J. Appl. Phys. 30 (1991) 2730.
- 10) M. C. Tatham, J. F. Ryan and C. T. Foxon: Phys. Rev. Lett. 63 (1989) 1637.
- 11) W. H. Knox, C. Hirlimann, D. A. B. Miller, J. Shah, D. S. Chemla and C. V. Shank: Phys. Rev. Lett. 56 (1986) 1191.

## CHAPTER 4

### Time Resolved Studies of Excitonic Absorption Bleaching in Type-II GaAs/AlGaAs/AlAs Tunneling Bi-Quantum-Well

#### 4.1 Introduction

In chapter 2 and 3, we reported the fast recoveries from the excitonic absorption bleaching in resonant and non-resonant TBQ structures.<sup>1-3)</sup> TBQs show fast recoveries as fast as 1 ps with the reduction of the barrier thickness down to 1.7-nm-thick barriers. However, disadvantage of those TBQ structures is the optical absorption of wide wells. Since the band gap of narrow wells is larger than that of the wide wells, the excitation of e1-hh1 excitons in the narrow wells results in the coexcitation of the wide wells (Fig. 4-1).

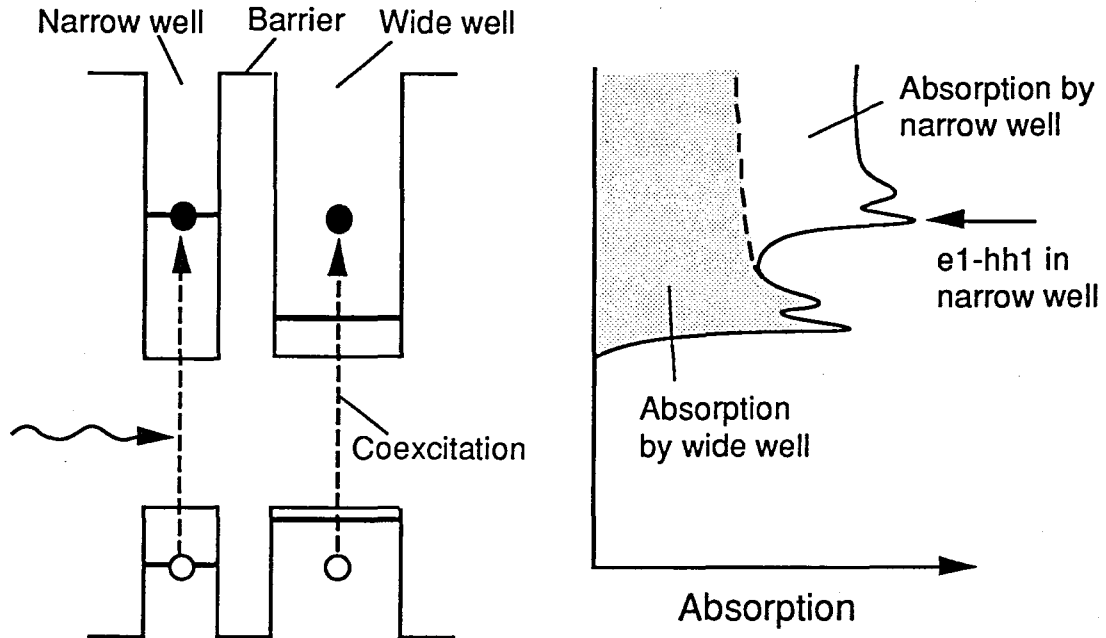


Fig. 4-1. Schematic band diagram and absorption spectrum of TBQ.

This additional optical absorption severely limits the applicability of TBQ for optical devices such as MQW etalon.<sup>4,5)</sup> MQW etalon uses a change in refractive index near the excitonic absorption peak for optically bistable operation. To use the change in refractive index efficiently, we must tune the wavelength in the lower energy side of the excitonic absorption peak where the absorption is relatively small and the index change,  $\Delta n$ , is relatively large<sup>6)</sup> (Fig. 4-2).

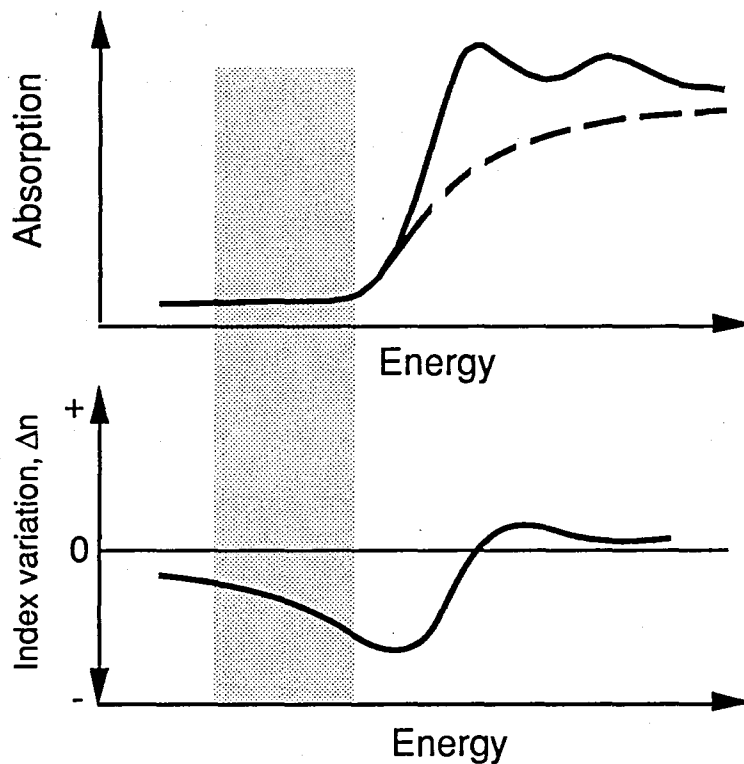


Fig. 4-2. Schematic absorption spectrum and change in the refractive index by excitonic absorption saturation in MQW. In the lower energy side of the exciton peak (shaded region), absorption is small but the index change is relatively large. The dashed line shows the excitonic absorption bleaching.



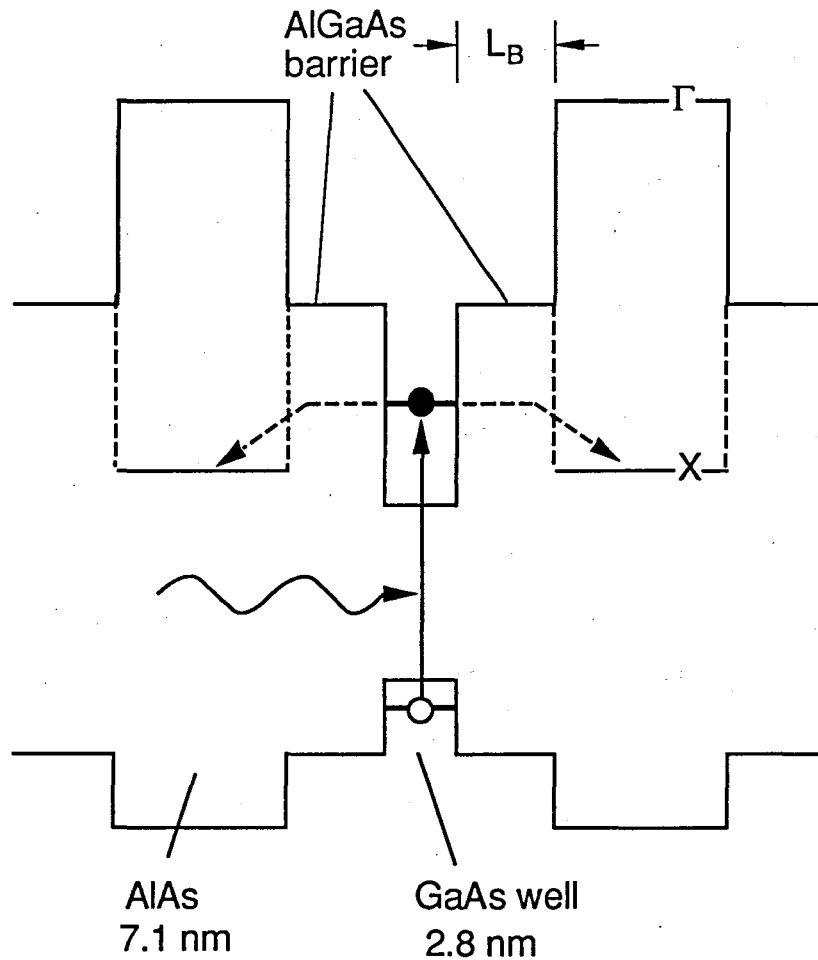


Fig. 4-3. Energy band diagram of type-II TBQ structure. The Type-II TBQ structure consists of GaAs wells, AlGaAs barriers and AlAs layers. The photoexcited electrons in GaAs wells escape through AlGaAs barriers by tunneling toward X states in AlAs layers.

One way to eliminate the optical absorption of the wide wells is to use a material which has a wider energy gap than that of the GaAs narrow wells. We studied the type-II tunneling bi-quantum wells<sup>7)</sup> consisting of a series of GaAs wells, AlGaAs barriers and AlAs layers as shown in Fig.4-3. Since the lowest direct transition energy in the

AlAs layers is larger than that of the GaAs wells, no significant optical absorption occurs in the AlAs layers during the excitation of the GaAs wells. If the lowest electron state in the GaAs well is higher in energy than the X state in the AlAs layer, the photo-excited electrons in the GaAs well escape by tunneling through AlGaAs barrier toward the X state in the AlAs layer. In GaAs/AlAs type-II MQWs, the lowest electron state in the GaAs well becomes higher than the X state in the AlAs layer when the GaAs well thickness is equal to or smaller than 12 monolayers.<sup>8,9)</sup> Some reports have already been made on the time resolved measurements of electron transfer in type-II GaAs/AlAs or GaAlAs/AlAs MQWs.<sup>10-13)</sup> However, the controllability of the absorption recovery time of the type-II MQWs is restricted. In our structure, the absorption recovery time is controlled directly by the AlGaAs barrier thickness.

## 4.2 Experiment

### 4.2.1 Sample structures

The type-II TBQ structures we studied consist of 50 periods of GaAs quantum wells 2.8-nm-thick, AlAs wells 7.1-nm-thick and  $\text{Al}_{0.51}\text{Ga}_{0.49}\text{As}$  barriers. We varied the thickness of  $\text{Al}_{0.51}\text{Ga}_{0.49}\text{As}$  barriers,  $L_B$ , from 4.0 nm (14 MLs) to 1.1 nm (4 MLs). All structures were grown on a semi-insulating (100) GaAs substrate by molecular beam epitaxy. After the growth, the substrate was removed by selective etching over a part of the sample.

Figure 4-4 shows the absorption spectra of the type-II TBQs at 300 K. The clear e1-hh1 excitonic absorption peak is observed around

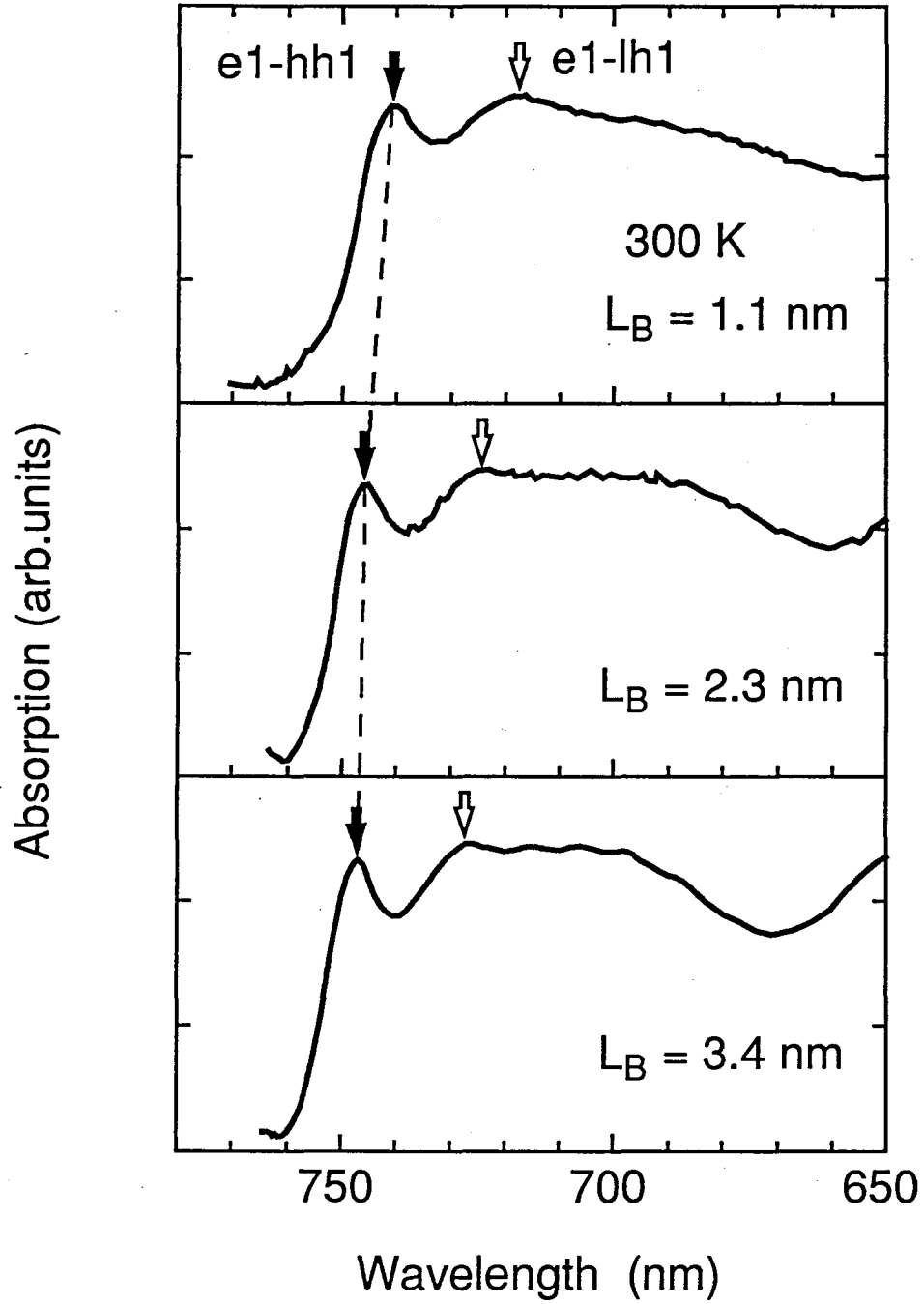


Fig. 4-4. Absorption spectrum for type-II TBQ structure at room temperature. The solid arrows show the e1-hh1 excitonic absorption peak (the electron heavy-hole exciton peak in GaAs wells). The open arrows show the e1-lh1 excitonic absorption peak.

745 nm at room temperature. The e1-hh1 absorption peak shifts from 747 nm to 740 nm as the barrier thickness decreases from 4.0 nm to 1.1 nm. This contrasts with the red shift in type-I TBQ with the reduced barrier thickness reported in chapter 2.<sup>2)</sup> In type-I TBQs, the red shift comes from the reduced confinement of excitons. However, in type-II TBQs, the reduction of the AlGaAs barrier thickness results in the increased energy of quantum levels due to the approach of the AlAs potential barriers toward the GaAs wells. Saeta et al. observed the e1-hh1 excitonic absorption peak at 700 nm at room temperature for type-II GaAs 3.1-nm-thick/AlAs 7.1-nm-thick MQWs, which can be regarded as type-II TBQ at  $L_B=0$ .<sup>10)</sup> This energy is about 100 meV larger than that of the e1-hh1 absorption peak of the present type-II TBQs.

The photoluminescence spectrum at 4.2 K is shown in Fig. 4-5 under the pumping of CW Kr ion laser at 530.9 nm. We confirm the direct e1-hh1 emission in GaAs wells at 704 nm. The indirect type-II emissions between the X-states in AlAs and the lowest heavy hole level in the GaAs wells are observed around 730 nm. The energy splitting between  $\Gamma-\Gamma$  and X- $\Gamma$  emission indicates that the lowest level of electrons in the GaAs wells is more than 40 meV higher than the X state of the AlAs wells.

#### 4.2.2 Time resolved absorption measurement

We measured the time dependence of excitonic absorption bleaching of the e1-hh1 excitonic transition. We used ordinary time-resolved pump-probe absorption measurement and lock-in amplification. A tunable mode-locked styryl dye laser synchronously

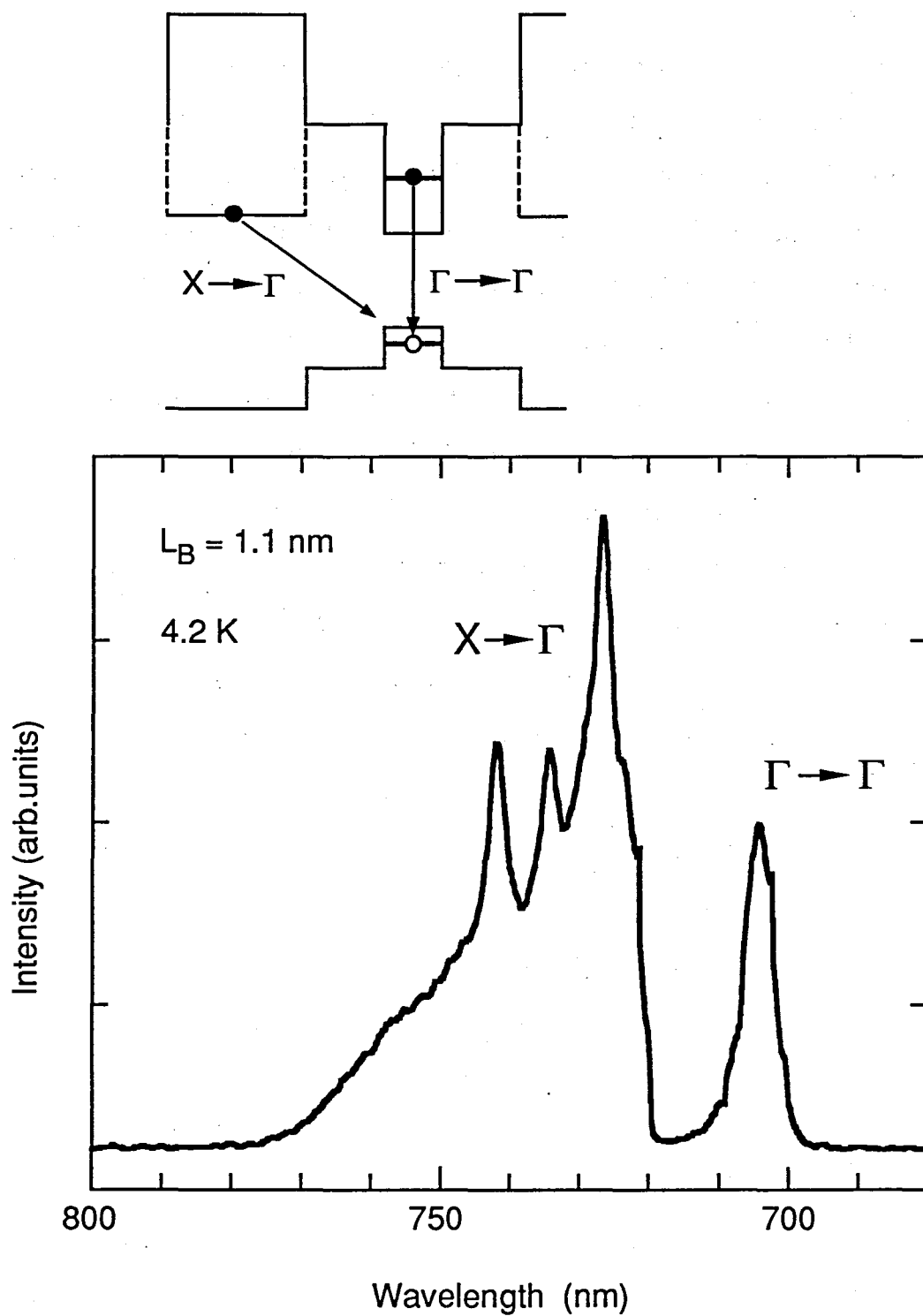


Fig. 4-5. Photoluminescence spectrum at 4.2 K. The photoluminescence peak at 704 nm is the direct e1-hh1 emission in GaAs wells. The peaks around 730 nm are the indirect type-II X- $\Gamma$  emissions.

pumped by compressed YAG laser pulses was used to generate optical pump and probe pulses of 1 ps duration at 12 ns intervals. The optical delay of 660 ps stroke was moved by a stepping motor. The pump beam intensity was 0.3-0.8 mW in front of the sample and focused on a 15- $\mu\text{m}$ -diameter spot. The density of photoexcited electrons per well was calculated to be low (about 1 to  $3 \times 10^{10} \text{ cm}^{-2}$ ).

Figure 4-6 shows the observed transmission-time dependence at the lowest heavy-hole exciton peak in narrow wells. For the fast component of the initial decay, type-II TBQs show a recovery time on the order of picoseconds. The recovery time is reduced to 8 ps for barrier thickness of 1.1 nm (4 MLs). There are also slow recovery tails after the fast relaxations. Such tails have a time constant slower than 1 ns and a magnitude of about 50% of the initial absorption change like the type-I TBQ.<sup>1,2)</sup> Since only electrons can escape from the wells, we attribute the slow recovery tail to the holes remaining in the GaAs wells.

The abrupt drop of the signal before time 0 in the upper part of Fig.4-6 was obtained by cutting the pumping light. This fact indicates that the carrier accumulation is large enough for absorption bleaching to be present even after about 12 ns from the previous photo-excitation. In type-II MQW systems, it is known that the carrier lifetime through the indirect recombination between the X conduction band in AlAs and the  $\Gamma$  valence band in GaAs needs several microseconds.<sup>8,14)</sup> In our structure, this process is expected to be even slower because of the existence of AlGaAs tunneling barrier. The carrier accumulation evidenced in Fig.4-6 is consistent with a long carrier lifetime.

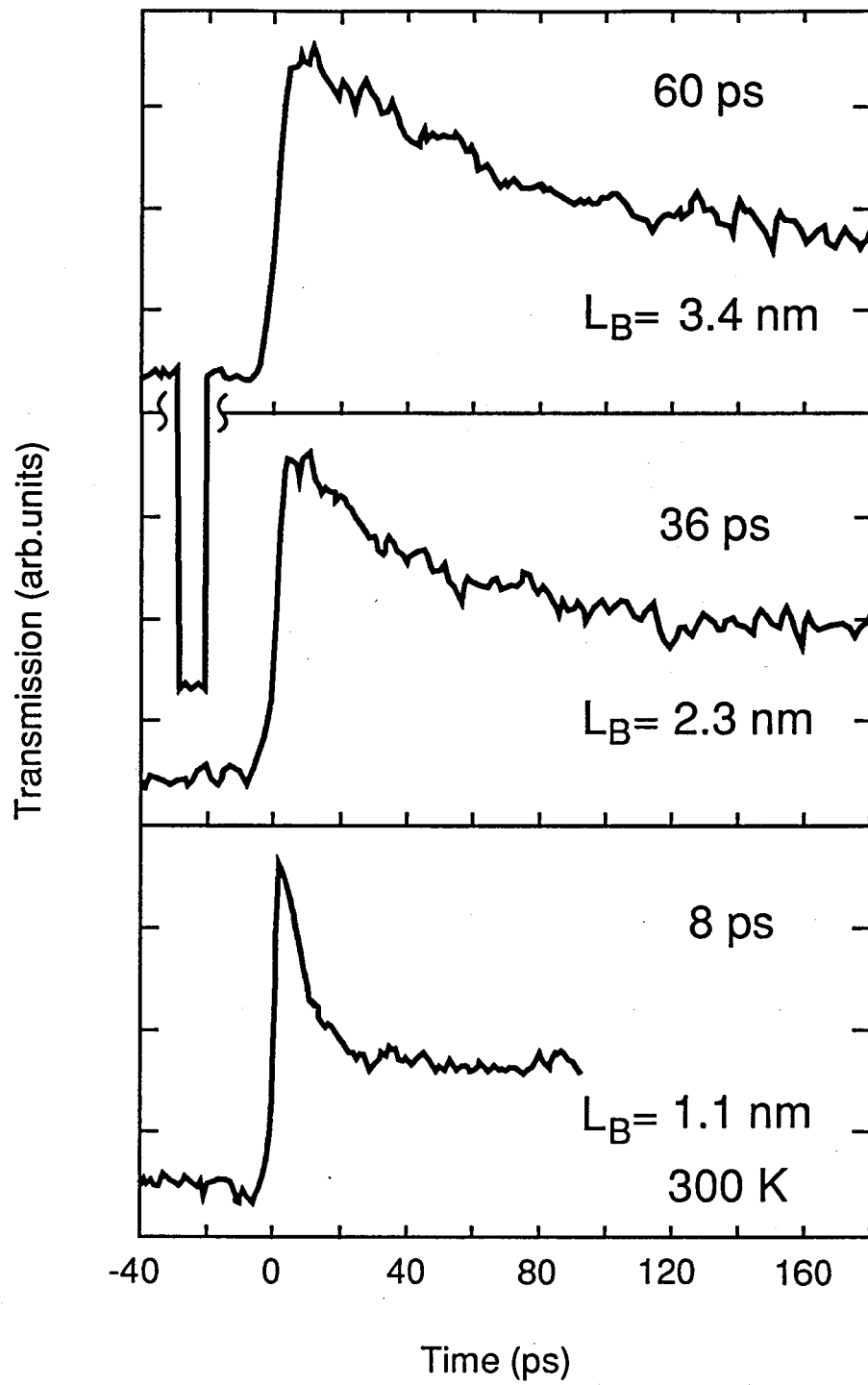


Fig. 4-6. Time-resolved transmission change of the lowest excitonic absorption peak in GaAs wells of type-II TBQs at room temperature. The abrupt drop of the signal before time 0 in the upper part of this figure is due to cutting the pumping light.

### 4.3 Discussion

The semilogarithmic plot of the experimental recovery time as a function of barrier thickness,  $L_B$ , is shown by the solid circles in Fig.4-7. The dashed line in Fig.4-7 indicates the slope (and not the magnitude) of the calculated tunneling time through AlGaAs barriers from the GaAs wells of the 2.8 nm thickness, which is obtained from the statelifetimes of the virtual states of resonant tunneling barrier structures.<sup>1)</sup> The result for GaAs 2.8 nm-thick/AlAs 6.7 nm-thick type-II MQW by Feldmann et al. is also shown (x in Fig.4-7).<sup>11)</sup> Although the calculated slope does not include the effect of the blue shift of the exciton peak which leads to the increased tunneling probability for the thinner barriers, the calculated slope roughly agrees with the experimental data. The clear dependence of the recovery time on the barrier thickness proves the controllability of the recovery time in a wide range through barrier thickness.

The open circles show the absorption recovery time observed for the type-I TBQs which consists of the narrow GaAs wells of 4.5 nm-thick and the wide GaAs wells of the 9.0 nm-thick.<sup>2)</sup> Note that the dependence of the recovery times for type-II TBQs is similar to that for the type-I TBQs. In chapter 2, we showed that the calculated tunneling times of the type-I TBQs for various scattering mechanisms are linearly dependent on the barrier thickness on a semilogarithmic plot, with nearly the same slope in the dashed line in Fig.4-7.<sup>15)</sup> The calculated slopes of the tunneling times are independent of the scattering mechanisms such as LO-phonon emission (absorption), deformation potential, and alloy scattering. The dependence of the



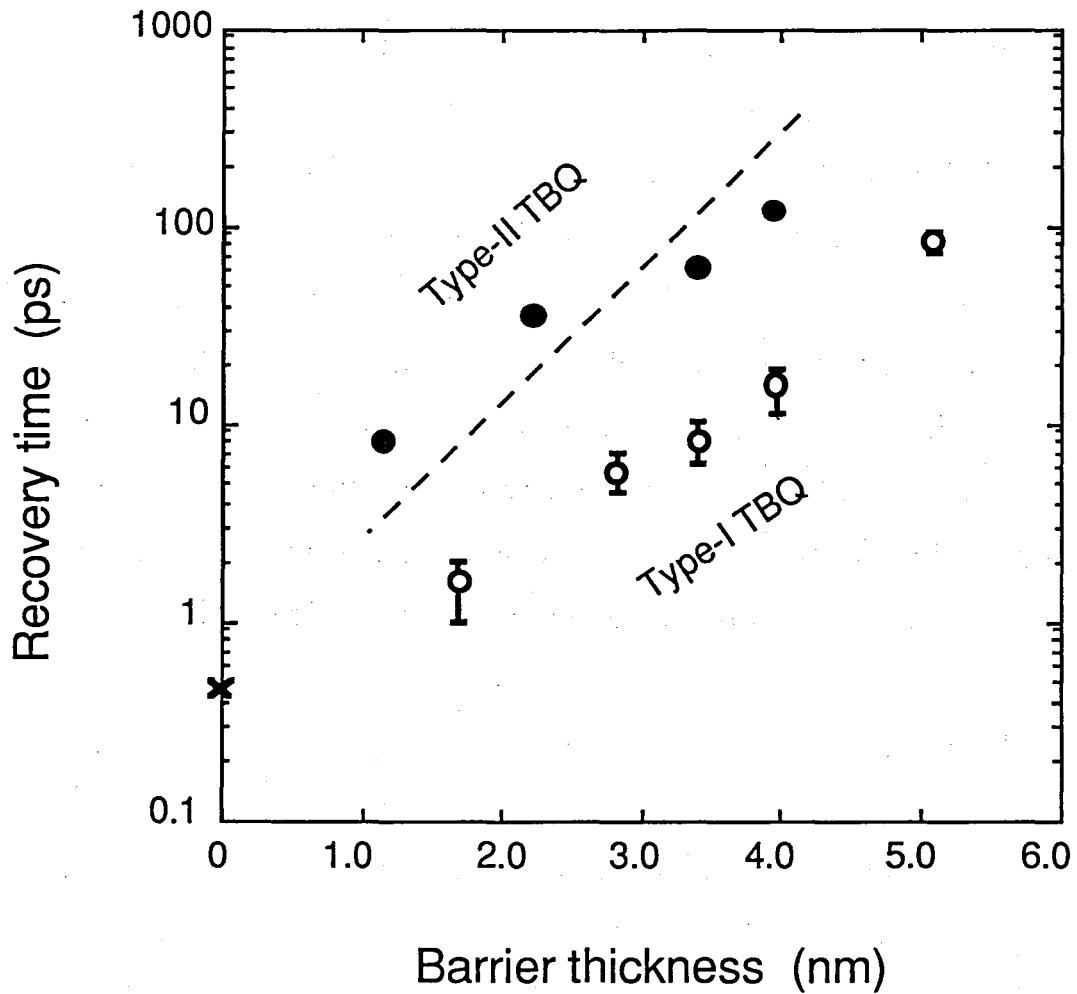


Fig. 4-7. The dependence of the recovery time on barrier thickness for type-II and type-I TBQs. The solid circles and open circles show the absorption recovery times of type-II and type-I TBQs, respectively. The dashed line indicates the slope (not the magnitude) of the calculated tunneling time through AlGaAs barriers from GaAs wells of the 2.8 nm thickness. Also shown is the datum from Feldmann et al. (Ref.11, X) on the type-II MQW.

tunneling time on the barrier thickness comes from the overlap integral of the wavefunctions of electron states for both the narrow wells (the GaAs wells) and the wide wells (the AlAs layers) for type-I (type-II) TBQs. The difference in the scattering mechanism affects only the

magnitude of the tunneling time, which results in a parallel translation of the semilogarithmic plot. Therefore, the similarity in the type-I and type-II TBQ tendencies indicates that the absorption recovery in type-II TBQs is also governed by a tunneling process. In type-I TBQs, the LO-phonon emission is the dominant scattering mechanism which assists the non-resonant tunneling. As for the type-II TBQs, we have not yet identified the dominant scattering mechanism. The non-resonant intervalley phonon scatterings from the  $\Gamma$  to the X electron states and the interface scatterings due to the interface mixing potential or due to the potential fluctuations<sup>11,13)</sup> are possible candidates.

#### 4.4 Summary

We reported the time evolution of excitonic absorption bleaching in type-II TBQs. Type-II TBQs consist of a series of GaAs wells, AlGaAs barriers and AlAs layers. Since the lowest direct transition energy in the AlAs layers is larger than that of the GaAs wells, no significant optical absorption occurs in the AlAs layers during the excitation of the GaAs wells. We observed the energy shift of the e1-hh1 absorption peak from 747 nm to 740 nm as the barrier thickness decreases from 4.0 nm to 1.1 nm. This contrasts with the red shift in type-I TBQ with the reduced barrier thickness. In type-II TBQs, the reduction of the AlGaAs barrier thickness results in the increased energy of quantum levels due to the approach of the AlAs potential barriers toward the GaAs wells. We showed that the recovery time of the excitonic absorption bleaching of the GaAs wells is reduced to 8 ps for the AlGaAs barrier thickness of 1.1 nm. The dependence of the

recovery time on the barrier thickness for type-II TBQs is similar to that for the type-I TBQs. The similarity indicates that the absorption recovery in type-II TBQs is also governed by a tunneling process. Type-II TBQs show picoseconds absorption recovery with no significant optical absorption except for by GaAs wells.

## REFERENCES

- 1) A. Tackeuchi, S. Muto, T. Inata, and T. Fujii: Jpn. J. Appl. Phys. 28 (1989) L1098.
- 2) A. Tackeuchi, S. Muto, T. Inata, and T. Fujii: Appl. Phys. Lett. 58 (1991) 1670.
- 3) A. Tackeuchi, T. Inata, S. Muto, and T. Fujii: Jpn. J. Appl. Phys. 30 (1991) 2730.
- 4) H. M. Gibbs, S. L. McCall, T. N. C. Venkatesan, A. C. Gossard, A. Passner and W. Wiegmann: Appl. Phys. Lett. 35 (1979) 451.
- 5) A. Migus, A. Antonetti, D. Hulin, A. Mysyrowicz, H. M. Gibbs, N. Peyghambarian, and J. L. Jewell: Appl. Phys. Lett. 46 (1985) 70.
- 6) S. H. Park, J. F. Morhange, A. D. Jeffery, R. A. Morgan, A. Chavez-Pirson, H. M. Gibbs, S. W. Koch, N. Peyghambarian, M. Derstine, A. C. Gossard, J. H. English, and W. Weigmann: Appl. Phys. Lett. 52 (1988) 1201.
- 7) A. Tackeuchi, T. Inata, Y. Sugitama, Y. Nakata, S. Nakamura, and S. Muto: to be published in J. Jpn. Appl. Phys. (1991).
- 8) E. Finkman, M. D. Sturge, and M. C. Tamargo: Appl Phys. Lett. 49 (1986) 1299.
- 9) J. Ihm: Appl. Phys. Lett. 50 (1987) 1068.
- 10) P. Saeta, J.F. Federici, R.J. Fisher, B.I. Greene, L. Pfeiffer, R.C. Spitzer, and B.A. Wilson: Appl. Phys. Lett. 54 (1989) 1681
- 11) J. Feldmann, R. Sattmann, E.O. Göbel, J. Kuhl, J. Hebling, K. Ploog, R. Muraliharan, P. Dawson, and C.T. Foxon: Phys. Rev. B42 (1990) 5809.
- 12) Y. Masumoto, T. Mishina, F. Sasaki, and M. Adachi: Phys. Rev. B40 (1989) 8581.

- 13) J. Nunnenkamp, J. Kuhl, K. Ploog, J. Feldmann, E. Göbel, P. Dawson, and C.T. Foxon in *Ultrafast Phenomena VII*, Springer Series in Chemical Physics, Vol.53, edited by C.B. Harris, E.P. Ippen, G.A. Mourou and A.H. Zewail (Springer-Verlag Berlin, Heidelberg 1990), pp.236-238
- 14) P. Dawson, K. J. Moore, C. T. Foxon, G. W. 't Hooft, and R. P. M. van Hal: *J. Appl. Phys.* 65 (1989) 3606.
- 15) S. Muto, T. Inata, A. Tackeuchi, Y. Sugiyama, and T. Fujii: *Appl. Phys. Lett.* 58 (1991) 2393.

## CHAPTER 5

# Picosecond Excitonic Absorption Recovery of 100-nm GaAs/AlGaAs Narrow Multiple-Quantum-Well Wires

### 5.1 Introduction

Until here, we have described the approaches to shorten the absorption recovery time in quantum wells using tunneling effect. In this chapter, we report another approach to reduce carrier lifetime without the sacrifice of the optical efficiency. That is to use surface recombination on the sidewalls of wire structures (Fig. 5-1). In the wire structure, photo-excited carriers diffuse toward the side walls, and recombine on the side wall surfaces. Surface recombination on the sidewalls was shown to be practical in reducing the nonlinear response time by Jewell et al. in their Fabry-Perot micro resonators.<sup>1)</sup> They reduced the recovery time of bulk GaAs etalon down to 150 ps using 1.5- $\mu\text{m}$ -square micro structures. Mayer et al.<sup>2)</sup> have observed a reduced carrier lifetime of 20 ps at 40 K for their 400-nm GaAs/AlGaAs wires using photoluminescence measurements. The present problem of those wire structures is that damages are liable to invade the net region of wire during the fabrication process. Those damages can not only shorten the carrier lifetime but also deteriorate the excitonic optical nonlinearity. We did the time-resolved absorption measurement of narrow multiple-quantum-well (MQW) wires in order to investigate their excitonic optical nonlinearity. We show that the strong optical nonlinearity of excitons is preserved, even in wires on the order of 100 nm width, and having a fast recovery time in the picosecond region.<sup>3)</sup>

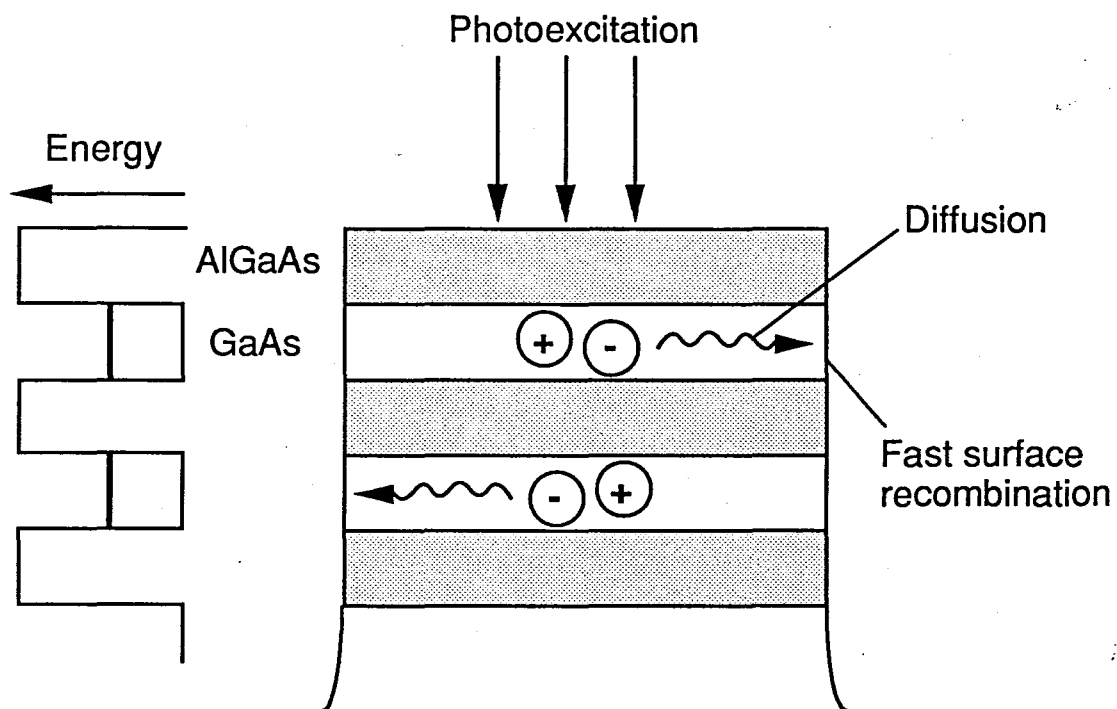


Fig. 5-1. Schematic structure and concept of MQW wire.

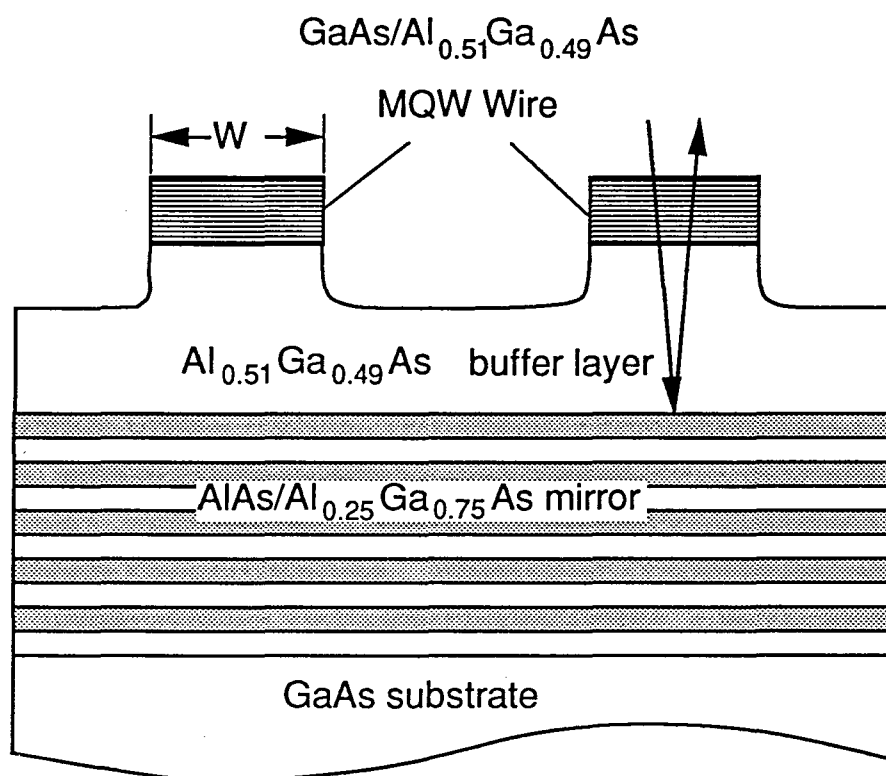


Fig. 5-2. Sample structure of MQW wires.

## 5.2 Experiment

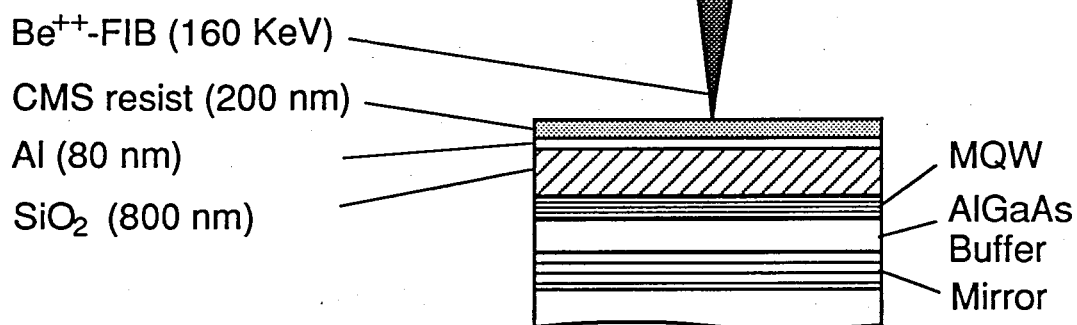
### 5.2.1 Sample structures and Fabrication process

Samples used for this study were prepared using molecular-beam-epitaxy growth on semi-insulating (100) GaAs substrates. As shown in Fig. 5-2, each structure consist of 40 periods of 4.5-nm GaAs and 4.0-nm  $\text{Al}_{0.51}\text{Ga}_{0.49}\text{As}$  MQWs, a 700-nm-thick  $\text{Al}_{0.51}\text{Ga}_{0.49}\text{As}$  buffer layer, and 10 pairs of 66.5-nm AlAs and 57.8-nm  $\text{Al}_{0.25}\text{Ga}_{0.75}\text{As}$  layers (quarter-wave semiconductor Bragg-reflector stack<sup>4)</sup>). We measured the light reflected by the buried Bragg reflector to obtain the transmission ratio of the MQW wires. This method prevent removing the GaAs substrate to measure the transmitted light directly. The lateral dimension of the MQW wires,  $W$ , varies from 130 nm to 970 nm. The separation between each wire is fixed at about 200 nm.

The nanostructures were fabricated using both focused-ion-beam (FIB) lithography and reactive-ion-beam (RIB) etching by electron-cyclotron resonance (ECR) chlorine-plasma as shown in Fig. 5-3.<sup>5)</sup> We used the trilevel resist structure, consisting of a 200 nm partially-chloromethylated-polystyrene (CMS) negative electron beam resist, a 80 nm Al, and a 800 nm  $\text{SiO}_2$ .  $\text{SiO}_2$  film works as the ion stopper for FIB exposure. At first, the  $\text{Be}^{++}$ -FIB (160keV) was scanned to expose line-arrays of 400  $\mu\text{m}$  squares (Fig.5-3-a). Next, the resist patterns were transferred into the intermediate Al film by reactive ion etching (RIE) in a  $\text{BCl}_3 + 5\%\text{CCl}_4$  plasma (Fig.5-3-b). The Al mask patterns were then transferred into the thick bottom  $\text{SiO}_2$  layer by the second RIE with  $\text{CHF}_3$  plasma (Fig.5-3-c). The wire structure fabrication of a

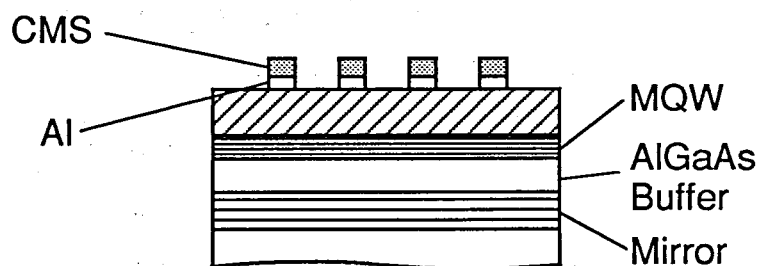


a. FIB Lithography



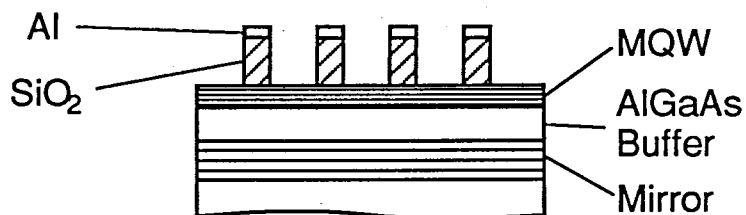
b. Al - RIE

BCl<sub>3</sub>+5%CCl<sub>4</sub>



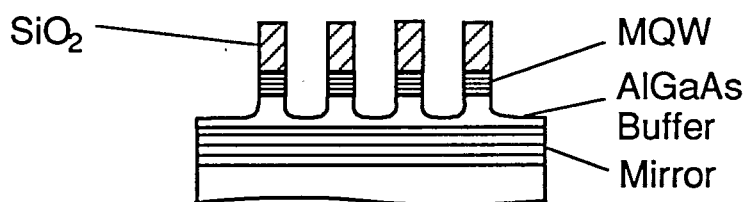
c. SiO<sub>2</sub> - RIE

CHF<sub>3</sub>



d. MQW - RIBE

Cl<sub>2</sub>



e. Removal of SiO<sub>2</sub>

Wet etching

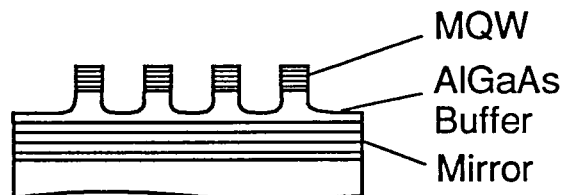


Fig. 5-3. Fabrication process of MQW wires using FIB lithography.

GaAs/AlGaAs MQW was carried out by the subsequent reactive ion beam etching (RIBE) using electron cyclotron resonance (ECR) chlorine-plasma (Fig.5-3-d). At last, the remained SiO<sub>2</sub> pattern was selectively removed by chemical etching (Fig.5-3-e).

### 5.2.2 Absorption spectra of MQW wires

Figure 5-4 shows the absorption spectra of MQW wires obtained by measuring the light reflected by the buried Bragg reflector.<sup>6)</sup> These spectra consist of three components: the true absorption due to MQW wires, the reflection spectrum of the buried Bragg reflector as shown in the lower part in Fig. 5-4 and the optical interference between the top layer of the MQW and the buried Bragg reflector. The peak around 795 nm indicates the lowest electron-heavy-hole excitonic absorption. Also, the small peak around 780 nm for 130-nm and 180-nm wires shows the electron-light-hole excitonic absorption. The large peak at 784 nm of MQW is due to optical interference. In the MQW spectrum, the excitonic absorption peak at 795 nm lies on the shoulder of this large interference peak. The problem in fabricating wire structure is that the damage may invade the wire's net region during fabrication and degrade the excitonic properties of the material. These spectra show that the excitonic absorption peaks are preserved even for wires as thin as 130 nm wide without critical reduction as compared with unprocessed MQW. This indicates that damage which degrades the exciton formation is not in the net area of our samples.

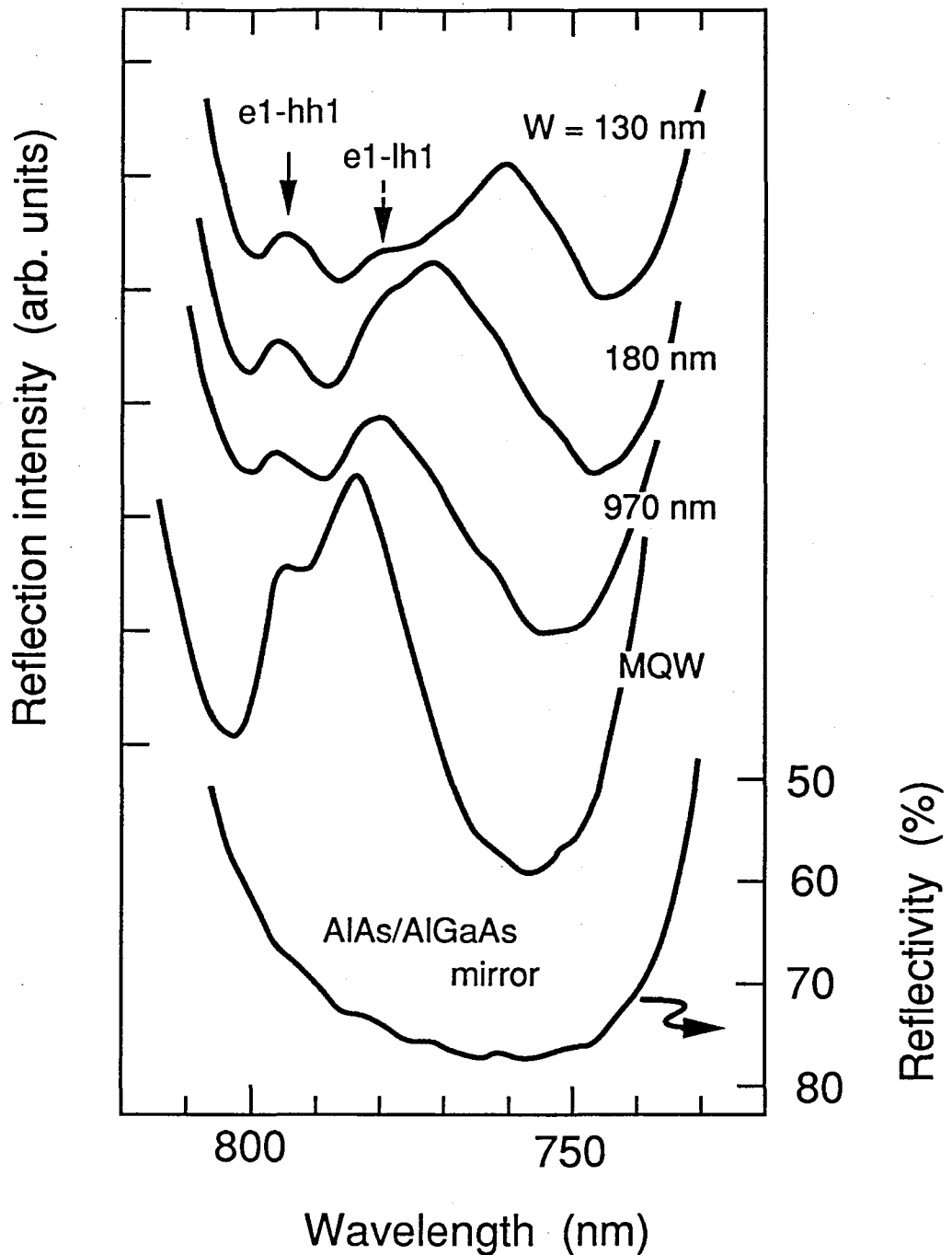


Fig. 5-4. Absorption spectra of MQW wires and the reflection spectrum of the buried Bragg reflector. Absorption spectra were obtained by measuring the light reflected by the buried Bragg reflector. These spectra consist of three components: the true absorption due to MQW wires, the reflection spectrum of the buried Bragg reflector and the optical interference between the top surface of the sample and the buried Bragg reflector. The peaks around 795 nm indicate the lowest electron-heavy-hole excitonic absorption peaks. Also, the small peaks around 780 nm for 130-nm and 180-nm wires show the electron-light-hole excitonic absorption peaks.

### 5.2.3 Time resolved absorption measurement

We measured the time dependent absorption of the lowest electron heavy-hole exciton transition, e1-hh1, of MQW wires. We used conventional time-resolved pump-probe absorption measurement which uses lock-in amplification as shown in Fig. 5-5. Optical pump and probe pulses of 1-2 ps duration at 12 ns intervals were obtained from a tunable mode-locked styryl dye laser ( $\lambda \sim 794$  nm) synchronously pumped by compressed YAG laser pulses. The optical delay was moved by a stepping motor. The pump beam intensity was 0.2 to 0.5 mW in front of the sample and was focused on a 15- $\mu\text{m}$ -diameter spot. All measurements were done at room temperature.

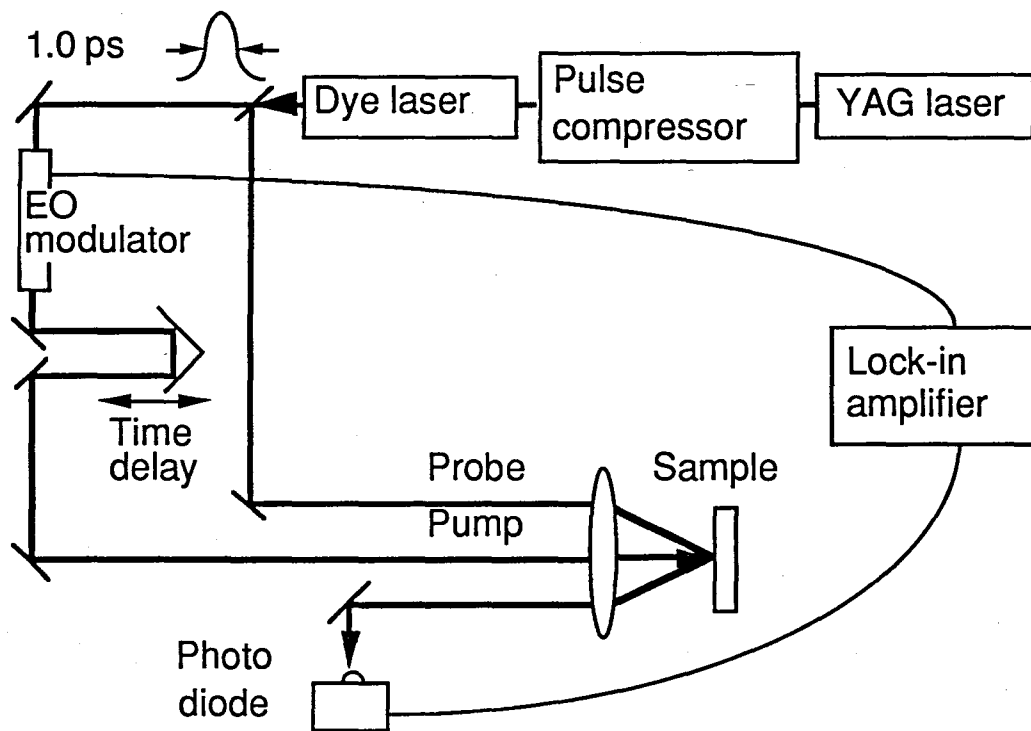


Fig. 5-5. Time resolved absorption measurement system.

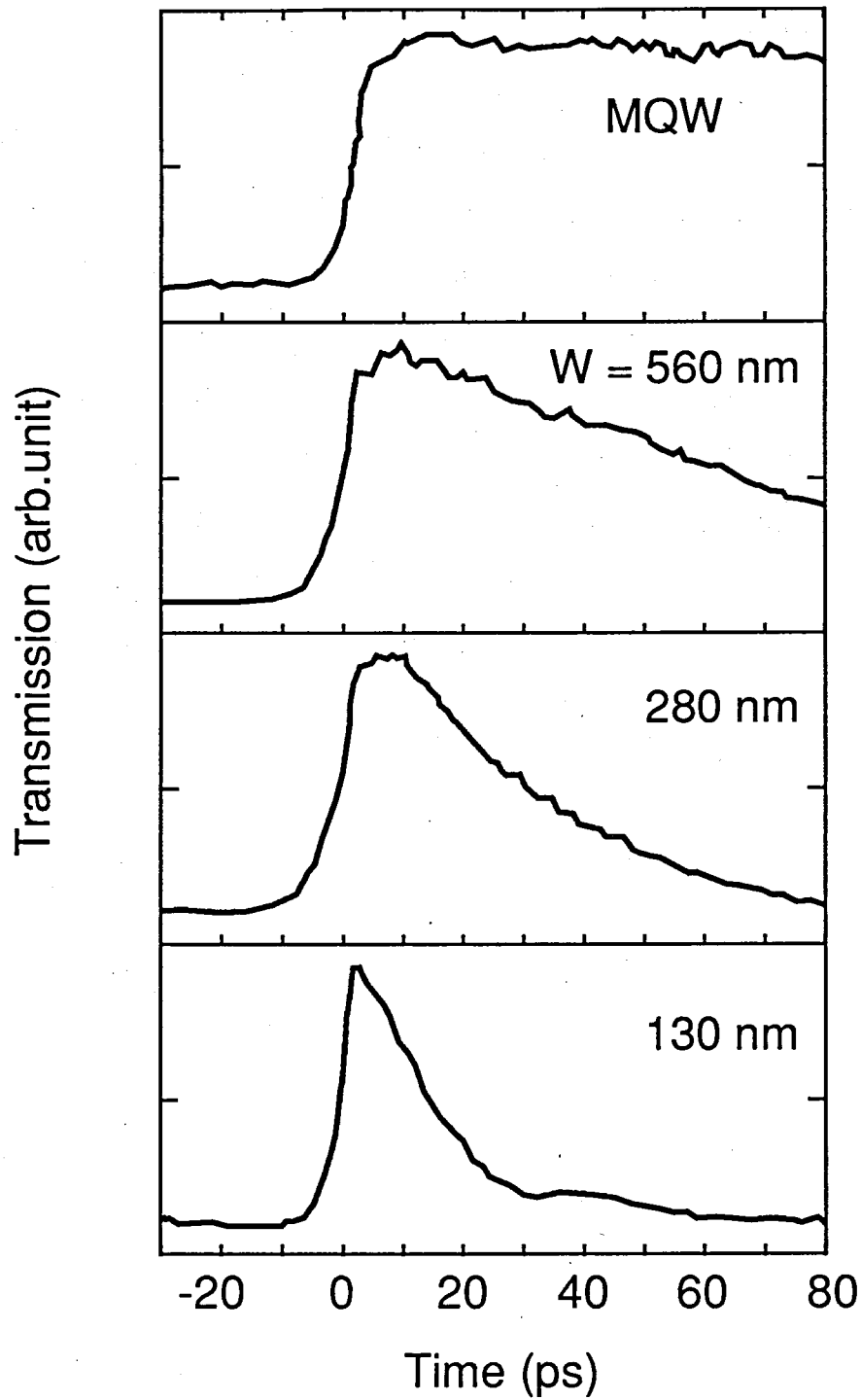


Fig. 5-6. Time-resolved transmission of the lowest excitonic absorption peak of quantum-well wires. The transmission change of a conventional MQW is also shown.

Figure 5-6 shows the observed time-dependent transmission at the lowest heavy-hole exciton transition in MQW wires. After photoexcitation, the unprocessed MQW does not show a clear absorption recovery in this time region indicating a lifetime of nanoseconds. However, the recovery time of MQW wires is remarkably reduced to 11 ps for 130-nm-wide wires. Note also that they show a complete recovery. This means that MQW wires can be applied to picosecond optical devices operating at a high repetition rate. Figure 5-7 shows the initial absorption change, normalized by wire areas, after the photoexcitation of MQW wires. The striking feature is that these absorption change, even for wires as small as 130 nm in

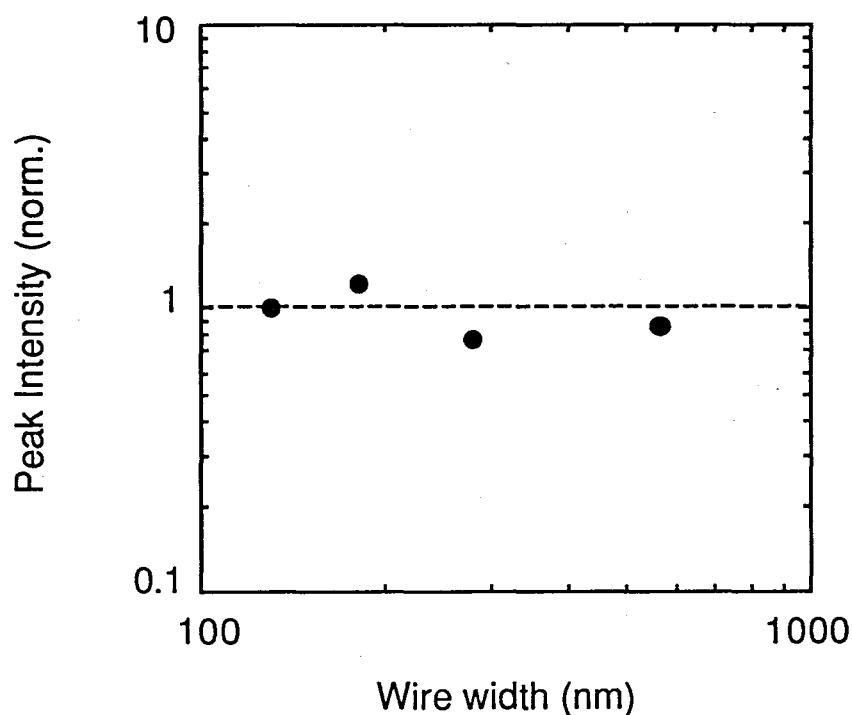


Fig. 5-7. The magnitude of the initial absorption change, normalized by the wire area, after the photoexcitation of MQW wires. The absorption change of MQW is normalized to 1.

width, are almost the same as those of conventional MQWs. These results indicate that the damages which deteriorate the excitonic optical nonlinearity are not in the net area of our samples.

### 5.3 Discussion

The experimental recovery time is plotted logarithmically as a function of the wire width in Fig. 5-8. The reduction of the recovery time dependent on the wire width indicates that most of the recombination is not achieved through damages in the net area of wires. Assuming that the lateral diffusion of photoexcited carriers and subsequent recombination at the sidewalls to be the main absorption recovery mechanism, we solve the diffusion equation:<sup>7,8)</sup>

$$\frac{\partial n}{\partial t} = D \frac{\partial^2 n}{\partial x^2} - \frac{n}{\tau_0} ;$$

$$\left( \pm D \frac{\partial n}{\partial x} = -S n, \text{ at } x = \pm \frac{W}{2} \right) , \quad (5-1)$$

where  $n$  is the carrier concentration,  $D$  the diffusion coefficient,  $\tau_0$  the intrinsic lifetime of the carrier,  $S$  the surface recombination rate. The solid line in Fig. 5-8 indicates the calculated result when we use surface velocity ( $S$ ) of  $5 \times 10^5$  cm/s and diffusion coefficient of  $20 \text{ cm}^2/\text{s}$ . The surface velocity is consistent with the room temperature recombination velocity at the free GaAs-surface ( $\sim 10^6$  cm/s).<sup>9,10)</sup> In the condition that diffusion controls the absorption recovery, the recovery time is expected to be proportional to square of the wire width because of the

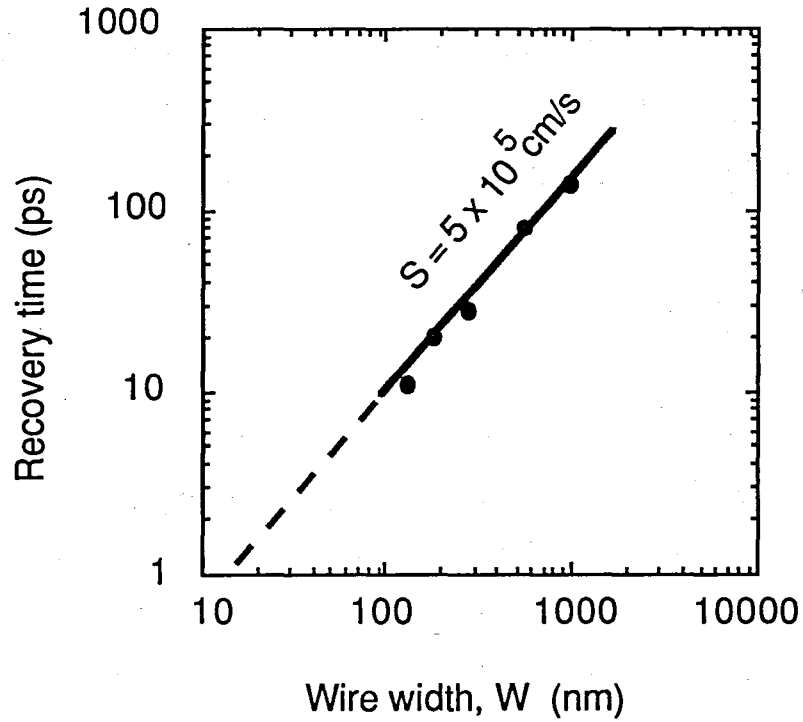


Fig. 5-8. The dependence of recovery time on wire width. The solid line indicates the calculated recovery time for diffusion coefficient of  $20 \text{ cm}^2/\text{s}$  and surface velocity of  $5 \times 10^5 \text{ cm/s}$ .

random walk process of diffusion. However if surface recombination controls the absorption recovery, the recovery time is proportional to the wire width.<sup>7)</sup> The almost linear dependence of our experimental data shows that the slow surface velocity controls the absorption recovery in our wire structures.

The clear dependence of the recovery time on the wire width suggests that the recovery time could be tuned in practical applications. From the extrapolation of experimental data, we expect a 1-ps-recovery for quantum-well wires having a width less than 20 nm.



## 5.4 Summary

We studied the excitonic absorption bleaching of GaAs/AlGaAs MQW wires by the time-dependent absorption measurement. In MQW wires, photoexcited carriers diffuse toward the sidewall surfaces and recombine there faster than the recombination lifetime in bulk. We made MQW wires as small as 130 nm using FIB lithography and electron cyclotron-resonance chlorine-plasma etching. We showed that the strong optical nonlinearity of excitons is preserved, even in wires on the order of 100 nm, and that the recovery time is reduced to 11 ps for 130-nm-width wires showing a complete recovery. The clear dependence of the recovery time on the wire width suggests that the recovery time could be tuned in practical applications. We believe that these results indicate the high potential of the narrow MQW wires for high speed optical device applications. By reducing the present MQW wire width to 20 nm, there is a possibility to produce quantum wires with a 1 ps recovery at room temperature.

## REFERENCES

- 1) J. L. Jewell, A. Scherer, S. L. McCall, A. C. Gossard, and J. H. English: Appl. Phys. Lett. 51 (1987) 94.
- 2) G. Mayer, B. E. Maile, R. Germann, A. Forchel, P. Grambow, and H. P. Meier: Appl. Phys. Lett. 56 (1990) 2016.
- 3) A. Tackeuchi, H. Kitada, H. Arimoto, Y. Sugiyama, A. Endoh, Y. Nakata, T. Inata, and S. Muto: Appl. Phys. Letters 59 (1991) 1114.
- 4) J. P. van der Ziel and M. Ilegens: Applied Optics 14 (1975) 2627.
- 5) H. Kitada, Y. Arimoto, A. Endoh, A. Tackeuchi, Y. Sugiyama, T. Inata, and S. Muto, unpublished.
- 6) A. Tackeuchi, H. Kitada, H. Arimoto, T. Inata, Y. Sugiyama, Y. Yamaguchi, Y. Nakata, S. Nakamura, and S. Muto, to be published in Surf. Science.
- 7) G. Mayer, B. E. Maile, R. Germann, A. Forchel, and H. P. Meier: Superlattices and Microstructures 5 (1989) 579.
- 8) A. Endoh, H. Kitada, H. Arimoto, A. Tackeuchi, Y. Yamaguchi, Y. Nakata, Y. Sugiyama, T. Inata, and S. Muto, unpublished.
- 9) H. C. Casey, Jr., E. Buehler: Appl. Phys. Lett. 30 (1977) 247.
- 10) C. J. Sandroff, R. N. Nottenburg, J. C. Bischoff, and R. Bhat: Appl. Phys. Lett. 51 (1987) 33.

## CHAPTER 6

### Direct observation of picosecond spin relaxation of excitons in GaAs/AlGaAs quantum wells using spin-dependent optical nonlinearity

#### 6.1 Introduction

Spin relaxation is of interest from the viewpoints of fundamental physics as well as possible applications of "spin dependent optical nonlinearity". Spin relaxation of carriers in semiconductors has been studied by measuring the steady-state luminescence<sup>1)</sup> and the time-resolved luminescence<sup>2)</sup> with circular polarization. Both measurements, however, have limitations. In steady-state luminescence measurements, several assumptions have to be made to derive the spin relaxation time.<sup>1)</sup> The resolution of time-resolved luminescence has been on the order of 10 ps.<sup>3)</sup> Also, in both measurements, it has been difficult to obtain the spin relaxation time at 300 K, the most practical temperature, due to the low luminescence efficiency. Therefore, the understanding of the spin relaxation kinetics at high temperatures or in the high-speed region has remained vague. In this chapter, we report the first direct observation of the spin relaxation kinetics of excitons in multiple quantum wells (MQWs) at room temperature with a time resolution of 1ps, using time-resolved polarization absorption measurements.<sup>4)</sup>

#### 6.2 Rate equations of spin relaxation

Spin-aligned carriers are created<sup>5)</sup> when electrons are excited by circularly polarized light as shown in Fig. 6-1. By matching the excitation laser wavelength to the electron-heavy hole transition energy,

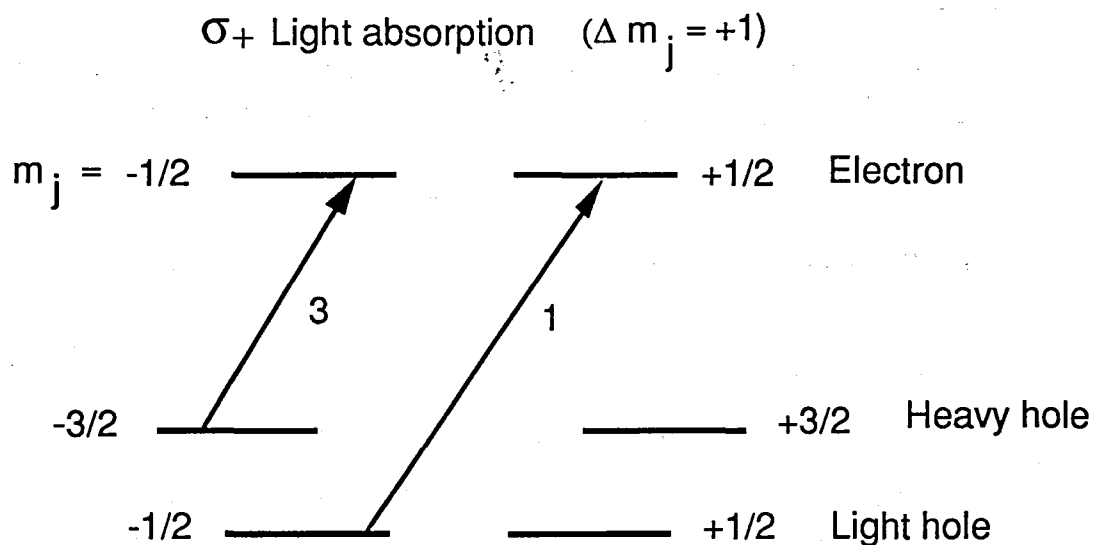


Fig. 6-1. Absorption transitions for GaAs quantum wells with circular polarized light. The transitions involving heavy ( $m_j = 3/2$ ) and light ( $m_j = 1/2$ ) holes have relative strengths of 3 and 1. The quantization axis is normal to the QW interfaces.

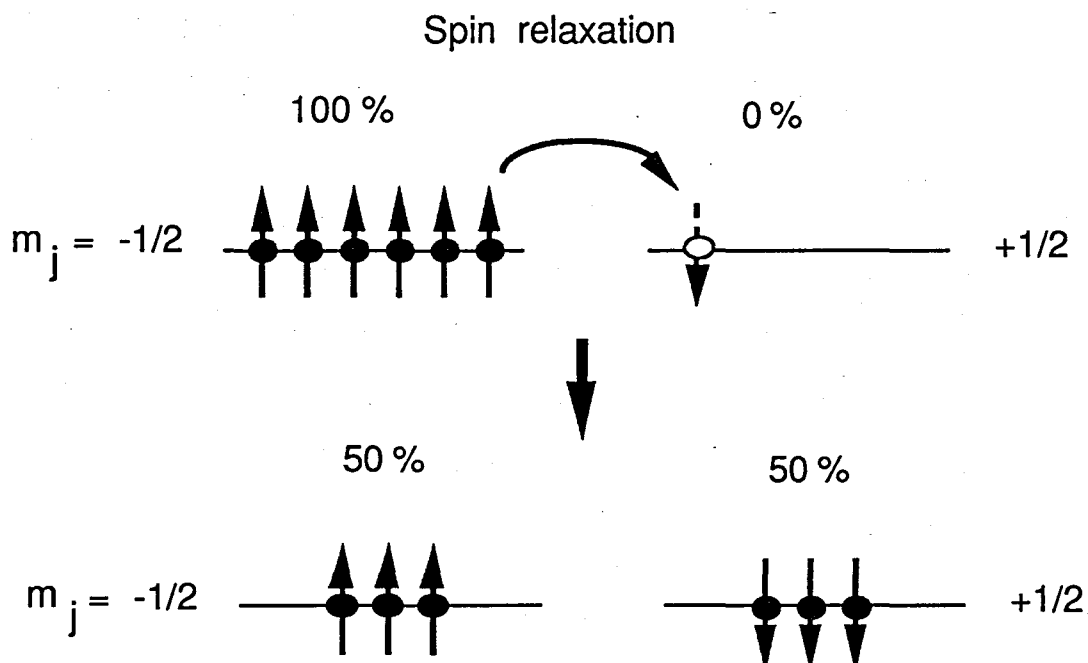


Fig. 6-2. Schematic diagram of spin relaxation process.

we can excite the fully spin-polarized electrons from the heavy hole level in quantum wells. In the absence of magnetic field, the fully spin-polarized electrons relax with a spin relaxation time,  $\tau_s$ , to an equilibrium with 50%-up and 50%-down spins (Fig. 6-2).

The population change of spin-polarized carriers resulting from a  $\delta$ -excitation pulse is described by the following rate equations:<sup>2)</sup>

$$\frac{dN_+}{dt} = -\frac{N_+}{\tau_r} - \frac{N_+}{\tau_s} + \frac{N_-}{\tau_s}, \quad (6-1)$$

$$\frac{dN_-}{dt} = -\frac{N_-}{\tau_r} + \frac{N_+}{\tau_s} - \frac{N_-}{\tau_s}. \quad (6-2)$$

$\tau_r$  is the recombination time and  $\tau_s$  is the spin relaxation time. The solutions are

$$N_+ = \frac{N_0}{2} \left(1 + e^{-\frac{2t}{\tau_s}}\right) e^{-\frac{t}{\tau_r}}, \quad (6-3)$$

$$N_- = \frac{N_0}{2} \left(1 - e^{-\frac{2t}{\tau_s}}\right) e^{-\frac{t}{\tau_r}}. \quad (6-4)$$

Here,  $N_0$  is the initial population of spin-up carriers. For  $\tau_r \gg \tau_s$ , the population of spin-up carriers exponentially decays after the excitation with a time constant of  $\tau_s/2$  toward an equilibrium value of  $N_0/2$  (Fig. 6-3). Also, the population of spin-down carriers exponentially rises with a time constant of  $\tau_s/2$ . The sum of Eqs.(6-1) and (6-2) describes the decay of the total excited carrier population:

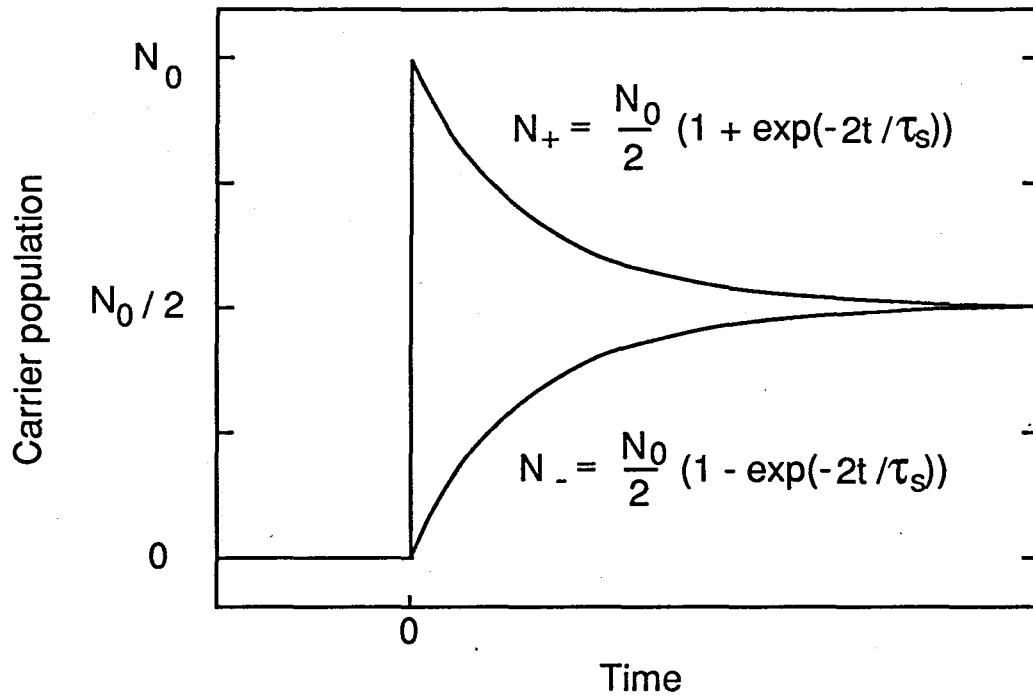


Fig. 6-3. Calculated population changes of carriers by spin relaxation after  $\delta$ -excitation for  $\tau_r \gg \tau_s$ .

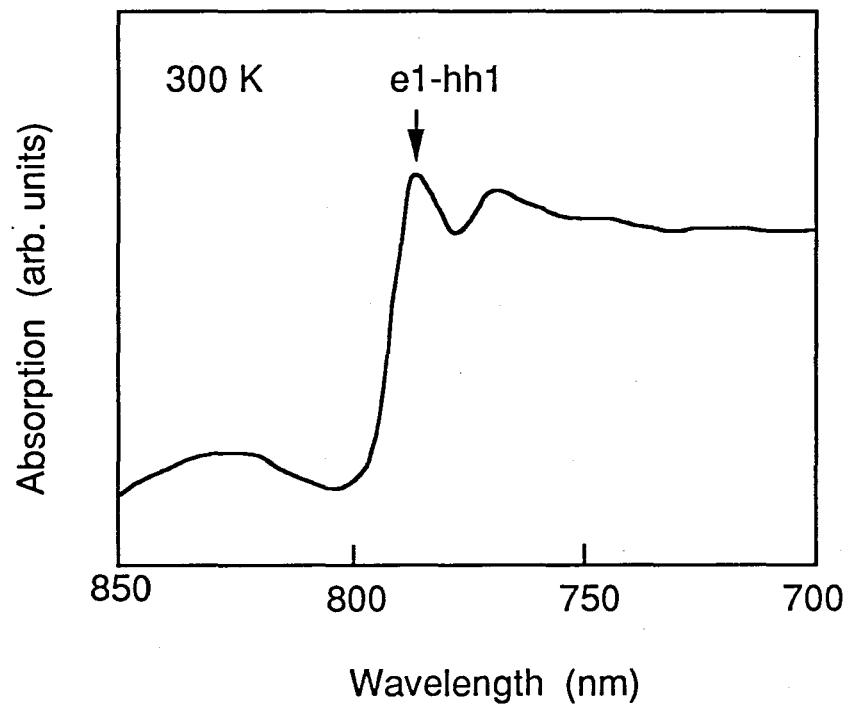


Fig. 6-4. Absorption spectrum of a GaAs/AlGaAs MQW. The arrow shows the excitonic absorption peak studied.

$$\frac{d(N_+ + N_-)}{dt} = -\frac{N_+ + N_-}{\tau_r} \quad (6-5)$$

This time transient can be observed independently using a linearly polarized light.

### 6.3 Experiment

The sample we investigated consists of 120 periods of alternating 4.5-nm-thick GaAs quantum wells and 4.0-nm-thick  $\text{Al}_{0.51}\text{Ga}_{0.49}\text{As}$  barriers. This structure was grown on a semi-insulating (100) GaAs substrate by molecular beam epitaxy. After the growth, the substrate was removed by selective etching over a part of the sample. Figure 6-4 shows the absorption spectrum of the MQW. The arrow shows the studied e1-hh1 exciton peak.

We used spin-dependent optical nonlinearity for the observation of spin relaxation process as shown in Fig. 6-5. After right circularly polarized photoexcitation,  $\sigma_+^{\text{pump}}$ , the populations of carriers,  $N_+$  ( $N_-$ ), with up (down) spin along the direction of light propagation, are probed by right (left) circularly polarized probe pulse,  $\sigma_+^{\text{probe}}$  ( $\sigma_-^{\text{probe}}$ ). In the small signal regime, the absorption change is proportional to the carrier population. Therefore, the absorption change for  $(\sigma_+^{\text{pump}}, \sigma_+^{\text{probe}})$  shows the population change of up-spin carriers pumped by the right-circular light. Also, the absorption change for  $(\sigma_+^{\text{pump}}, \sigma_-^{\text{probe}})$  shows the population change of down-spin carriers. The orthogonal linear polarization case corresponds to the spin-independent carrier relaxation described by Eq. (6-5).

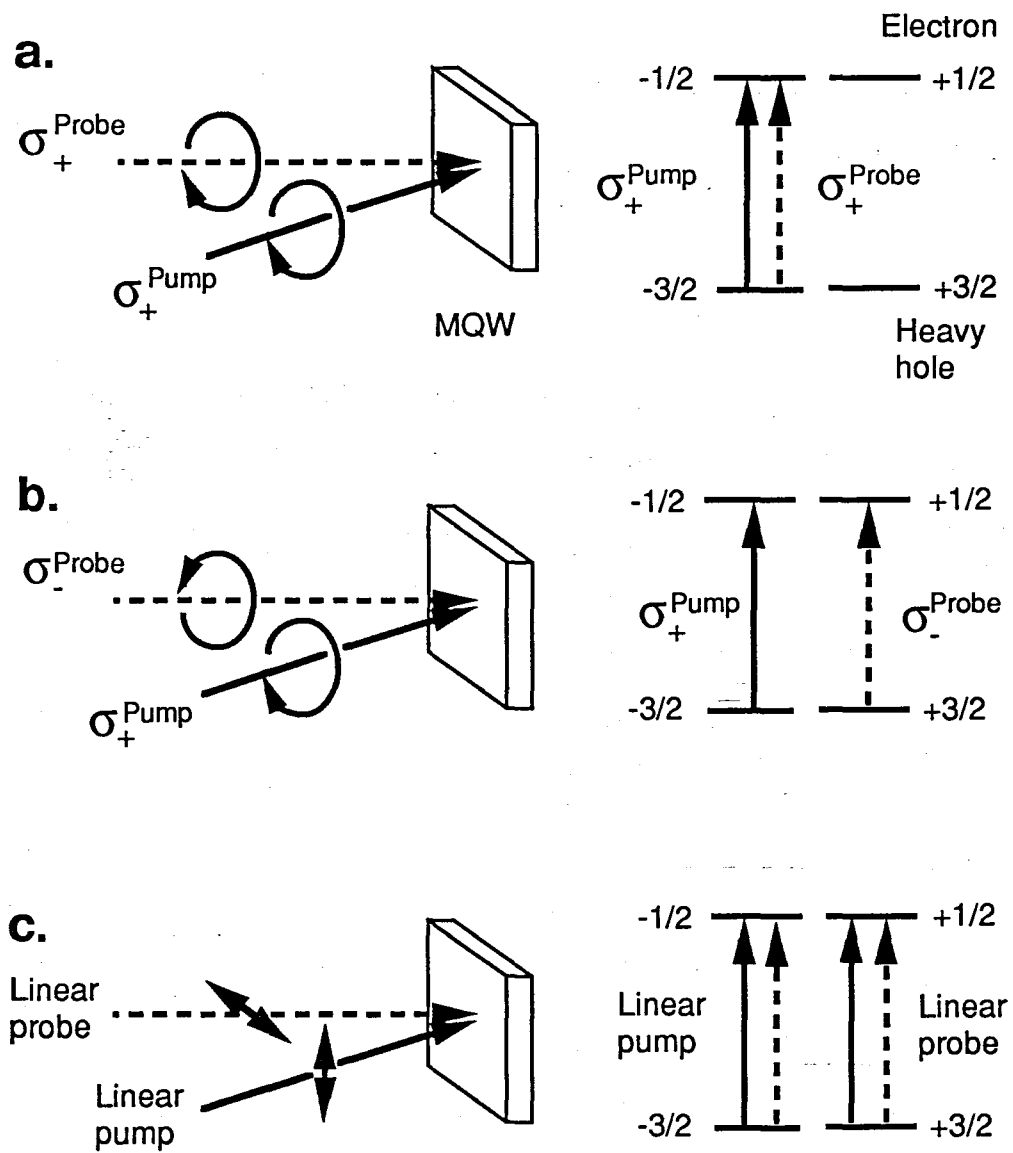


Fig. 6-5. Measurement principle using the spin-dependent optical nonlinearity.



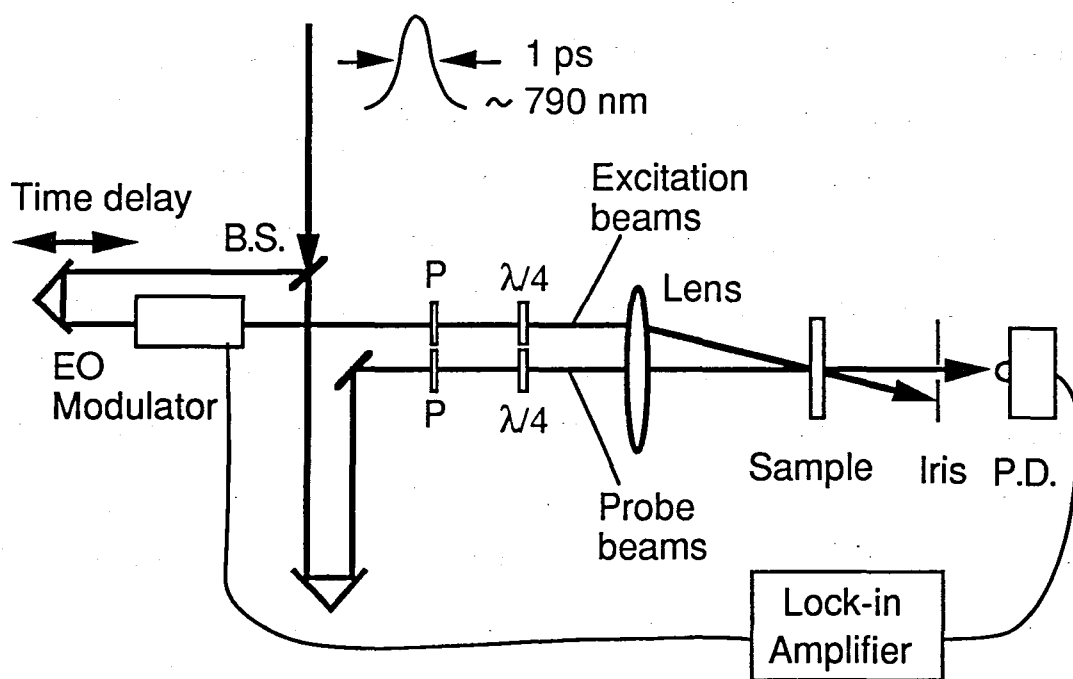


Fig. 6-6. Experimental setup of time-resolved polarization absorption measurements: B.S., beamsplitter; P, polarizer;  $\lambda/4$ , quarter-wave plate; P.D., photodiode.

Fig. 6-6 shows the pump-probe absorption measurement system. Time resolution in this system is determined only by the duration of the optical pulses. We used 1 ps optical pump and probe pulses at 12 ns intervals. These were produced by a tunable mode-locked styryl dye laser synchronously pumped by compressed neodymium YAG laser pulses. The wavelengths of the pump and probe pulses were tuned to the lowest electron-heavy hole excitonic absorption peak at 787 nm marked by the arrow in Fig. 6-4. The linearly polarized outputs of the laser pass through a quarter-wave plate with an optic axis orientation that can be rotated to produce either left or right circularly polarized light. The pump beam is chopped by an electro-optic modulator at 6 MHz to avoid dye laser noise in low-frequency region. For all the measurements, the

pump beam intensity was 0.3 mW in front of the sample, and the probe beam intensity was fixed to about one-tenth the pump beam intensity. They were focused on a spot 15  $\mu\text{m}$  in diameter on the sample. The probe signal was synchronously detected by a lock-in amplifier.

The observed time dependence of transmission at the heavy hole exciton peak is shown in Fig. 6-7. We observed a clear exponential decay for circular polarization ( $\sigma_{+}^{\text{pump}}, \sigma_{+}^{\text{probe}}$ ), and a clear exponential rise for anti-circular polarization ( $\sigma_{+}^{\text{pump}}, \sigma_{-}^{\text{probe}}$ ). The initial absorption change for the same circularly polarized case is about twice that for the linear perpendicular case, and decays toward a steady-state level half its initial value. The absorption change for the anticircularly polarized case rises from 0 and levels off at the same steady-state level. The magnitude of the absorption change after about 30 ps is almost the same in all cases. The observed absorption change indicates the decay in the population of up-spin carriers pumped by the right-circular light and the accumulation of down-spin carriers described by Eqs. (6-3) and (6-4). It should be noted that this is the first direct observation of the transient behavior of spin relaxation from the moment of excitation with a sufficiently high time resolution (1 ps). It is especially interesting that the symmetrical behavior of up-spin carrier decay and down-spin carrier accumulation is clearly observed. In linear polarization, however, we did not observe any exponential decay within the full optical delay stroke of 120 ps. Since this case corresponds to the spin-independent carrier relaxation described by Eq. (6-5), this means that the lifetime,  $\tau_r$ , of carriers in our sample is much longer than the spin relaxation time,  $\tau_s$ .

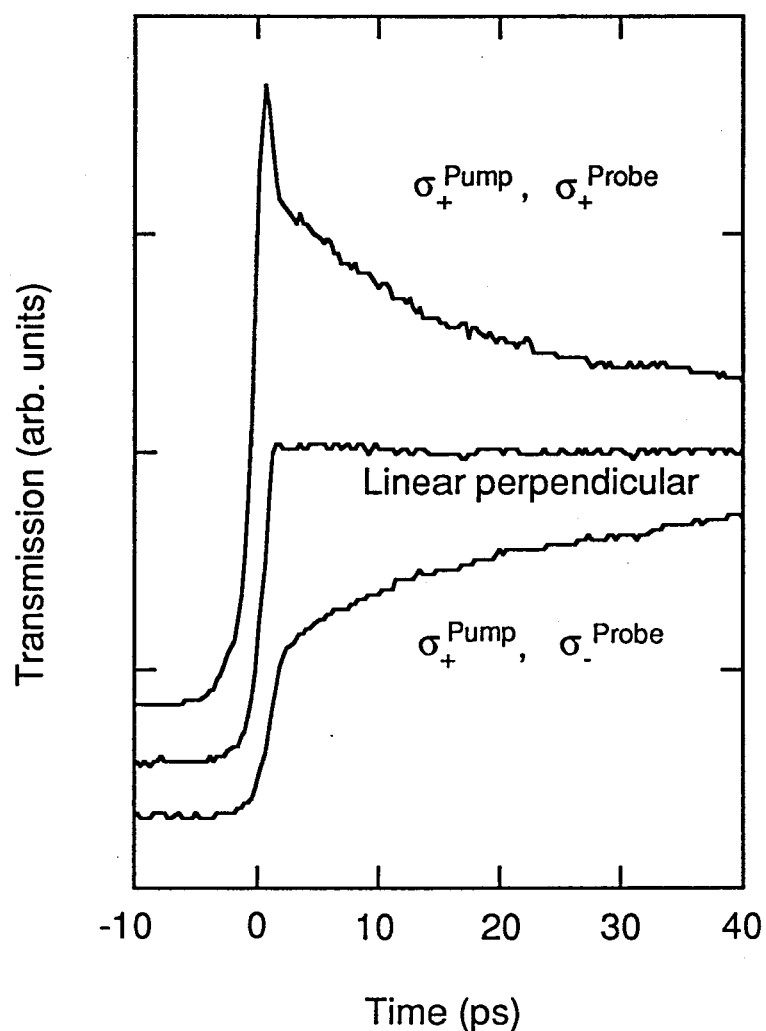


Fig. 6-7. Time evolution of the transmission of the excitonic absorption peak. " $\sigma_+^{\text{Pump}}, \sigma_+^{\text{Probe}}$ " indicates right circularly polarized excitation and right circularly polarized probe. " $\sigma_+^{\text{Pump}}, \sigma_-^{\text{Probe}}$ " indicates the right circularly polarized excitation and left circularly polarized probe. "Linear perpendicular" indicates the linear polarized excitation and linear polarized probe perpendicular to the excitation polarization.

To better understand the spin relaxation kinetics, we subtracted the result of the anticircular polarization from the result of the linear polarization, as shown in Fig. 6-8. The clear initial peaks in curve (a) and in the same circularly polarization result ( $\sigma_{+}^{\text{pump}}$ ,  $\sigma_{+}^{\text{probe}}$ ) curve in Fig. 6-8 can be attributed to the coherent artifact<sup>6)</sup> that is generated due to pump beam diffraction by the optical transient grating in the sample. The reduction of the peak in curve (b) compared to curve (a) is consistent with the fact that the coherent artifact becomes relatively small for anticircular polarization and linear perpendicular polarization.<sup>7,8)</sup> Except for these peaks, Fig. 6-8 clearly shows the exponential decays of the spin relaxation.

The shape of the decay was calculated from the rate equations (6-1) and (6-2) with the addition of an excitation term corresponding to a gaussian laser pulse of 1.0 ps at full width of half maximum. Since the lifetime is much longer than the spin relaxation time, we neglected the term for lifetime ( $\tau_r$ ). The dashed curves in Fig. 6-8 show fits of single exponential decay of 15 and 16 ps for curves (a) and (b) respectively. From curve (b) which has the little effect of coherent artifact, we deduced the relaxation time,  $\tau_s/2$ , of 16 ps.

## 6.4 Discussion

Fundamentally, the mechanism of spin relaxation in MQWs is not yet clear. It is known that in a GaAs crystal no hole polarization is observed,<sup>9)</sup> indicating that the holes have a spin-flip rate too high to be observed. Therefore, we could attribute the observed spin relaxation to the electron spin. The D'yakonov-Perel (DP) mechanism<sup>10,11)</sup> is

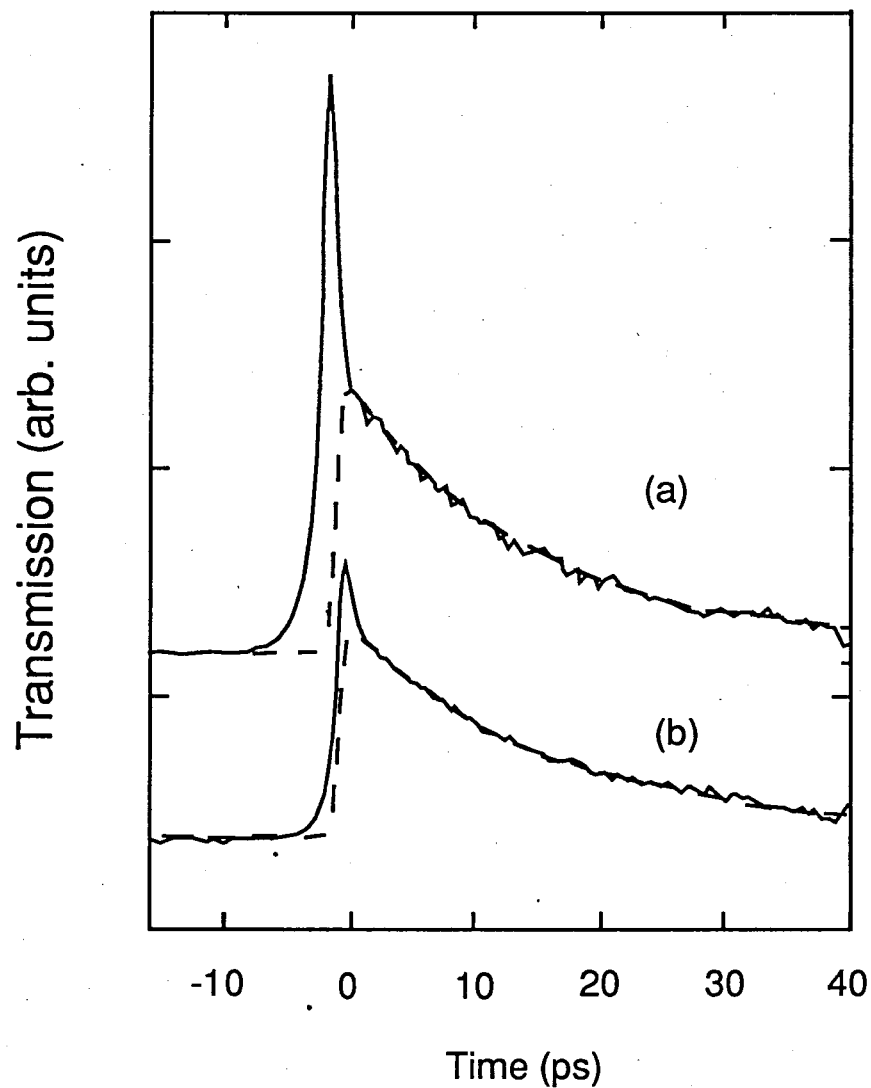


Fig. 6-8. (a) The data obtained (from Fig. 6-7) by subtraction of "Linear perpendicular" from " $\sigma_{+}^{\text{pump}}, \sigma_{+}^{\text{probe}}$ " (solid line) and the fitted curve (dashed line) with spin-relaxation time  $\tau_S$  of 30 ps. (b) The data obtained by subtraction of " $\sigma_{+}^{\text{pump}}, \sigma_{-}^{\text{probe}}$ " from "linear perpendicular" (solid line) and the fitted curve (dashed line) with spin-relaxation time  $\tau_S$  of 32 ps.

believed to determine the spin relaxation kinetics of electrons at high temperatures.<sup>12,13)</sup> The DP mechanism is due to a precession of the electron spin in a pseudomagnetic field caused by a spin-orbital splitting of the conduction band in III-V compounds. Clark et al.<sup>12,13)</sup> reported an electron spin relaxation time, dominated by the DP mechanism, of about 10 ps at 300 K for the  $\text{Al}_{0.18}\text{Ga}_{0.82}\text{As}$  crystal using steady-state experiments. Also, Miller et al.<sup>14)</sup> reported using steady-state experiments that the DP process is relevant to spin relaxation in a  $\text{GaAs}/\text{Al}_{0.28}\text{Ga}_{0.72}\text{As}$  MQW between 70 and 150 K. Although the DP mechanism usually works for free electrons in the conduction band, this mechanism of free electrons would work to relax the electron spin in excitons through the fast thermalization (0.2-0.3 ps<sup>15,16)</sup>) of electrons in free or excitonic states. Therefore, it seems natural to believe that we observed the electron spin relaxation by the DP mechanism in a MQW at room temperature. However, more experimental and theoretical studies are needed to unravel the spin relaxation mechanism in MQWs.

Since excitons in MQWs show a clear optical nonlinearity even at room temperature, there have been many optical device applications<sup>17-18)</sup> using normal excitonic optical nonlinearity. From this practical point of view, the observed rapid relaxation time  $\tau_s/2$  of 16 ps, which is two orders of magnitude shorter than the recombination lifetime and the large spin-dependent transmission change whose magnitude doubles that of a normally excited transmission change, as shown in Fig. 6-7, are quite attractive. We believe that spin-dependent optical nonlinearity characterized by a fast relaxation and by a large transmission change will open doors to new optical device applications.

## 6.5 Summary

We have directly observed the time transient of spin relaxation in GaAs/AlGaAs MQW using time-resolved polarization absorption measurement for the first time. The measurement uses a pump probe time resolve technique with a time resolution of 1 ps. We obtained a fast decay of spin-up carriers and a fast accumulation of spin-down carriers with a spin relaxation time of 32 ps at room temperature. The observed decay and accumulation process show a clear symmetrical time transient expected from simple rate equations. We have thus demonstrated the usefulness of this technique in extracting information on spin relaxation kinetics in semiconductors, and also shown the high potentiality of spin-dependent optical nonlinearity.

## REFERENCES

- 1) R. R. Parsons: Phys. Rev. Lett. 23 (1969) 1152.
- 2) R. J. Seymour and R. R. Alfano: Appl. Phys. Lett. 37 (1980) 231.
- 3) W. A. J. A. van der Poel, A. L. G. J. Severens, H. W. van Kesteren, and C. T. Foxon: Superlatt. Microstruct. 5 (1989) 115.
- 4) A. Tackeuchi, S. Muto, T. Inata, and T. Fujii: Appl. Phys. Letters 56, (1990) 2213.
- 5) G. Lampel: Phys. Rev. Lett. 20 (1968) 491.
- 6) E. P. Ippen and C. V. Shank, in ultrashort Light Pulses, edited by S. L. Shapiro (Springer, New York, 1977), Vol. 18, p.83.
- 7) Z. Vardeny, and J. Tauc: Opt. Commun. 39 (1981) 396.
- 8) H. J. Eichler, P. Gunter, and D. W. Pohl, Laser-Induced Dynamic Gratings (Springer, Berlin, 1986), pp. 18 and 213.
- 9) A. N. Titkov and V. I. Safarov, and G. Lampel, in Proceedings of the 14th International Conference on the Physics of Semiconductors, Edinburgh, 1979, edited by B. L. H. Wilson (Institute of Physics, Bristol, 1979), p.1031.
- 10) M. I. D'yakonov and V. I. Perel': Fizika Tverdogo Tela. 13 (1971) 3581 [Sov. Phys. Solid State 13 (1972) 3023].
- 11) M. I. D'yakonov and V. I. Perel': Zh. Eksp. Teor. Fiz. 65 (1973) 362 [Sov. Phys. JETP 38 (1974) 177].
- 12) A. H. Clark, R. D. Burnham, D. J. Chadi, and R. M. White: Phys. Rev. B 12 (1975) 5758.
- 13) A. H. Clark, R. D. Burnham, D. J. Chadi, and R. M. White: Solid State Commun. 20 (1976) 385.
- 14) R. C. Miller, D. A. Kleinmann, W. A. Nordland, Jr., and A. C. Gossard: Phys. Rev. B22 (1980) 863.



- 15) W. H. Knox, C. Hirlimann, D. A. B. Miller, J. Shah, D. S. Chemla, and C. V. Shank: Phys. Rev. Lett. 56 (1986) 1191.
- 16) W. H. Knox, R. L. Fork, M. C. Downer, D. A. B. Miller, D. S. Chemla, C. V. Shank, A. C. Gossard, and W. Wiegmann: Phys. Rev. Lett. 54 (1985) 1306.
- 17) H. M. Gibbs, S. S. Tarng, J. L. Jewell, D. A. Weinberger, K. Tai, A. C. Gossard, S. L. McCall, A. Passner, and W. Wiegmann: Appl. Phys. Lett. 41 (1982) 221.
- 18) A. Migus, A. Antonetti, D. Hulin, A. Mysyrowicz, H. M. Gibbs, N. Peyghambarian, and J. L. Jewell: Appl. Phys. Lett. 46 (1985) 70.

## CHAPTER 7

# Picosecond Characterization of InGaAs/InAlAs Resonant Tunneling Barrier Diode by Electro-Optic Sampling

### 7.1 Introduction

Recently researchers have been greatly interested in resonant tunneling<sup>1,2)</sup> and its applications.<sup>3)</sup> The applications of resonant tunneling, represented by resonant tunneling barrier (RTB) diode, use the switching over its negative differential resistance (NDR) region to do a new logic operation. There is a new aspect about the switching process between the peak and the valley in the I-V characteristic curve, since it is not governed by electric factors such as RC time constant alone. The new factor is a quantum-mechanical state-lifetime,<sup>4-6)</sup>  $\tau_s$  ( $= \hbar / \Delta E_{FWHM}$ , where  $\Delta E_{FWHM}$  is the full energy width at half maximum of tunneling probability), of carriers in the RTB diode's quantum well. The carriers confined in the well need a finite time for escape using tunneling. Usually the statelifetime is equal or faster than picoseconds and the switching time is also in picoseconds region. This makes the observation of the switching process difficult. Mourou et al.<sup>7,8)</sup> were the first to use electro-optic sampling (EOS)<sup>9)</sup> for the measurement of the RTB diode's switching. EOS has a very high time resolution of about 1 ps. They reported the observation of the 1.9 ps-switching for a GaAs/AlAs RTB diode.

In this chapter, we study the switching of InGaAs/InAlAs RTB diodes using electro-optic sampling.<sup>10,11)</sup> InGaAs/InAlAs RTB diodes<sup>12,13)</sup> have a high peak-to-valley ratio over 5 at room temperature. This is better than that of the conventional GaAs/AlGaAs RTB diodes between 2 and 3. We made three kinds of InGaAs/InAlAs

RTB diodes with different barrier thickness. The RTB samples were designed to have sufficiently longer switching times than the EOS time-resolution to ensure experimental accuracy. We propose a new equivalent circuit model of the RTB diode including quantum mechanical effect and compare it with the experimental switching behavior.

## 7.2 Experiment

### 7.2.1 Sample structures of RTB diodes.

Three symmetrical RTB structures were studied. These structures have an identical 4.4 nm InGaAs quantum well and 5.3 nm, 5.6 nm, and 5.9 nm InAlAs barriers. These RTB regions were sandwiched between two Si-doped n-InGaAs (electrode) layers (900 nm,  $N_d=1 \times 10^{17} \text{ cm}^{-3}$ ) with thin undoped InGaAs spacer layers (1.5 nm) as shown in Fig. 7-1.

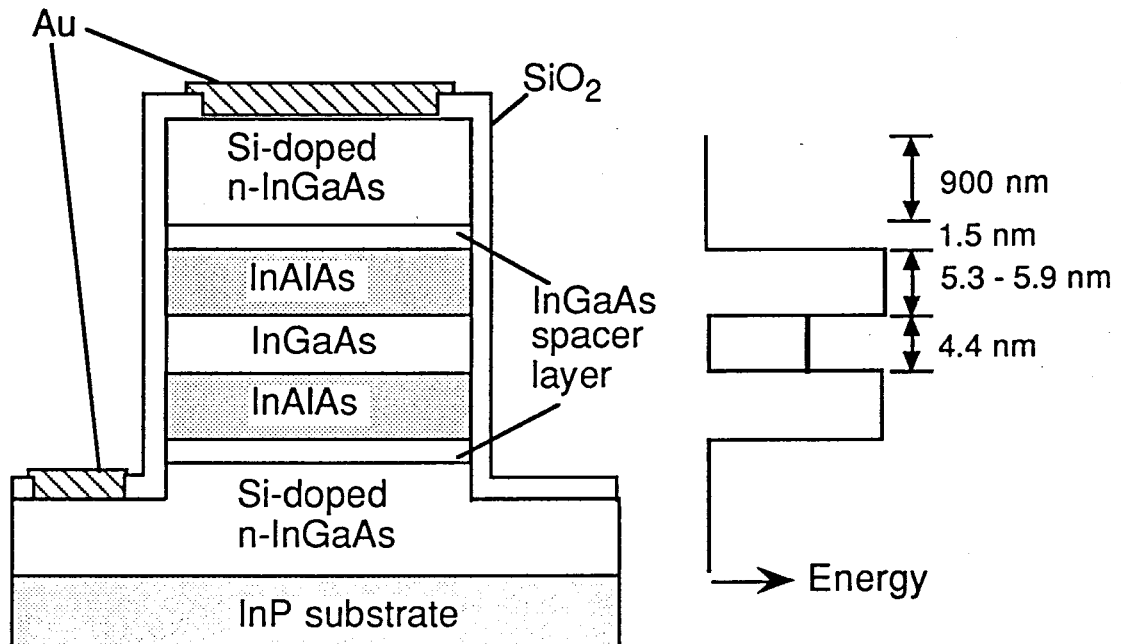


Fig. 7-1. Sample structure of the RTB diodes.

The diodes were isolated by mesa etching ( $7 \times 7 \mu\text{m}^2$ ). We calculated state-lifetime,  $\tau_c (= \hbar / \Delta E_{\text{FWHM}})$ , in an unbiased condition, using potential barrier height of 0.53 eV.<sup>14,15</sup> Its value for these structures is 7, 10, 16 ps, for the increasing order of the barrier thickness. Figure 7-2 shows the I-V characteristics of the RTB diode having a 5.9 nm InAlAs barrier layer. The I-V curve shows a large peak to valley ratio of 8 at room temperature. We measured the switching behavior from the peak to the valley using electro-optic sampling.

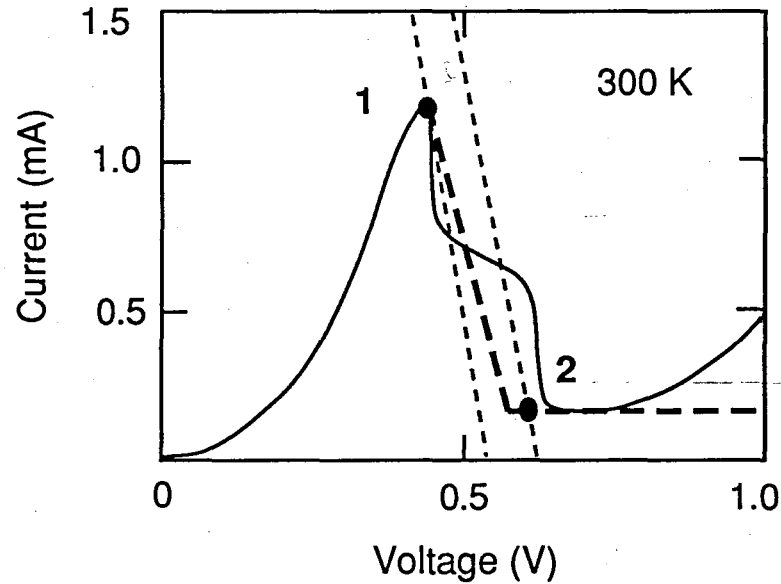


Fig. 7-2. I-V characteristics of the RTB diode with 5.9 nm InAlAs barrier layer. The thin dashed lines show the load lines. The upper load line intersects with the intrinsic I-V curve at point 1 in the peak condition. The thick dashed lines show the approximated resistance in the piece-wise-linear model.

### 7.2.2 Electro-optic sampling of RTB diodes

Electro-optic sampling is a kind of pump-probe measurement (Fig. 7-3). We divide the optical pulses into the pump pulses to excite the photoconductive switch and probe pulses to detect the electric signal. By changing the optical path length, we generate the time difference between the pump and the probe pulses. The EOS head we used consists of a GaAs photoconductive switch and the InGaAs/InAlAs RTB diode formed on a semi-insulating (100) InP substrate. 50  $\mu\text{m}$  coplanar transmission lines between the GaAs photoconductive switch and RTB diode are wire bonded. A LiTaO<sub>3</sub> crystal coated with a highly reflective dielectric mirror is pasted on the coplanar lines near the diode to detect the electrical response. Fig.7-4 shows the geometry of the detection part of the sampling head. The electric field of the transmission line changes the birefringence of LiTaO<sub>3</sub> crystal due to Pockels effect. The transmitted light intensity through Pockels cell inserted into two orthogonal polarizers is given by<sup>16)</sup>

$$I = I_0 \sin^2 \left( \frac{\pi V}{2V_\pi} \right), \quad (7-1)$$

where  $V$  is the applied voltage and  $V_\pi$  is the half-wave voltage (about 5kV in LiTaO<sub>3</sub>). In order to maintain the almost linear relationship between the applied voltage and the transmitted light intensity, the modulator must be biased near  $V_\pi/2$  (Fig.7-5). This condition is realized optically by the insert of a quarter wave plate between two orthogonal polarizer as shown in Fig.7-3. Near the bias point, we can rewrite eq.(7-1) as

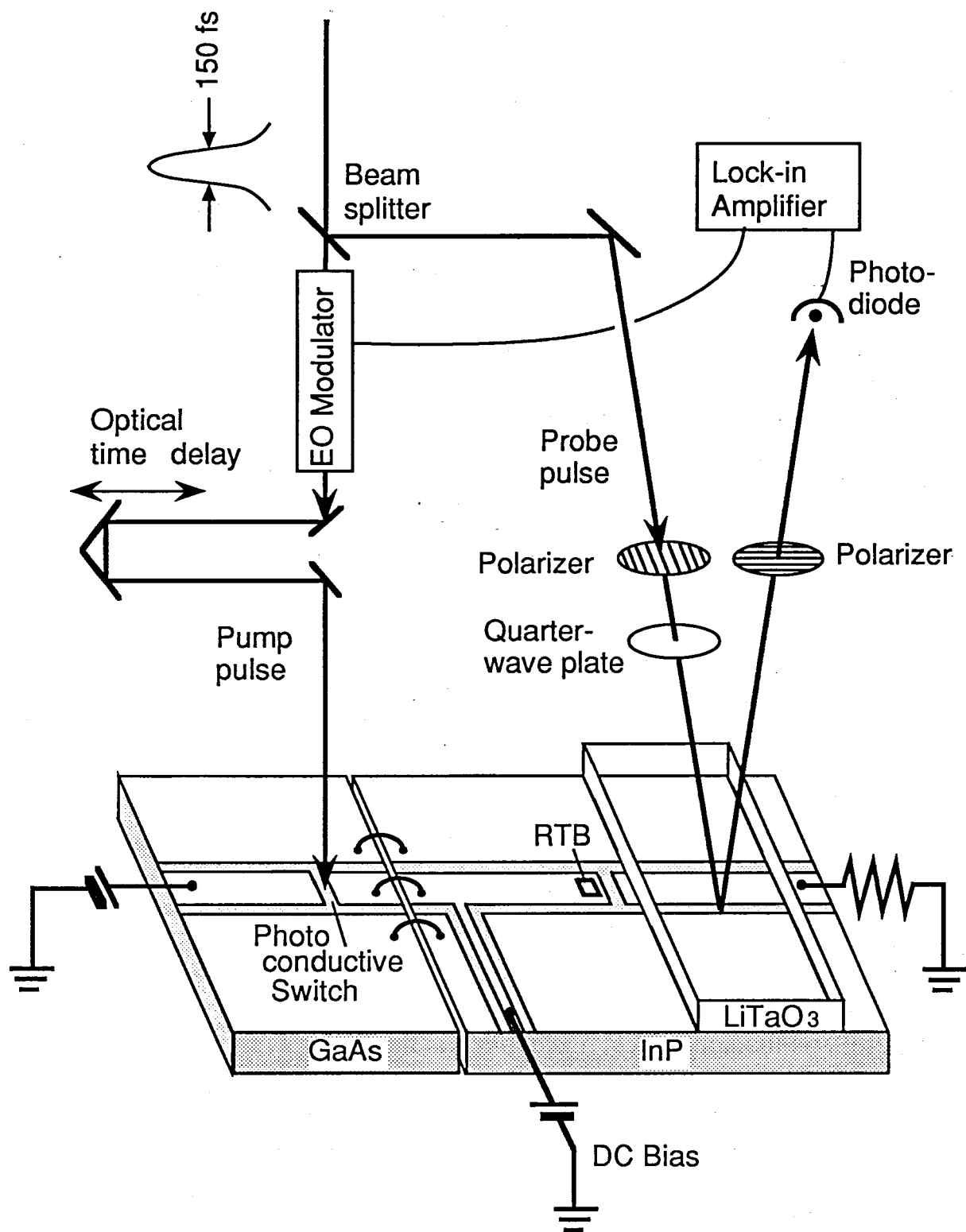


Fig. 7-3. Electro-optic sampling system.

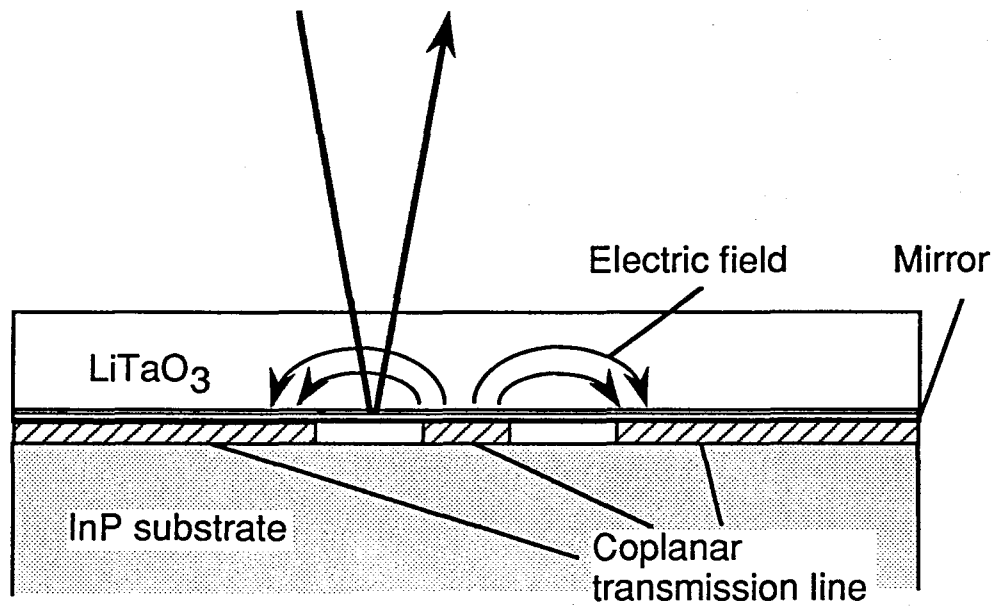


Fig. 7-4. Geometry of the detection part of the sampling head.

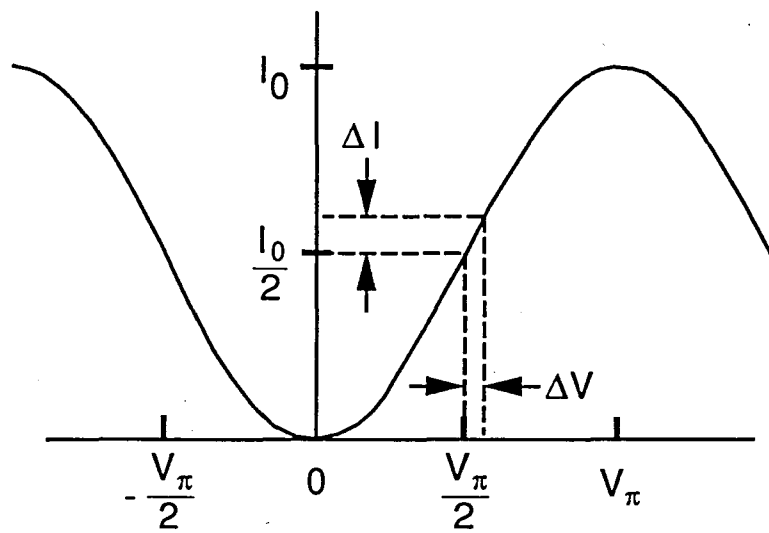


Fig. 7-5. Transmitted light intensity versus the applied voltage.

$$\Delta I = \frac{I_0}{2} \sin\left(\frac{\pi \Delta V}{V_\pi}\right) \quad (7-2)$$

Since the voltage change,  $\Delta V$ , is smaller than 120 mV, the intensity change,  $\Delta I$ , is almost proportional to  $\Delta V$ .

We used 150 fs optical pulses generated by a colliding pulse mode-locked dye laser. During the switching measurements, the DC bias is kept below the NDR region. Electric pulses produced at the photoconductive switch by the optical pump pulse travel along the transmission line and switch the RTB diode. The response of the RTB diode is detected by probe pulses using Pockels effect. The optical delay of 130 ps stroke is moved by a stepping motor. The lock-in amplification was used with an electro-optic modulator of 6 MHz chopping. The time resolution of our measurement system was 1.1 ps.

Figure 7-6 shows the applied electric signal and the switching signals of the RTB diode. The peak voltage of the applied signal was, 120 meV, 80 meV, and 40 meV for the 5.3 nm, 5.6 nm, and 5.9 nm barrier RTB diodes, respectively. Current drops (90 to 10%) with fall times of 12 ps, 28 ps, and 35 ps were observed for the 5.3 nm, 5.6 nm, 5.9 nm barrier RTB diodes, respectively. Note that the switching time decreases with the barrier thickness.

### 7.3 Discussion

We analyze the switching behavior using a new equivalent circuit model of the RTB diode. In RTB diode, the escape time of the electrons from the well is governed not only by the electric RC time



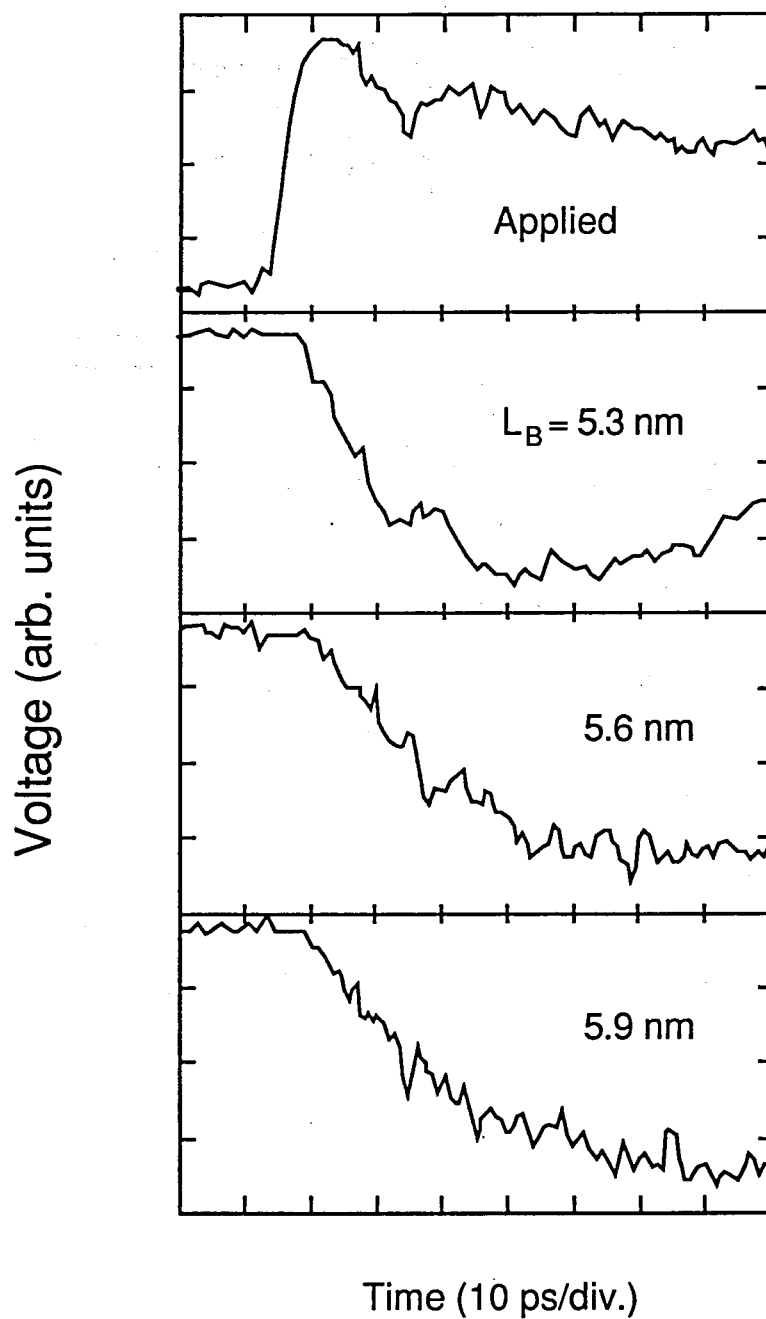


Fig. 7-6. Electro-optic signals of the applied electric signals and the response signals of the RTB diode.

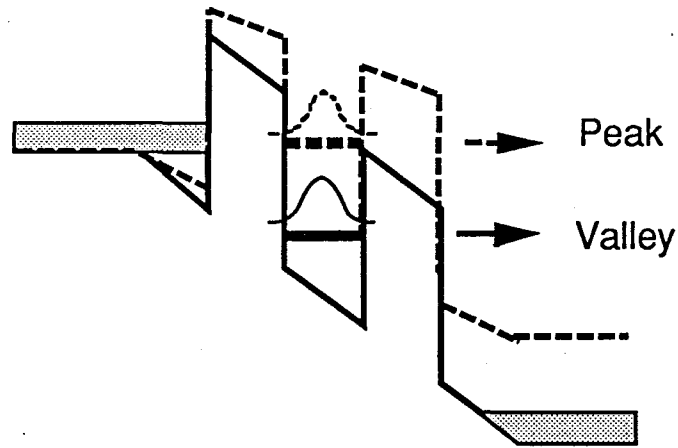


Fig.7-7. Schematic band diagram under the abrupt bias change.

constant but also by the state-lifetime. For example, after the step-like switching of the electric bias from the peak to the valley voltage, electrons remains in the well during the quantum mechanical state-lifetime (Fig.7-7). Therefore we assume that the tunneling current relaxes exponentially with the state-lifetime when the applied bias suddenly changes to the valley condition. To meet this requirement, we propose a new model shown in Fig.7-8(b). This model uses a pseudocapacitance,  $C'$ , in series with a resistance,  $R$ , as the voltage expression of the nonlinear resistance (NLR) for the tunneling current,  $I_t$ ; and uses voltage  $V_{C'}$  of pseudo-capacitance  $C'$  divided by  $R$  as the tunneling current expression. In this model, the tunneling current,  $I_t$ , is written as

$$I_t = \frac{V_{C'}}{R}, \quad (7-3)$$

and the internal voltage,  $V_{RTB}$ , of the RTB diode except the series

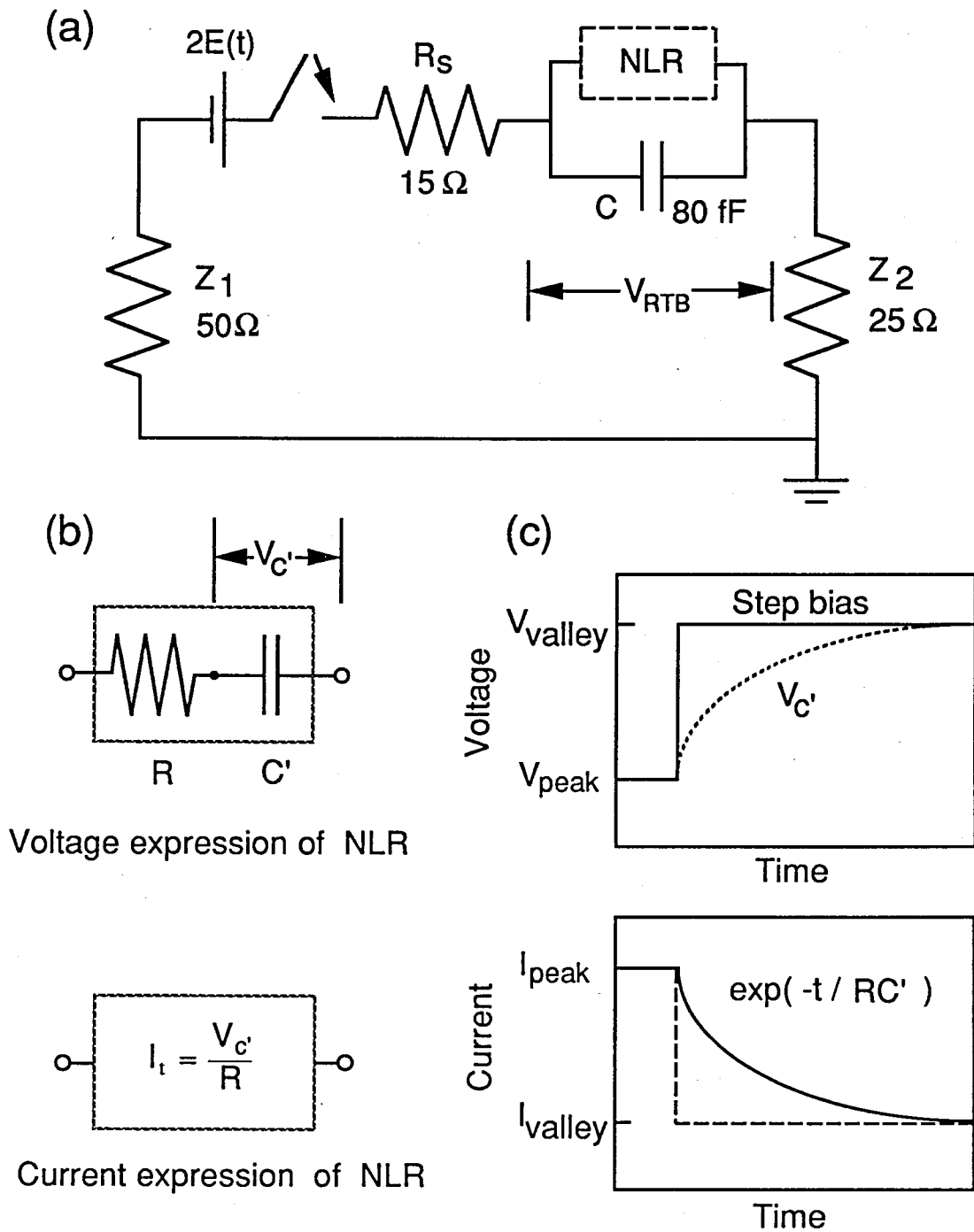


Fig. 7-8. (a) Equivalent circuit of the measurement.

(b) New equivalent circuit model of the NLR in the RTB diode.

(c) Schematic current change through the NLR with a step-like voltage change. The dashed line shows the current change through the NLR of the Esaki diode model.

resistance is

$$V_{\text{RTB}} = V_{c'} + RC' \frac{dV_{c'}}{dt} \quad (7-4)$$

When a step bias is applied to the RTB diode in the peak condition, the tunneling current falls with time constant  $RC'$  as shown in Fig.7-8(c). By setting  $RC'$  equal to the state-lifetime, we can describe the effect of quantum mechanical carriers in the RTB diode. In the limit of  $C'=0$ , this model reproduces the Esaki diode model which consists of a capacitance,  $C$ , in parallel with a resistance,  $R$ .

The circuit equation of the measurement shown in Fig.7-8(a) is

$$2 E(t) = (Z_1 + Z_2 + R_s) (I_t + C \frac{dV_{\text{RTB}}}{dt}) + V_{\text{RTB}}, \quad (7-5)$$

in terms of the tunneling current,  $I_t$ , and the internal voltage,  $V_{\text{RTB}}$ , given by eqs.(7-3) and (7-4). The smoothed curve of the actually applied signal shown in Fig.7-6 was used as  $E(t)$ . The characteristic impedance,  $Z_1$ , of the coplanar transmission lines and the characteristic impedance,  $Z_2$ , of the transmission lines under the  $\text{LiTaO}_3$  were designed to be 50 and 25  $\Omega$ , respectively. As for the parameters of the RTB diode, the capacitance,  $C$ , was estimated to be 80fF in consideration of the charge distribution around the RTB, and the series resistance,  $R_s = 15 \Omega$ , was obtained from the I-V curves of the control diode which had the same structure as the RTB diode except that RTB section was replaced by an n-InGaAs layer. The I-V characteristics of the RTB diode was approximated by the piecewise-

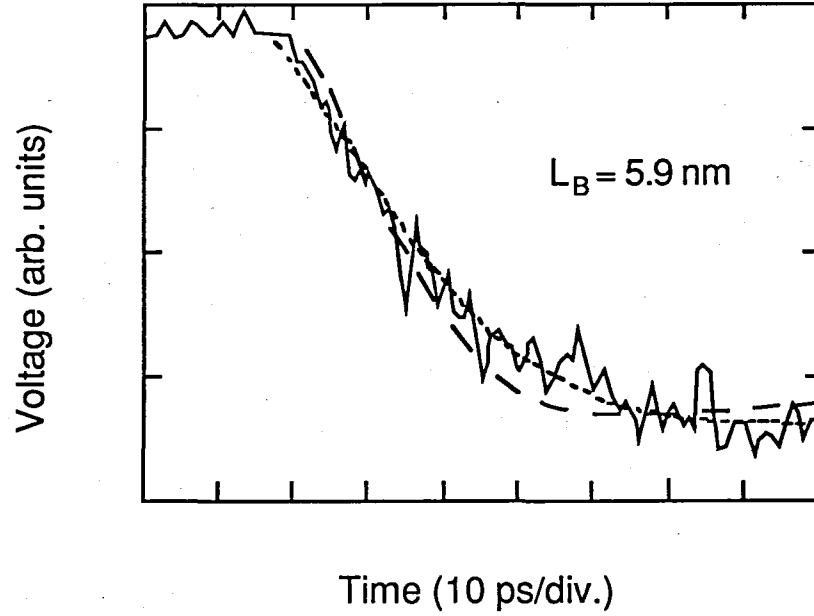


Fig. 7-9. Simulated switching curve using equivalent circuit model. The dotted line shows the best-fit curve of  $RC' = \tau_c/2$ . The dashed line shows the best-fit curve of  $RC' = 0$ .

linear model as shown in Fig.7-2. For the value of  $R$  in the NDR region, where we cannot rely on the measured I-V curve in Fig. 7-2 because of circuit oscillation, we used a fitting parameter. The resistance,  $R$ , was varied around the slope of a line connecting the points 1 and 2. Above the valley voltage, the current was approximated as constant. As another fitting parameter, we also varied the  $RC'$  time constant between  $\tau_c$ ,  $\tau_c/2$ , and 0, where  $\tau_c$  is the calculated state-lifetime. In the transient response simulation, we numerically solved circuit eqs. (7-3)-(7-5) by iteration.

For  $RC' = 0$ , we could not describe the experimental signal better than for  $RC' = \tau_c$  and  $\tau_c/2$  as shown in Table I and shown in Fig. 7-9. The deviation (residual sum of squares) of the simulated best fitting curve of  $RC' = 0$  from the experimental data became 1.3 and 2 times the

value for the new model, for the 5.6 and 5.9 nm barrier diodes, respectively. This indicates the validity of new equivalent circuit model including the quantum mechanical effect. E. R. Brown et al.<sup>17)</sup> proposed the similar equivalent circuit model of the RTB diode including quantum effect independently of us. Their model has a different circuit expression as ours, but it has the same physical character and the same transient behavior as ours. They also obtained good agreement between the new model and the electric high frequency oscillation measurement.

Table I. The electrical characteristics of the RTB diodes in the peak condition and the residual sum of squares of curve fitting.

LB (nm)	I <sub>p</sub> (mA)	V <sub>p</sub> (mV)	Residual sum of squares, $\sum (\Delta\xi_j)^2$		
			RC'=0	$\tau_c/2$	$\tau_c$
5.3	3.5	597	1	0.96	0.89
5.6	2.9	543	1	0.74	0.76
5.9	1.5	444	1	0.47	0.45

$\Delta\xi_j$  is the residual between the simulated best fitting curve and the experimental data. The residual sum of squares is normalized by the RC'=0 case.

#### 7.4 Summary

We performed dynamic characterization of the InGaAs/InAlAs RTB diode. Picoseconds switching from the peak to the valley was observed using electro-optic sampling with high time resolution. It was confirmed that the actual switching time is reduced with the reduction

of the barrier thickness. We proposed a new equivalent circuit model of the RTB diode including quantum-mechanical state-lifetime phenomenologically. The simulated switching behavior of the RTB diode using the new equivalent circuit model showed the better agreement with the experimental results than old model. This result shows that the inclusion of the quantum effect is indispensable for the circuit description of RTB diode. To realize faster switching, we must reduce both of the statelifetime and the RC time constant.

## REFERENCES

- 1) R. F. Kazarinov and R. A. Suris: Sov. Phys. Semicond. 5 (1971) 707.
- 2) R. Tsu and L. Esaki: Appl. Phys. Lett. 22 (1973) 562.
- 3) N. Yokoyama and K. Imamura: Electron. Lett. 22 (1986) 1228.
- 4) B. Ricco and M. Ya. Azbel: Phys. Rev. B29 (1984) 1970.
- 5) H. C. Liu and D. D. Coon: Appl. Phys. Lett. 50 (1987) 1246.
- 6) T. C. L. G. Sollner, E. R. Brown, W. D. Goodhue and H. Q. Le: Appl. Phys. Lett. 50 (1987) 332.
- 7) G. Mourou, K. Meyer, J. Whitaker, M. Pessot, R. Grongin and C. Caruso, Proc. 2nd OSA-IEEE (LEOS), Incline Village, Nevada, 1987 (Springer-Verlag, Berlin, 1987) p.40.
- 8) J. F. Whitacker, G. A. Mourou, T. C. L. G. Sollner and W. D. Goodhue: Appl. Phys. Lett. 53 (1988) 385.
- 9) J. A. Valdmanis, G. A. Mourou and C. W. Gabel: Appl. Phys. Lett. 41 (1982) 211.
- 10) A. Tackeuchi, T. Inata, S. Muto, and E. Miyauchi, Proc. Ultrafast phenomena, Mt. Hiei, Kyoto, 1988 (Springer-Verlag, Berlin, 1988) p.182.
- 11) A. Tackeuchi, T. Inata, S. Muto, and E. Miyauchi: Jpn. J. Appl. Phys. 28 (1989) L750.
- 12) Y. Sugiyama, T. Inata, S. Muto, Y. Nakata and S. Hiyamizu: Appl. Phys. Lett. 52 (1988) 314.
- 13) S. Muto, T. Inata, Y. Sugiyama, Y. Nakata, T. Fujii and S. Hiyamizu: J. de Physique 48 (1987) Suppl. 11, p.C5-453.
- 14) Y. Sugiyama, T. Inata, T. Fujii, Y. Nakata, S. Muto, and S. Hiyamizu: Jpn. J. Appl. Phys. 25 (1986) L648.



- 15) T. Inata, S. Muto, S. Sasa, and E. Miyauchi: J. Cryst. Growth 95 (1989) 371.
- 16) B. H. Kolner, and D. M. Bloom: IEEE J. QE 22 (1986) 79.
- 17) E. R. Brown, C. D. Parker, and T. C. L.G. Sollner: Appl. Phys. Lett. 54 (1989) 934.

## CHAPTER 8

### Conclusions

We have investigated picosecond phenomena related to excitonic absorption bleaching in quantum wells and tunneling phenomena in superlattices. In particular, fast recovery of excitonic absorption after its bleaching in quantum wells is our main concern for all-optical device applications.

In chapter 2, fast recovery from the excitonic absorption bleaching in TBQ structures was proposed and demonstrated. The TBQ has a new feature that conventional superlattices will never have, that is, the control of absorption recovery time using tunneling. With the reduction of tunneling barrier thickness down to 1.7 nm, the recovery time is reduced to as short as 1 ps. This is by three orders of magnitude shorter than the recovery time of conventional MQWs, and that the fastest tunneling process ever observed, to our knowledge. We calculated the tunneling times for various scattering mechanisms and showed that the LO phonon emission process is the fastest one.

In chapter 3, we reported the time evolution of the excitonic absorption peak in resonant tunneling bi-quantum-well structures. In the resonant TBQ structure, e1-level in narrow well and e2-level in wide well are in resonant tunneling condition. We observed the reduction of absorption recovery time and the increased tail-to-peak ratio in resonant TBQ structures. By comparing with the e2-hh2 absorption change in MQW, we concluded that the increased tail-to-peak ratio in resonant TBQ can be attributed to the thermally remaining holes in the first excited subband of heavy holes.

In chapter 4, we proposed the type-II tunneling bi-quantum well (TBQ) structure which consists of a series of GaAs wells, AlGaAs barriers and AlAs layers. The type-II TBQ has no significant optical absorption except in the GaAs wells. The recovery time of the excitonic absorption bleaching of GaAs wells is reduced to 8 ps for the AlGaAs barrier thickness of 1.1 nm. Although the recovery time is slower than that of Type-I TBQs, the dependence of the recovery time on the barrier thickness is similar to that for the type-I TBQs.

In chapter 5, we studied the excitonic absorption bleaching in GaAs/AlGaAs MQW wires by the time-dependent absorption measurement. In MQW wires, photoexcited carriers diffuse toward the sidewall surfaces and recombine on the sidewall surface faster than the recombination lifetime in bulk. We made MQW wires as small as 130 nm using FIB lithography and electron cyclotron-resonance chlorine-plasma etching. We have shown that the strong optical nonlinearity of excitons is preserved, even in wires on the order of 100 nm, and that the recovery time is reduced to 11 ps for 130-nm-width wires showing complete recoveries.

In chapter 6, we observed directly the transient behavior of spin relaxation in GaAs/AlGaAs MQW using time-resolved polarization absorption measurement for the first time. We obtained a fast decay of spin-up carriers and a fast accumulation of spin-down carriers with a spin relaxation time of 32 ps at room temperature. The observed decay and accumulation processes show a clear symmetrical behavior in their time dependences, as expected from simple rate equations.

In chapter 7, we performed characterization of InGaAs/InAlAs RTB diode using electro-optic sampling. The switching time from peak

to valley is decreased with the reduction of the barrier thickness. We proposed a new equivalent circuit model of RTB diodes including quantum-mechanical state-lifetime phenomenologically. The simulated switching behavior of RTB diodes using a new equivalent circuit model shows a better agreement with the experimental results than by Esaki diode model.

## Acknowledgments

I am deeply indebted to Professor Kikuo Cho for his guidance and encouragement.

I wish to express my thanks to Professor Satoshi Hiyamizu, Professor Tetsuro Kobayashi, and Professor Hisao Nakashima for their advices and directions. I also would like to express my gratitude to Honorary Professor Akio Yoshimori for his encouragement.

I am grateful to Drs. Mikio Yamashita (now Professor at Hokkaido University) and Kenji Torizuka for their advices on the generation of ultrashort light pulses in Electrotechnical Laboratories.

Thesis work was done at Fujitsu Laboratories Ltd. I would like to thank Drs. Bun-ichi Oguchi (ex-chairman), Masaka Ogi (ex-president), Mikio Ohtsuki (president), and Kaneyuki Kurokawa (managing director) for their continuous support in this work. I also wish to express my sincere thanks to Drs. Takahiko Misugi (ex-managing director), Osamu Ryuzan, Masaaki Kobayashi, Koichi Dazai, Hajime Ishikawa (board director), Toyoshi Yamaoka, Osamu Ohtsuki, Hisao Hashimoto, Teruo Sakurai, Masashi Ozeki (general manager), Osamu Wada, Naoki Yokoyama, Eizou Miyauchi, and Toshio Fujii for their encouragements and support. I am grateful to collaborators, Drs. Shunichi Muto (section manager), Tsuguo Inata, Yoshihiro Sugiyama, Yoshiaki Nakata, Hiroshi Arimoto, Hideki Kitada, Satoshi Nakamura, Masaomi Yamaguchi, and Akira Endoh for their support and valuable discussions. Thanks are extended to Drs. Shigehiko Sasa, Hiroaki Ohnishi, Yasuhiro Yamaguchi, Hideaki Ishikawa, Toshio Kurihara, and Takayuki Kameda for their support and discussions.

## PUBLICATIONS AND PRESENTATIONS

### Papers and Letters\*

- \*1. "Picosecond Characterization of InGaAs/InAlAs Resonant Tunneling Barrier Diode by Electro-Optic Sampling":  
A. Tackeuchi, T. Inata, S. Muto, and E. Miyauchi:  
Jpn. J. Appl. Phys. 28 (1989) L750.
- \*2. "Fast Recovery of Excitonic Absorption Peaks in Tunneling Bi-Quantum-Well Structures":  
A. Tackeuchi, S. Muto, T. Inata, and T. Fujii:  
Jpn. J. Appl. Phys. 28 (1989) L1098.
3. "Picosecond Characterization of InGaAs/InAlAs Resonant Tunneling Barriers Grown by MBE":  
S. Muto, A. Tackeuchi, T. Inata, E. Miyauchi, and T. Fujii:  
Surf. Science 228 (1990) 370.
- \*4. "Direct Observation of Picosecond Spin Relaxation of Excitons in GaAs/AlGaAs Quantum Wells using Spin Dependent Optical Nonlinearity":  
A. Tackeuchi, S. Muto, T. Inata, and T. Fujii:  
Appl. Phys. Letters 56 (1990) 2213.
- \*5. "Fast Recovery of Excitonic Absorption Bleaching in Tunneling Biquantum Well Structures":  
A. Tackeuchi, S. Muto, T. Inata, and T. Fujii:  
Appl. Phys. Letters 58 (1991) 1670.
- \*6. "Longitudinal Optical Phonon Assisted Tunneling in Tunneling Bi-Quantum Well Structures":  
S. Muto, T. Inata, A. Tackeuchi, Y. Sugiyama, and T. Fujii:  
Appl. Phys. Letters 58 (1991) 2393.

- \*7. "Temperature Dependence of Photoluminescence Decay Time in Tunneling Bi-Quantum-Well Structures":  
Y. Sugiyama, A. Tackeuchi, T. Inata, and S. Muto:  
Jpn. J. Appl. Phys. 30 (1991) L1454.
  
- \*8. "Picosecond Excitonic Absorption Recovery of 100 nm GaAs/AlGaAs Narrow Multiple Quantum-well Wires":  
A. Tackeuchi, H. Kitada, H. Arimoto, Y. Sugiyama, A. Endoh, Y. Nakata, T. Inata, and S. Muto:  
Appl. Phys. Letters 59 (1991) 1114.
  
- 9. "Time Evolution of Excitonic Absorption Bleaching of Resonant Tunneling Bi-Quantum-Well Structures":  
A. Tackeuchi, S. Muto, T. Inata, and T. Fujii:  
Jpn. J. Appl. Phys. 30 (1991) 2730.
  
- 10. "Picosecond Absorption Recovery of 100 nm GaAs/AlGaAs MQW Wires":  
A. Tackeuchi, H. Kitada, H. Arimoto, Y. Sugiyama, T. Inata, Y. Yamaguchi, Y. Nakata, S. Nakamura, and S. Muto:  
Surf. Science 267 (1992) 267.
  
- \*11. "Fast Recovery from Excitonic Absorption Bleaching in Type-II GaAs/AlGaAs/AlAs Tunneling Bi-quantum Well":  
A. Tackeuchi, T. Inata, Y. Sugiyama, Y. Nakata, S. Nakamura, and S. Muto:  
to be published in Jpn. J. Appl. Phys. 31 (1992) Part 2, No.6A or 6B.
  
- \*12. "Fabrication of Sub-100nm Wires and Dots in GaAs/ AlGaAs Multiquantum Well by Focused Ion Beam Lithography":  
H. Kitada, H. Arimoto, A. Tackeuchi, Y. Yamaguchi, Y. Nakata, A. Endoh, and, S. Muto:  
to be published in Jpn. J. Appl. Phys. (1992).

## International Conferences

1. "Picosecond Characterization of InGaAs/InAlAs Resonant Tunneling Barrier Diode by Electro-Optic Sampling",  
A.Tackeuchi, T. Inata, S. Muto, and E. Miyauchi,  
The 6th International conference of Ultrafast Phenomena, Mt. Hiei, Kyoto, Japan, July 12-15, 1988.
2. "Picosecond characterization of InGaAs/InAlAs resonant tunneling barrier by Electro-Optic Sampling",  
A.Tackeuchi, T. Inata, S. Muto, E. Miyauchi, and T. Fujii,  
Electronic Materials Conference, MIT, USA, June 21-23, 1989.
3. "Fast Recovery of Excitonic Absorption Peaks in Tunneling Bi-Quantum-well Structures",  
A.Tackeuchi, T. Inata, S. Muto, and T. Fujii,  
The 16th International Symposium on Gallium Arsenide and Related Compounds, Karuizawa, Japan, Sept 25-29, 1989.
4. "Fast Recovery of Excitonic Absorption Peaks in Tunneling Bi-Quantum-Well Structures",  
A.Tackeuchi, S. Muto, T. Inata, and T. Fujii,  
The 7th International conference of Ultrafast Phenomena, Montrey, CA, USA, May 14-17, 1990.
5. "Picosecond Absorption Recovery of 100-nm GaAs/AlGaAs MQW Wires",  
A.Tackeuchi, H. Kitada, H. Arimoto, T. Inata, Y. Sugiyama, Y. Yamaguchi, Y. Nakata, S. Nakamura, and S. Muto,  
5th International Conference on Modulated Semiconductor Structures, Nara, Japan, July 8-12, 1991.



## Proceedings

1. "Picosecond Characterization of InGaAs/InAlAs Resonant Tunneling Barrier Diode by Electro-Optic Sampling",  
A. Tackeuchi, T. Inata, S. Muto, and E. Miyauchi:  
Ultrafast Phenomena VI, Proceedings of the 6th International conference of Ultrafast Phenomena, Mt. Hiei, 1988 (Springer-Verlag, Berlin 1988) P.182.
2. "Fast Recovery of Excitonic Absorption Peaks in Tunneling Bi-Quantum-Well Structures",  
A. Tackeuchi, T. Inata, S. Muto, and T. Fujii,  
Proceedings of the 16th International Symposium on Gallium Arsenide and Related Compounds, Karuizawa, 1989 (IOP Publishing Ltd, 1989) P.909.
3. "Fast Recovery of Excitonic Absorption Peaks in Tunneling Bi-Quantum-Well Structures",  
A. Tackeuchi, S. Muto, T. Inata, and T. Fujii:  
Ultrafast Phenomena VII, Proceedings of the 7th International conference of Ultrafast Phenomena, Montrey, 1990 (Springer-Verlag, Berlin 1990) P.265.

## PERSONAL HISTORY

Name                                      Atsushi Tackeuchi

Date of Birth:                      February 19, 1960.

### Educational Background

<u>Degree</u>	<u>Institution</u>	<u>Field</u>	<u>Graduated</u>
B.E.	Osaka University	Solid State Physics	1983
M.E.	Osaka University	Solid State Physics	1985

### Employment Experience

1985 to present:    Fujitsu Laboratories Ltd., Researcher

### Research Experience

In Osaka university, I studied surface science under Prof. Akio Yoshimori and Prof. Kikuo Cho. I made the Master's thesis titled "The theory of vibrations and thermal desorption of adsorbed hydrogen on Ni (110) surface" under the guidance of Prof. A. Yoshimori.

After joined Fujitsu Laboratories Ltd. in 1985, I stayed in Electrotechnical Laboratories from 1985 to 1986 (1 year) and studied a generation of ultrashort optical pulses using a colliding pulse modelocked dye laser under the guidance of Dr. Mikio Yamashita (now Prof. at Hokkaido Univ.).

From 1986, I have researched the picosecond phenomena in quantum confined structures of III-V compounds.

